CONSORZIO RFX
Ricerca Formazione Innovazione

Consiglio Nazionale delle Ricerche

Studies of Plasma Self-Organization in the Reversed-Field Pinch and Impact on Transport Properties

Susanna Cappello, D. Bonfiglio, G. Di Giannatale, D.F. Escande, M. Veranda, A. Kryzhanovskyy, the RFX team

CONSORZIO RFX
Associazione Euratom-ENEA sulla Fusione - PADOVA - ITALY
partnership involving ***CNR, ENEA, INFN and Padova University***

Collaborations: L. Chacon, *(LANL - USA)*
D. Grasso *(CNR-ISC Torino - IT)*
F. Pegoraro *(Pisa University -IT)*

Italy - Padova: Area della Ricerca del CNR

Consorzio RFX:

1) NBTF Neutral Beam Test Facilty for ITER

2) RFX: RFP Device

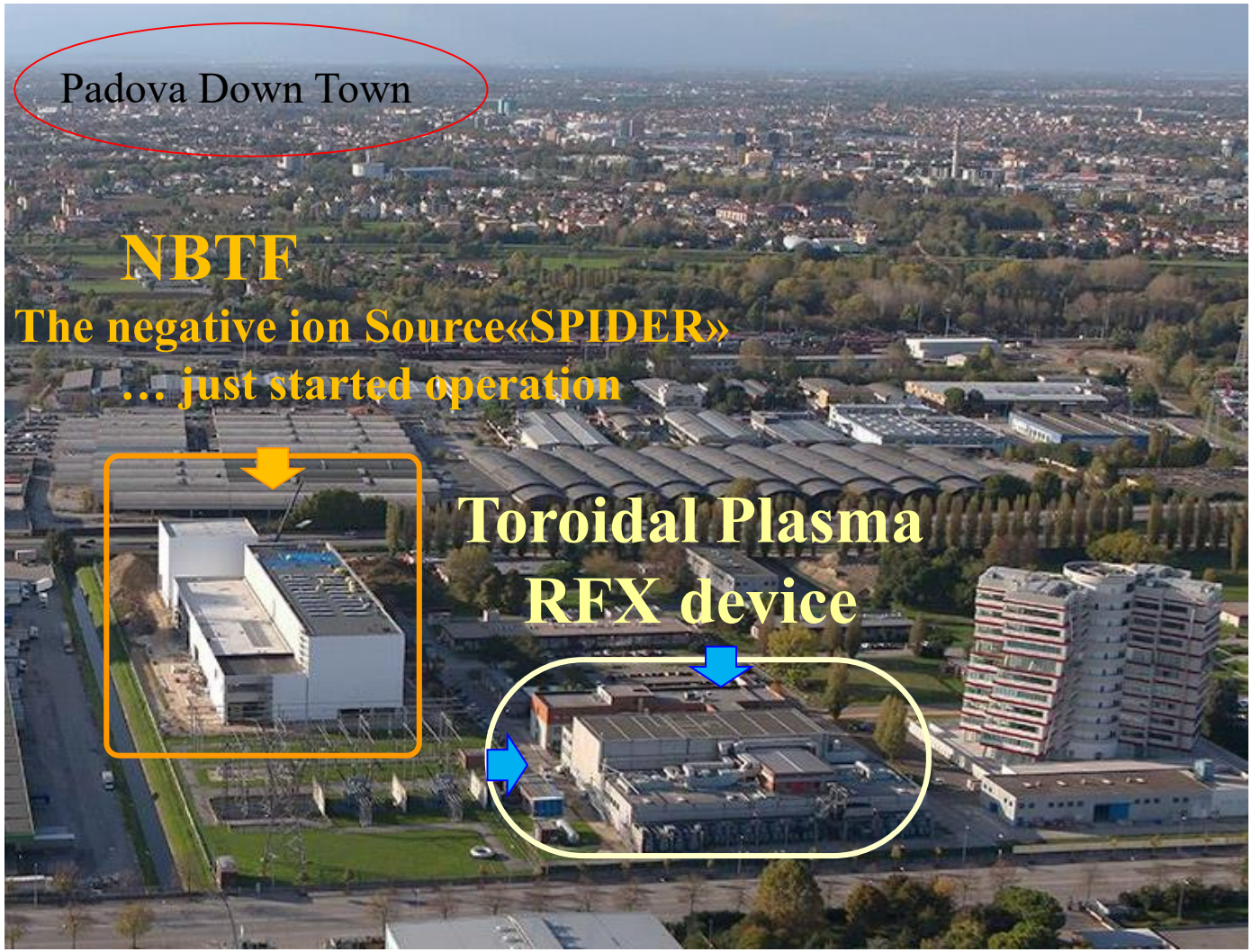

Reversed Field Pinch, RFP, partners:

USA - Sweden - Japan – China

The place of the RFP in MCF

Several common physics issues:
transport barrier formation, density limit, magnetic relaxation ..

Increasing plasma current

Steady state | Confinement | Light Tech expected

Coils Complexity | Disruption risk | Confinement

Stellarator

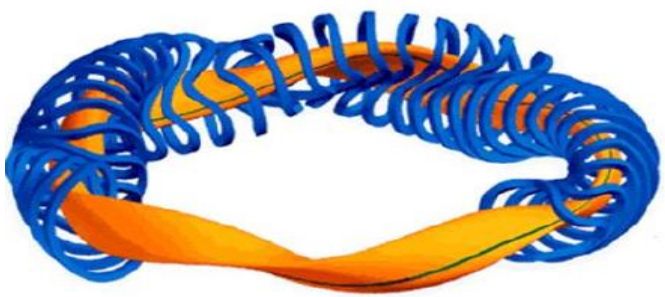

FIG. 1.14. Schematic of stellarator magnetic field coils and plasma configuration (
Ref. [1.62]).

R = 5.5 m W7-X

(R = 3.9 m LHD)

[*] Book: Fusion Physics IAEA 2012

Tokamak

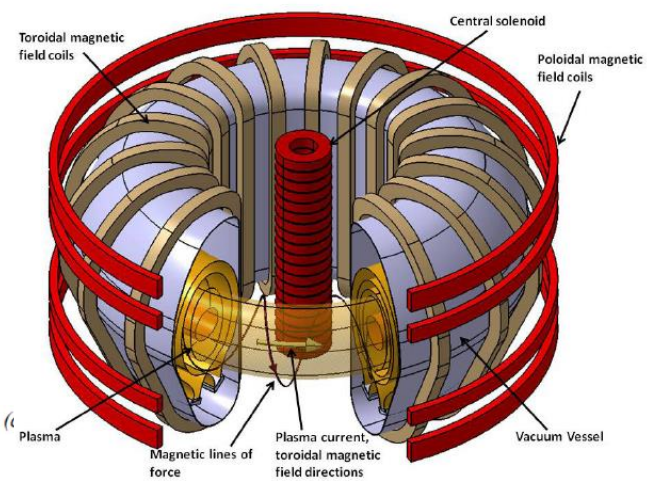

FIG. 1.12. Schematic of a tokamak.

R = 3 m JET

(R = 6.21 m ITER)

RFP

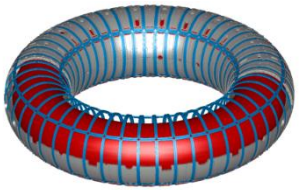

R = 2.0 m RFX

(1.5 m MST USA
1.4 m KTX Hefei China)

OUTLINE

Introduction to the RFP

a Pinch with Field Reversal – Helical selforganization – Transport Barriers

a. Overview of Experimental facts (mainly from RFX)

- Quasi helical states (QSH) in high current discharges (Ip > 0.8MA),
- Electron transport barriers (eITB), and Impurity screening effect;

b. 3D non linear MHD modeling and magnetic chaos healing

- Transition to helical regimes,
- Key role of edge Magnetic Perturbations (MP) and realistic Boundary conditions :

Non-Resonant and Resonant MPs … "synergistically interact" with helical self-organization process

- Magnetic chaos healing, Lagrangian Coherent Structures detection.

… New regimes to be experimentally explored in **RFX-mod2 from 2021**

RFP device and configuration set up

RFX device coils

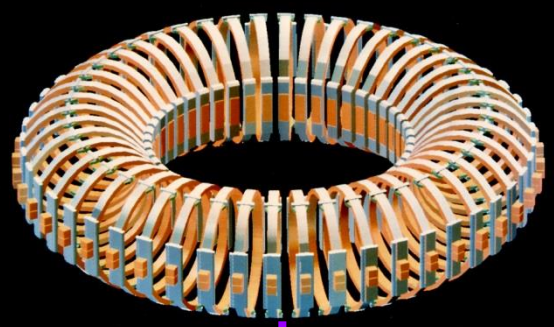

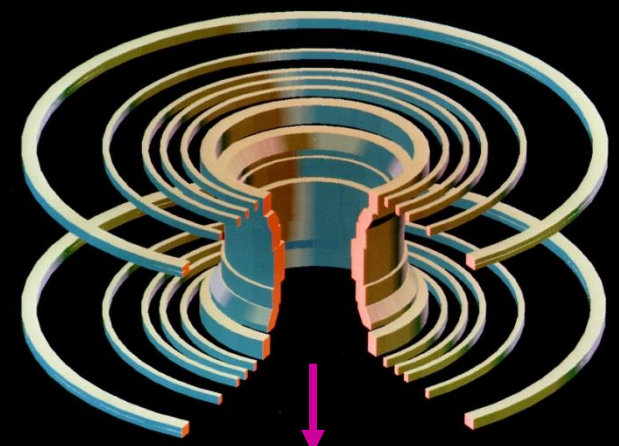

toroidal magnetic field

poloidal magnetic field

induction of plasma current

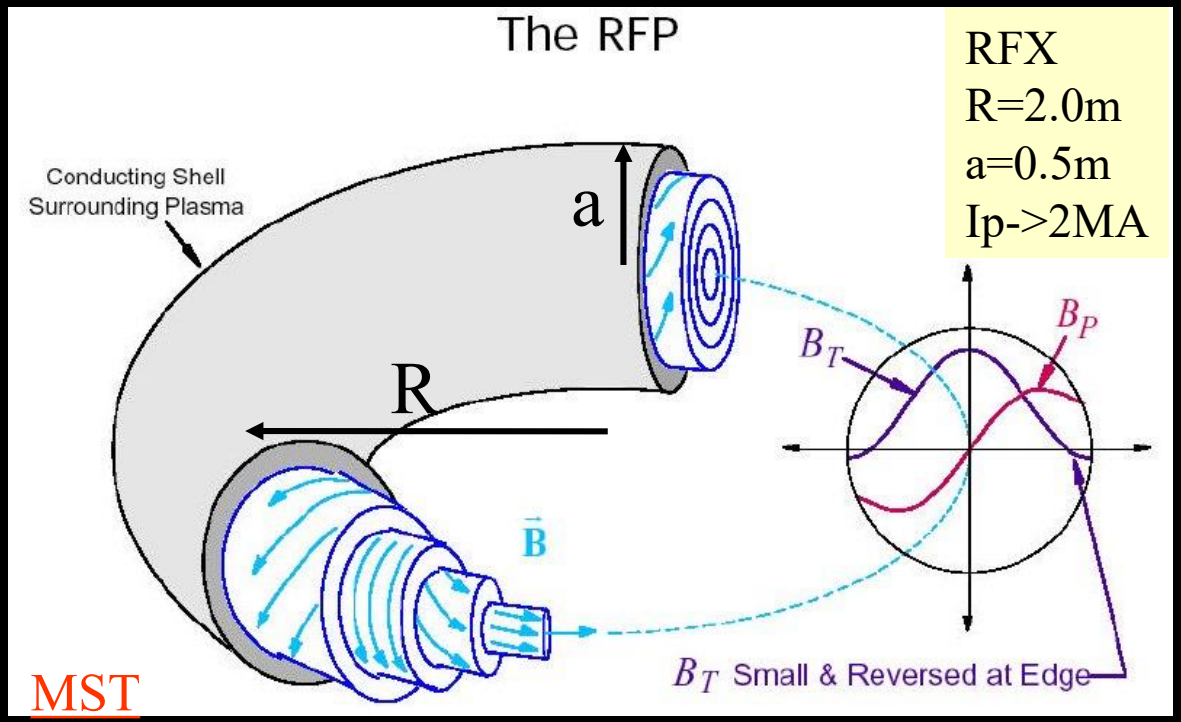

RFX
R=2.0m
a=0.5m
Ip->2MA

MST

mean magnetic field radial profiles

mainly produced by the plasma current

The RFP is a simple ohmic device.

No auxiliary systems – heating
– current drive
– momentum sources

(typically used in Tokamaks and Stellarators)

The RFP operational space

Two dimensionless parameters are routinely used:

F - Reversal parameter

$$F \equiv \frac{B_T(a)}{\langle B_T(r) \rangle}$$

$$\propto q\,(a)$$

Θ - Pinch parameter

$$\Theta \equiv \frac{B_P(a)}{\langle B_T(r) \rangle}$$

$$\propto \frac{I_{plasma}}{\Phi}$$

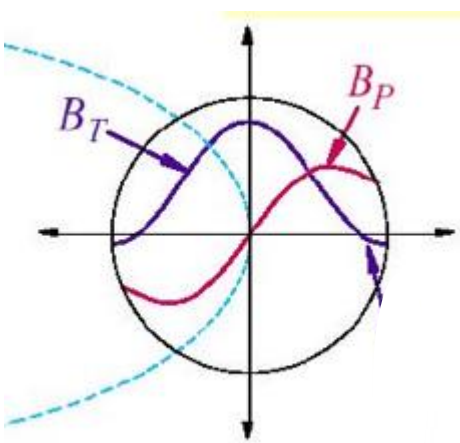

Reviews of Modern Physics, Vol. 58, No. 3, July 1986

Relaxation and magnetic reconnection in plasmas

J. B. Taylor

Culham Laboratory, Abingdon, Oxfordshire, OX14 3DB, England

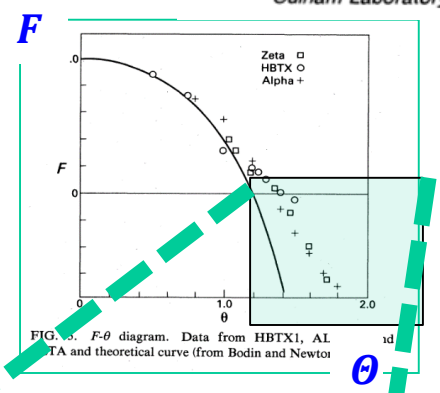

Bessel Function Model
BFM
minimum energy solutions: axisymmetric Bessel

Θ saturation predicted at Θ ~ 1.56

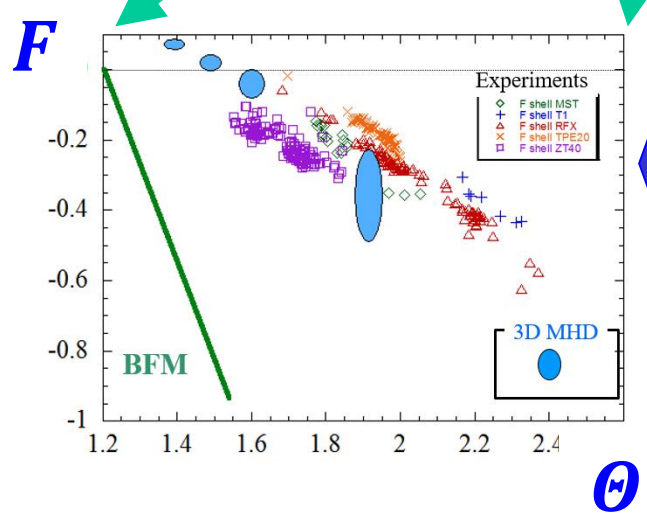

Experiments data base and 3D MHD predictions

Cappello PPCF2004

RFP self-organization

a) Overview of Experimental facts and b) Modeling results

Transition to helical states:

- Highlights of the phenomenology,
- Statistical data,
- Transport barrier formation Te,
- Impurity screening effect.

RFP self-organization

RFX

RFP ↔ saturated KINKED plasma

for Ip above ~ 1 MA

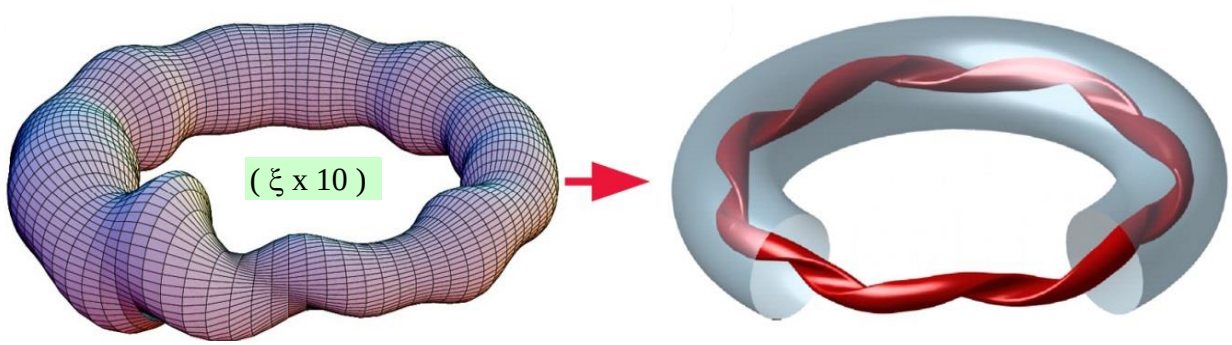

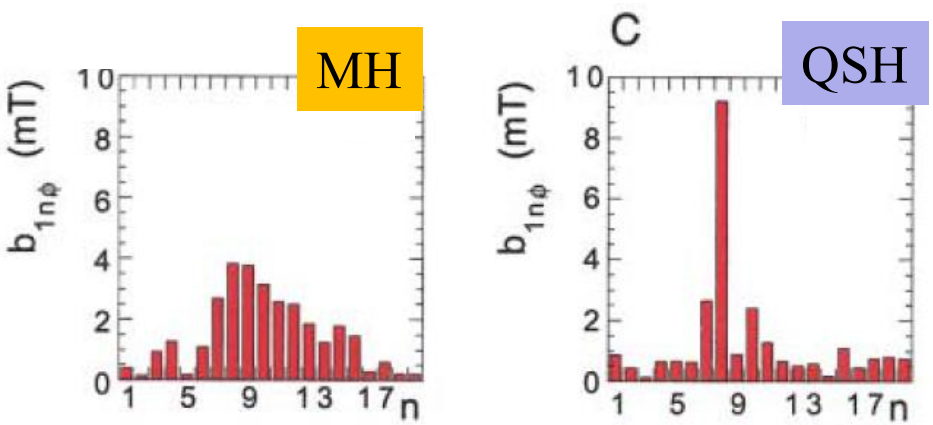

MHD spectrum: resistive kink-tearing modes

Advanced operation
required in RFX-mod

CLEAN MODE CONTROL
and/or
NON CONVENTIONAL
SCENARIOS (PPCD-OPCD)

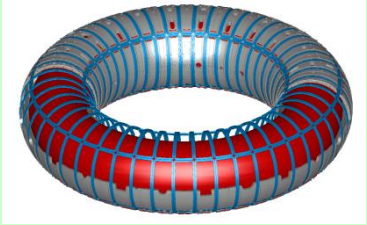

Feedback coils system
Typical operation:
Ip ~ 1.7 MA
Te up to 1.2 keV

RFP self-organization

RFX

RFP ↔ saturated KINKED plasma

for Ip above ~ 1 MA

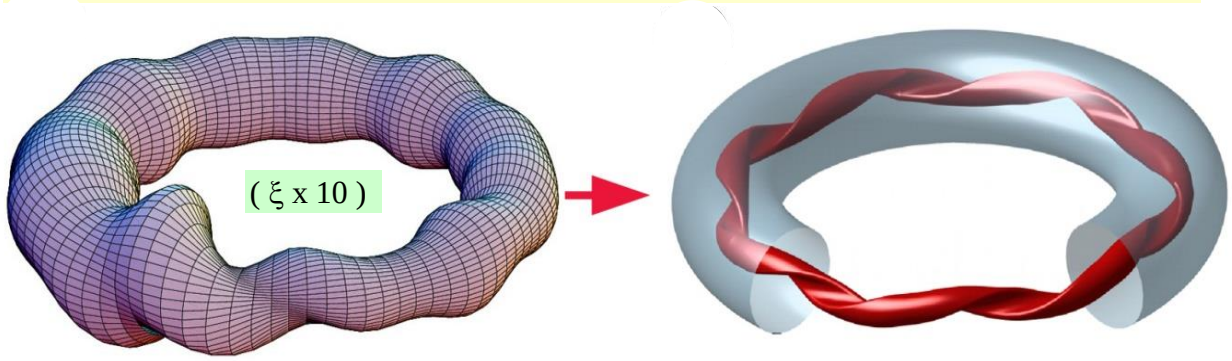

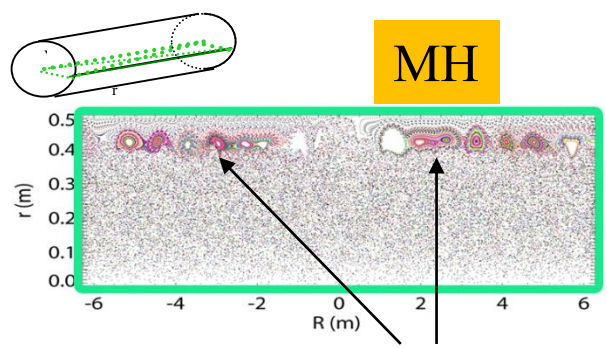

m=0 islands chain at reversal radius

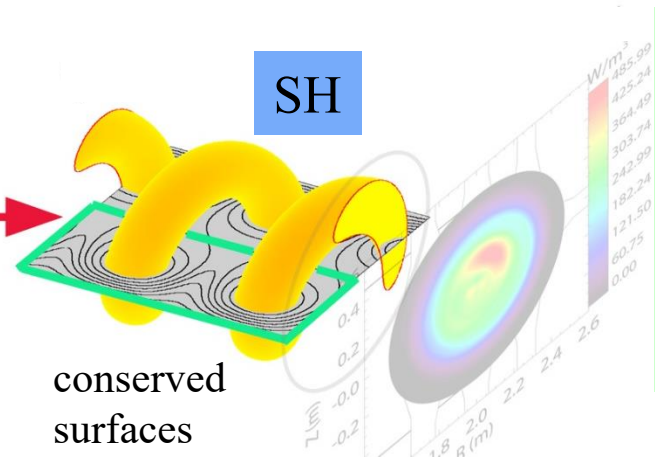

conserved surfaces

MHD spectrum impact on magnetic topology

Advanced operation required in RFX-mod

CLEAN MODE CONTROL
and/or
NON CONVENTIONAL SCENARIOS (PPCD-OPCD)

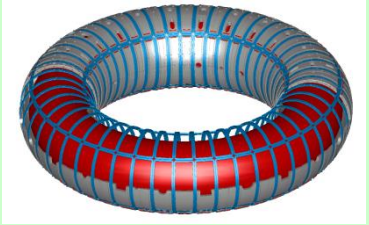

Feedback coils system
Typical operation:
Ip ~ 1.7 MA
Te up to 1.2 keV

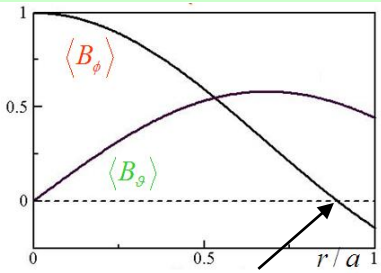

RFP helical self-organization: several experiments

RFX – TPE – MST –T2R

RFX

FIG. 3 (color). Schematic view of a $n = 7$ helical structure inside the RFX vessel.

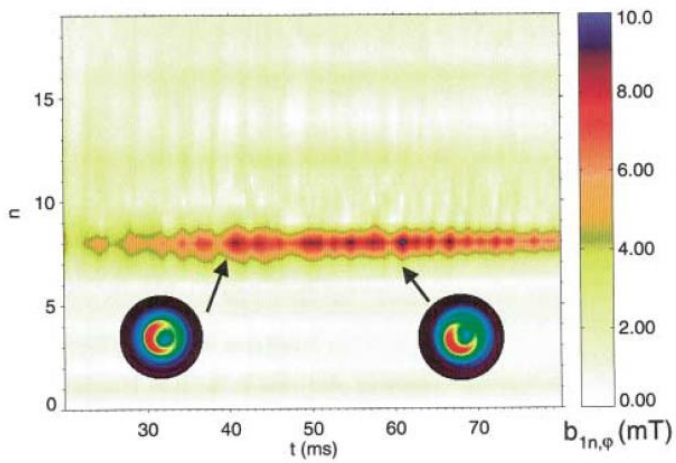

FIG. 5 (color). $m = 1$ modes n-spectrum vs time and SXR emissivity patterns at selected times ($t = 40$ ms and $t = 60$ ms) in a plasma (No. 11336) where the QSH state is permanent. The dominant mode in this case is $n = 8$.

Escande, Martin, Ortolani et al. PRL 2000

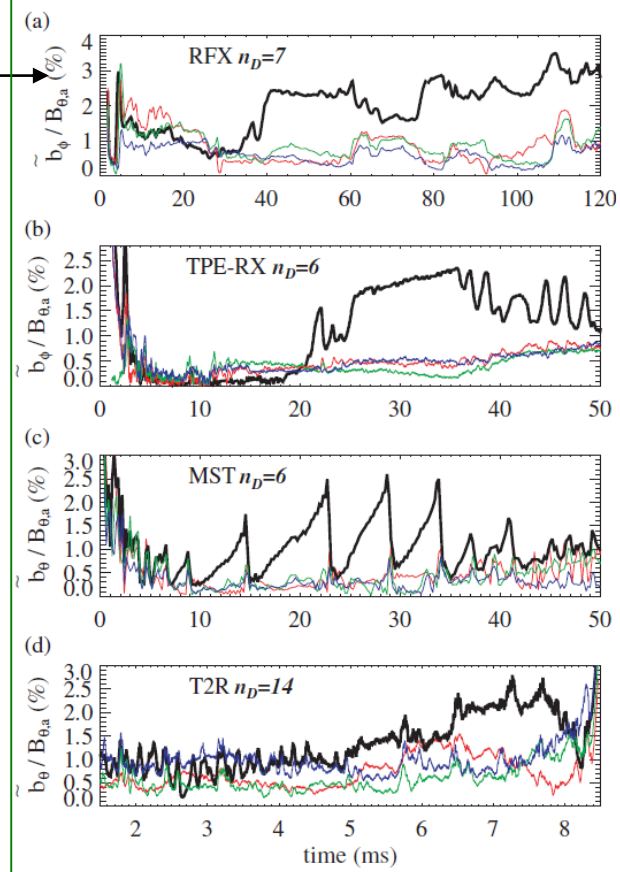

TPE-RX	Japan
MST	USA
T2R	Sweden

Martin, Marrelli, Spizzo et al. NF 2003

More recently also:
RELAX (Japan), KTX (Hefei- China)

RFP helical self-organization: a robust process

HELICAL persistency increases with current - up to > 85% of flat top

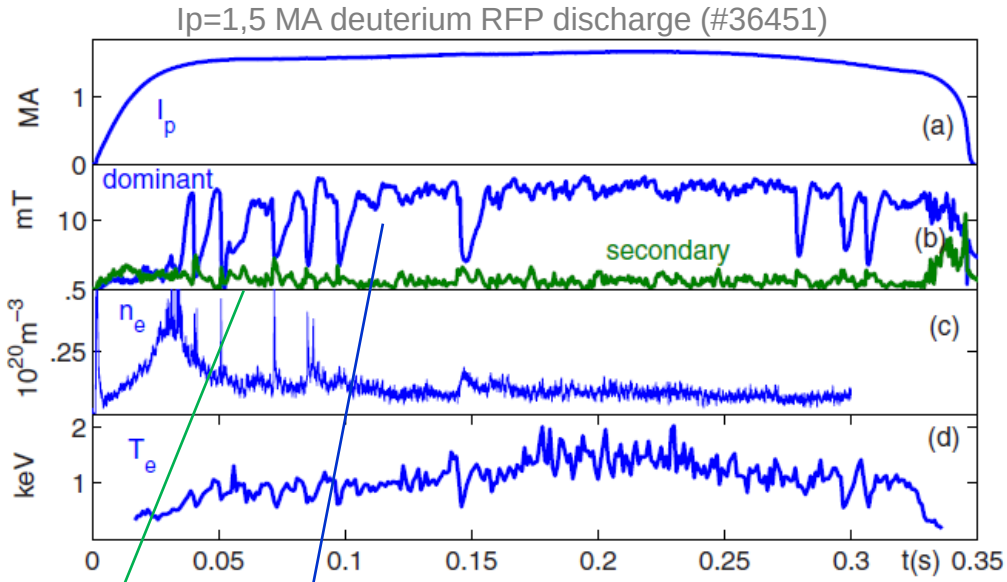

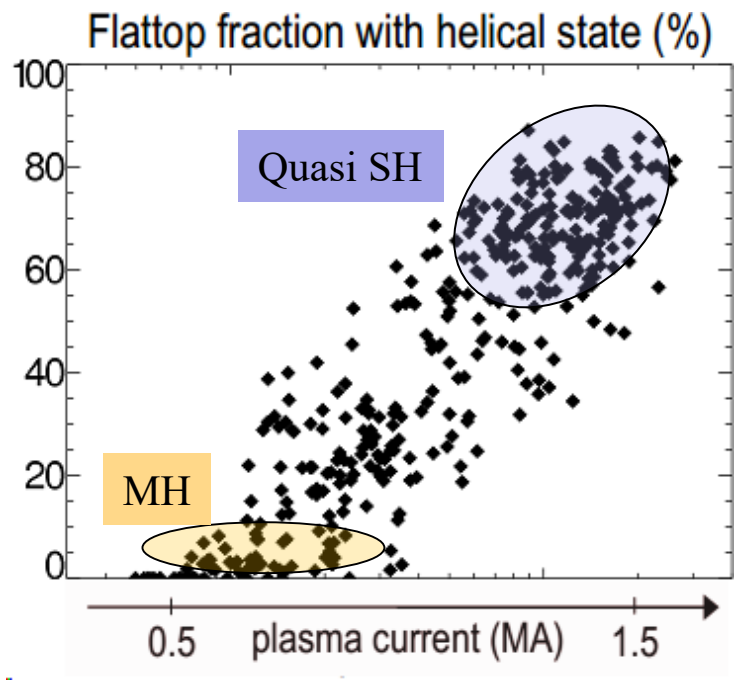

(hydrogen RFP discharges)

Piovesan, Zuin et al NuclFus 2009

Dominant mode (internal)

ave secondary modes

Puiatti, Dal Bello, Marrelli et al. NF 2015

Similar behavior in MST experiment:
- Chapman et al IAEA EX/P6-01 (2012)
- Sarff et al Nucl Fus 2013

RFP helical self-organization: barriers formation

Formation of e-Transport Barriers

24598, 117ms
I_P=1.3MA
n/n_G=0.20

22201, 35ms
I_P=0.7MA
n/n_G=0.22

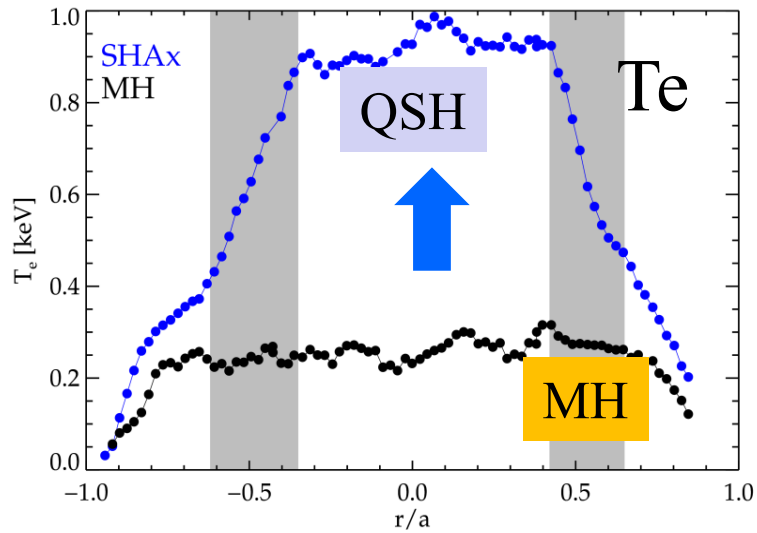

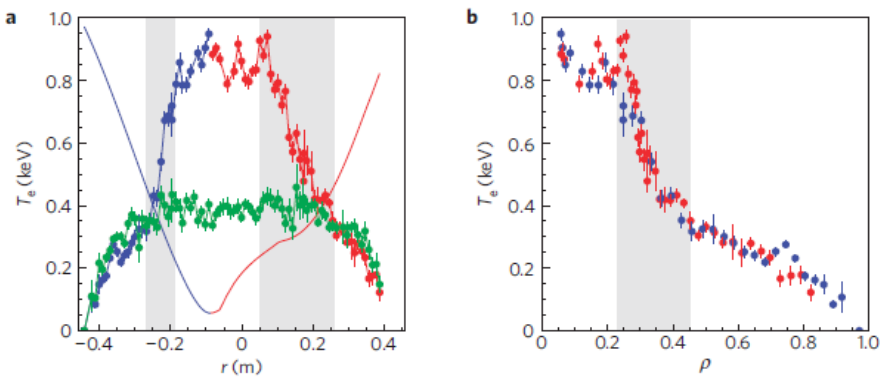

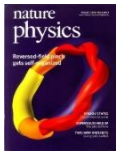

Lorenzini, Martines, Piovesan et al NatPhys 2009
Piovesan, Zuin, Alfier et al NF 2009

RFP helical self-organization: barriers formation

41st EPS Conference on Plasma Physics

… and Impurity screening effect

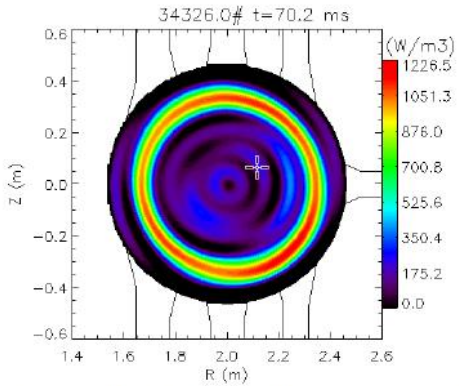

Fig.2 Experimental tomographic inversion of SXR emissivity at the maximum of the W LBO emission

Tungsten Laser Blow Off in QSH

a.u.

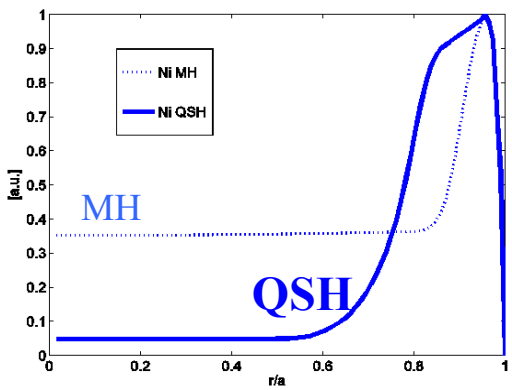

Simulation of Ni normalized total density at the steady state, after Ni target Laser Blow Off

Puiatti, Valisa, Agostini et al NF 2011
Carraro, Auriemma, Barbui et al EPS 2014
Menmuir, Carraro, Alfier et al PPCF 2010

TESPEL experiments (RFX-mod2) planned in collaboration with NIFS

RFP self-organization

a) Experiments and **b) Modeling**

Transition to helical states:

- Simple description from a toy model:
  current carrying wire in a flux conserver,

- 3D nonlinear viscoresistive Magnetohydrodynamic modeling:
  - ✓ Transition to helical regimes, and
  - ✓ Magnetic chaos healing

RFP *Toy model*: **intuitive RFP**

… a current carrying wire in a flux conserver:

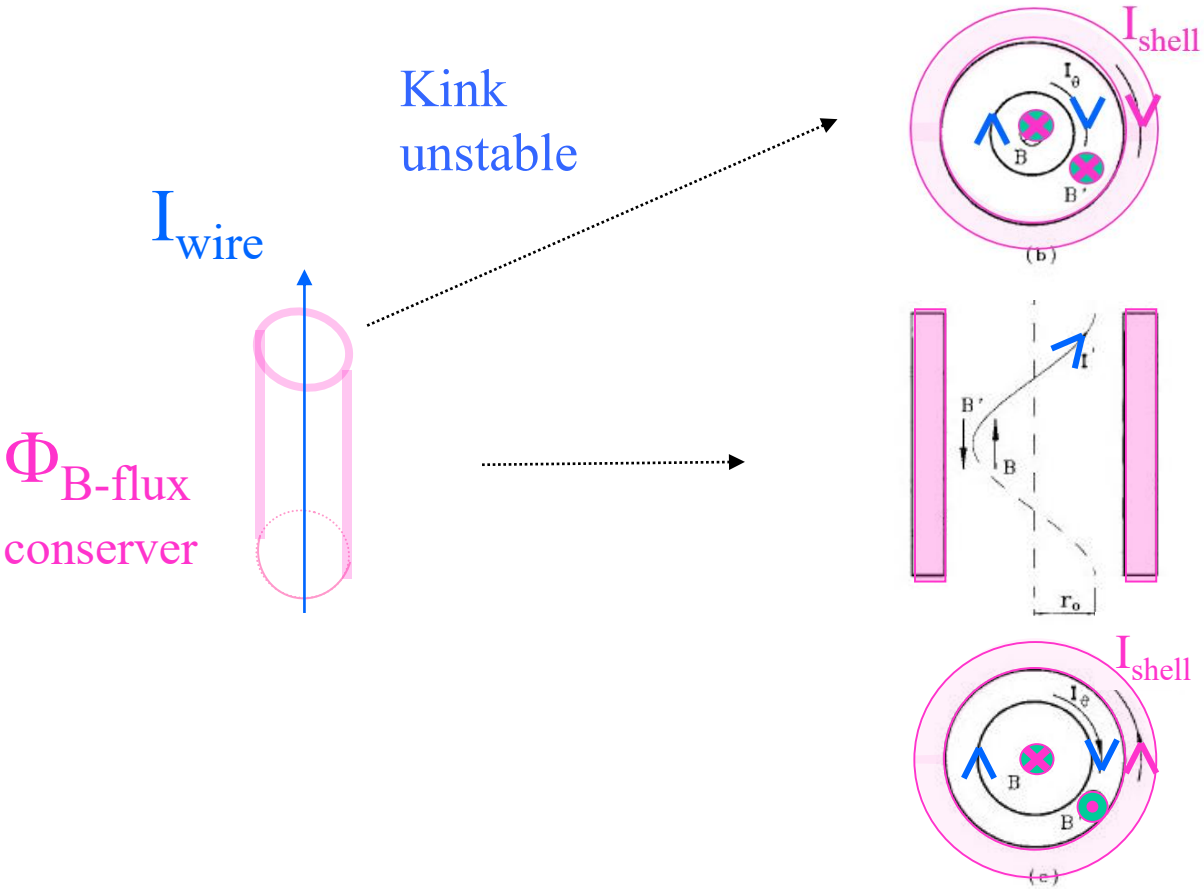

solenoidal effect by the wire itself

… saturates when edge field reversal is reached

Early elements:
Verhage-Furzer-Robinson NF 1978
Kadomtsev 1992 (Sawer PoF1959)

Elaborated in:
Benisti Escande EFTC 1998
Escande et al. PPCF 2000

$r_0 \rightarrow 1$ (disruption) for too small $\frac{I_{wire}}{\Phi}$
(Tokamak case)

Main NUMERICAL TOOLS involved on the modeling side

- **3D nonlinear MHD** – viscoresitive approximation:

  SpeCyl [a] - PIXIE3D [b] (benchmarked codes) [c]

- **Magnetic Field line integration**:

  NEMATO [d] (benchmarked vs ORBIT code [e])

- **Lagrangian Coherent Structures** detection [f, g]

[a] Cappello, Biskamp **NF** 1996
[b] Chacòn **CPC** 2004, Chacòn **PoP** 2008
[c] Bonfiglio, Chacon, Cappello **PoP** 2010
[d] Finn, Chacòn **PoP** 2005
[e] Ciaccio, Veranda, Bonfiglio, Cappello, Spizzo, White **PoP** (2013)
Recent collaboration with Borgogno (CNRS-Nice), Rubino and Grasso (CNR – ISC Torino, PoliTO) :
[f] Rubino, Borgogno, Veranda, Bonfiglio, Cappello, Grasso **PPCF** (2015)
[f] Di Giannatale, et al **POP** a,b (2019)
[f] Pegoraro, **PPCF** (2019)

3D nonlinear MHD

SpeCyl code - simple visco-resistive approx.

Cappello & Biskamp Nucl. Fus. 1996

$$\frac{\partial \boldsymbol{B}}{\partial t} = \nabla \wedge (\boldsymbol{v} \wedge \boldsymbol{B}) - \nabla \wedge (\eta \boldsymbol{J})$$

$$\frac{d\boldsymbol{v}}{dt} = \boldsymbol{J} \wedge \boldsymbol{B} + \nu \nabla^2 \boldsymbol{v}$$

$$\rho \equiv 1, \quad p \equiv 0$$

$\eta = \tau_A / \tau_R$

$\nu = \tau_A / \tau_v$

two dimensionless parameters with assigned radial profiles

Lundquist: $\mathbf{S = 1 / \eta}$

Viscous Lundquist $\mathbf{M = 1 / \nu}$

Magnetic Prandtl $\mathbf{P} = \nu/\eta = M/S$

Hartmann number $\mathbf{H} = (\nu\eta)^{-1/2}$

Cappello & Escande PRL 2000

r	Finite difference
θ, ϕ	Spectral formulation
t	Predictor-corrector + semi-implicit

Geometry: axially periodic cylinder

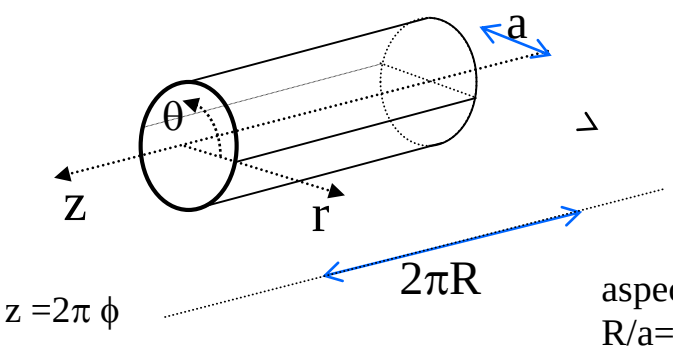

aspect ratio
R/a= 4 (RFX)

3D nonlinear MHD

SpeCyl code - simple visco-resistive approx.

Cappello & Biskamp Nucl. Fus. 1996

$$\frac{\partial \boldsymbol{B}}{\partial t} = \nabla \wedge (\boldsymbol{v} \wedge \boldsymbol{B}) - \nabla \wedge (\eta \boldsymbol{J})$$

$$\frac{\mathrm{d}\boldsymbol{v}}{\mathrm{d}t} = \boldsymbol{J} \wedge \boldsymbol{B} + \nu \nabla^2 \boldsymbol{v}$$

$$\rho \equiv 1, \quad p \equiv 0$$

$\eta = \tau_A / \tau_R$

$\nu = \tau_A / \tau_v$

two dimensionless parameters with assigned radial profiles

Lundquist: **$S = 1 / \eta$**

Viscous Lundquist **$M = 1 / \nu$**

r	Finite difference
θ, ϕ	Spectral formulation
t	Predictor-corrector + semi-implicit

Geometry: axially periodic cylinder

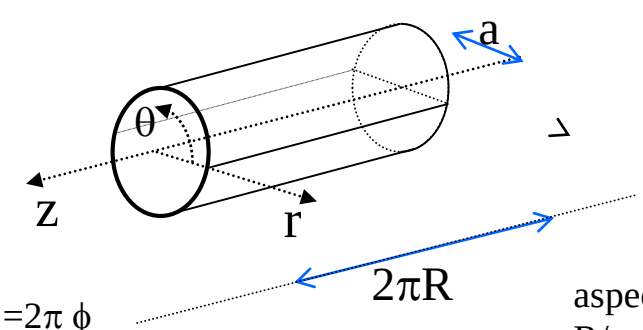

z =2π ϕ

aspect ratio
R/a= 4 (RFX)

"typical" boundary conditions:

- $B'_z = 0$ (**constant magnetic flux Φ**)
- Constant Ez (or **constant total toroidal current Iz**)
- velocity field: no slip.

m,n:
- Ideal boundary
- With MP on $B_{r\,m,n}$ (~ 2%, 4 %...)
- Thin shell + vacuum layer +ideal wall

initial conditions define Φ, Iz (i.e. Θ)

3D nonlinear MHD

Key role of boundary conditions
Allowing for finite Br at the plasma edge favors helical solutions

Next three slides: typical solutions for the choices

(Bonfiglio, Escande, Zanca, Cappello NF 2011)

"typical" boundary conditions:

- $B'_z = 0$ (**constant magnetic flux Φ**)
- Constant Ez (or **constant total toroidal current Iz**)
  - Ideal boundary
  - With MP on $B_{r\,m,n}$ (~ 2%, 4 %...)
  - Thin shell + vacuum layer +ideal wall
- velocity field: no slip.

3D nonlinear MHD

ideal BC: after the first strong relaxation to reversed state…

different regimes can be found

continuous transition ruled by *H number*

Cappello & Escande PRL 2000

Saturated kink
Single Helicity - SH

Nearly-periodic relaxations
Multiple Helicity - MH

High dissipation

Low dissipation

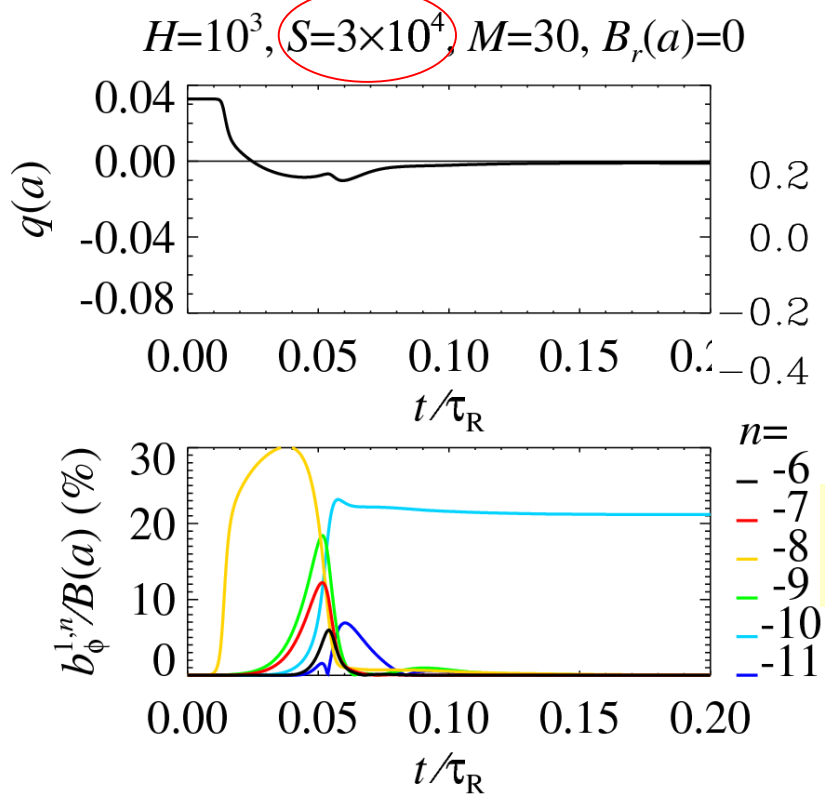

F(t)

Modes amplitude

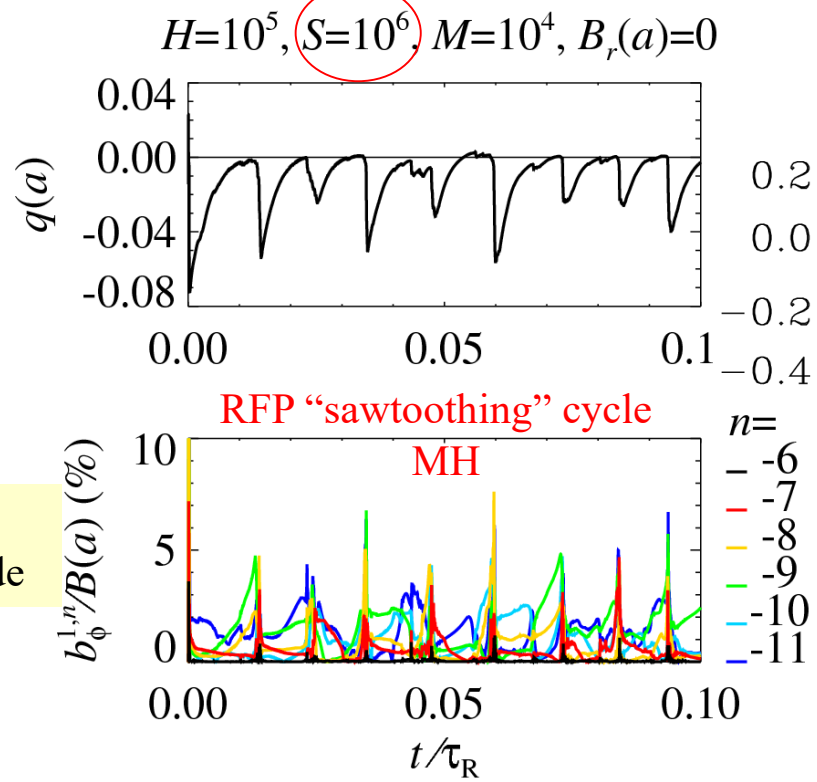

F

3D nonlinear MHD

ideal BC + MP (1,7) Sawtoothing cycle

with **systematic repetition of the MP stimulated mode**

Nearly-periodic relaxations
various degree of QSH persistence

Degree of helical order
ruled by *H* parameter & *MP*

Veranda to appear in NF 2019

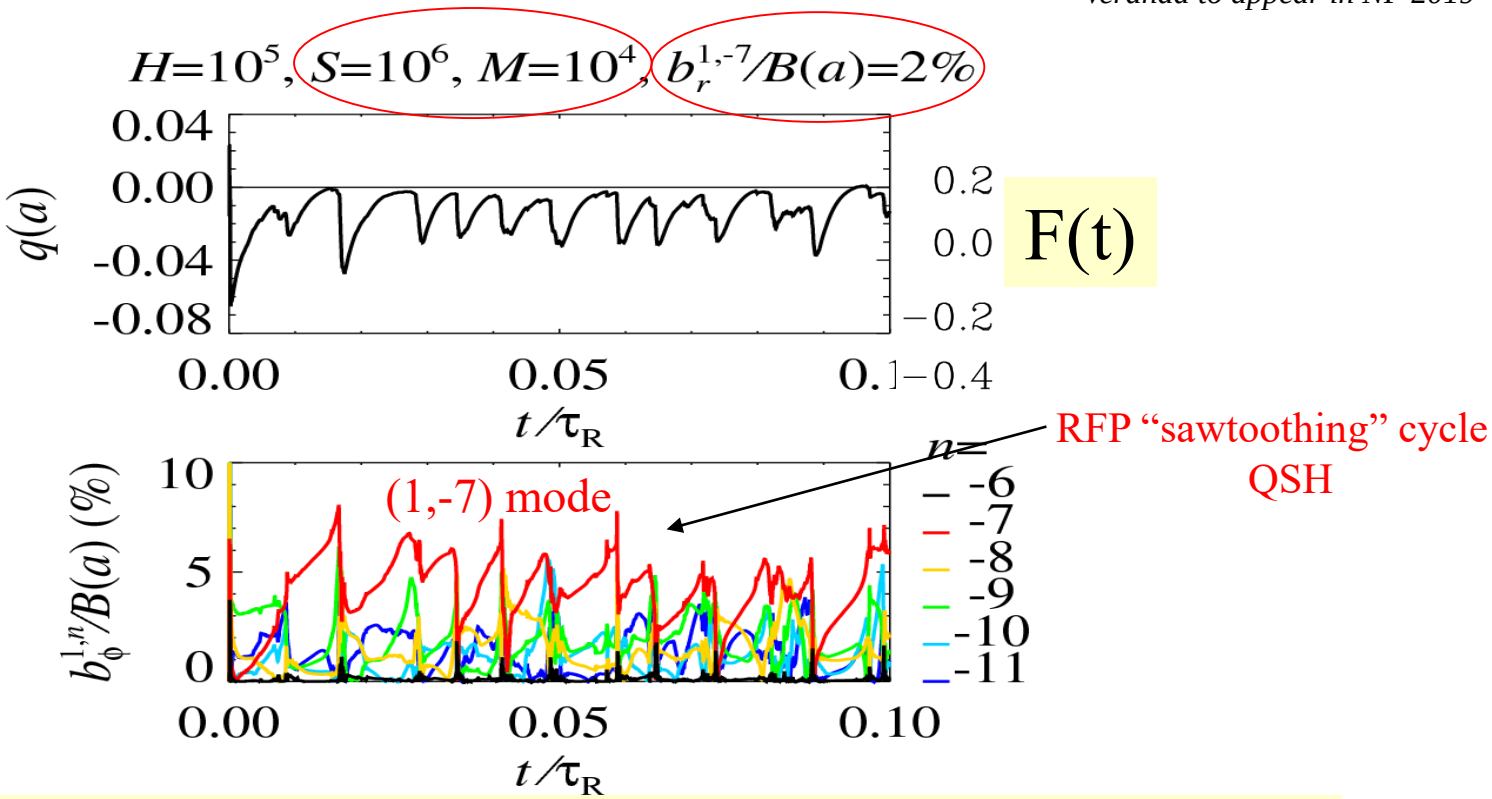

Bonfiglio NF 2011
Veranda PPCF 2013
Bonfiglio PRL 2013

The amplitude of secondary modes decreases with Lundquist, S,
The threshold MP% to excite a dominant mode decreases with S too.

3D nonlinear MHD

Thin Shell + Vacuum layer + Ideal wall + ~~no MP (1,7)~~:

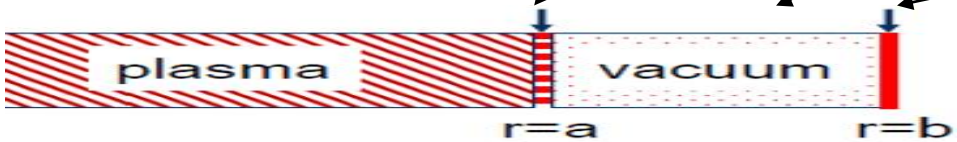

$S=10^6$, $M=10^4$, $b/a=1.2$, $\tau_W/\tau_R=10^{-2}$

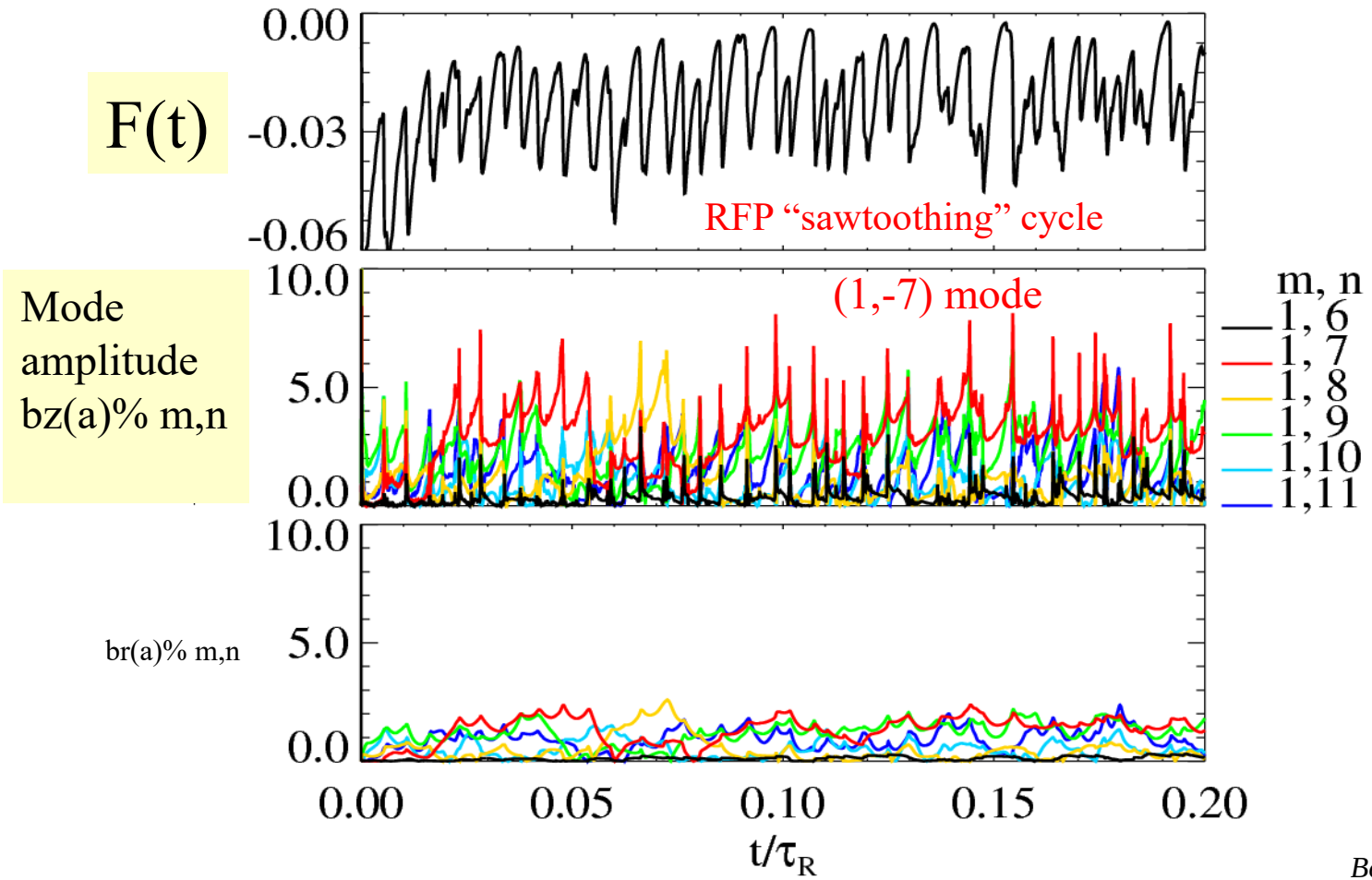

Poster session #2:
09/10/2019 15-17pm

P2-03 Bonfiglio Daniele
Effect of a refined magnetic boundary on MHD modelling of helical self-organization in the RFP

Bonfiglio EPS 2019
Bonfiglio AAPPS-DPP 2019

Hender Gimblett Robinson 1989
At low Θ -> distant shell tends to excite internal nonresonant modes

Chaos healing effect due to helical structure formation

Chaos healing effect due to helical structure formation

Next two slides:

Inspection of magnetic topology during a typical QSH sawtoothing cycle in simulations

We shall see an intermediate situation in between MH and SH

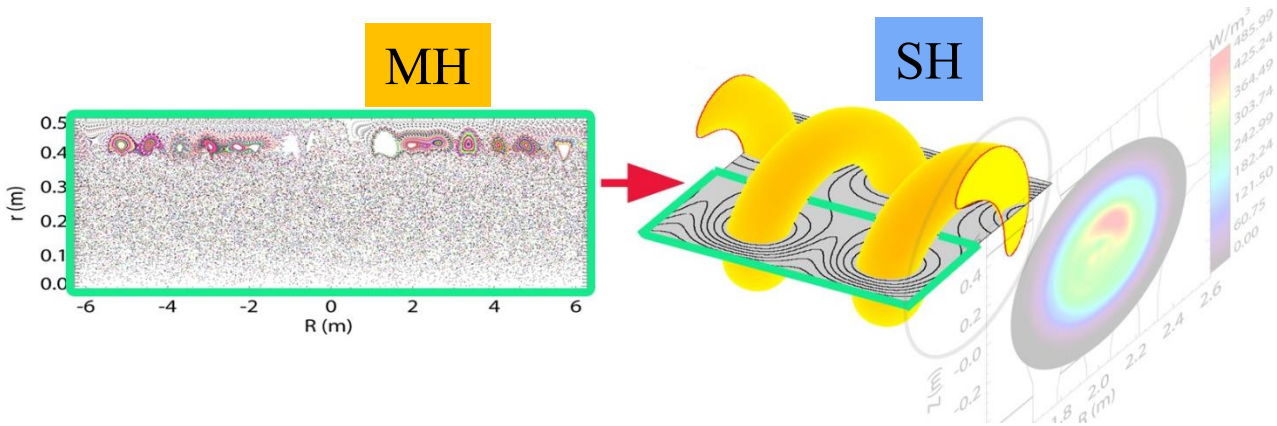

Chaos healing effect due to helical structure

[Dominant mode separatrix expulsion Escande et al PRL (2000)]

The width of conserved helical core evolves

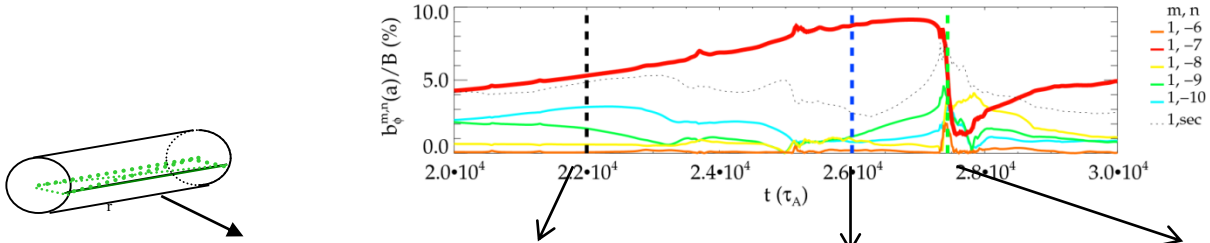

Core conserved surfaces are lost at slinky collapse

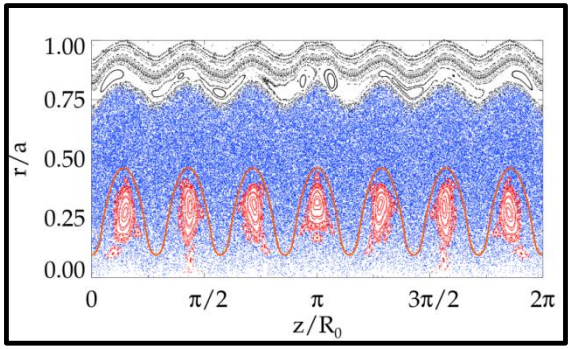

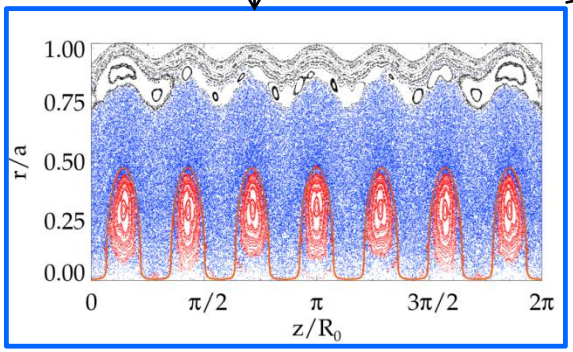

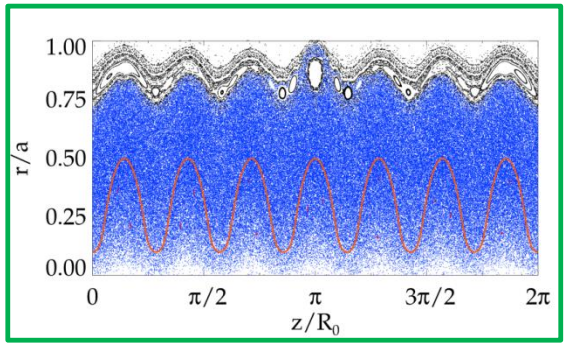

Max_q surface **(orange curve)** encompasses conserved magnetic surfaces

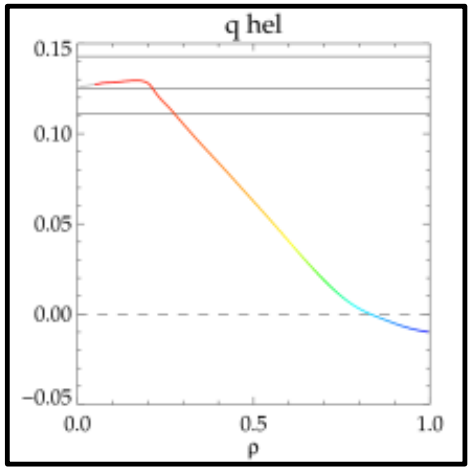

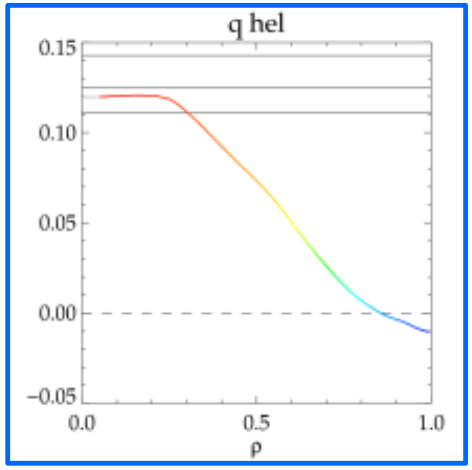

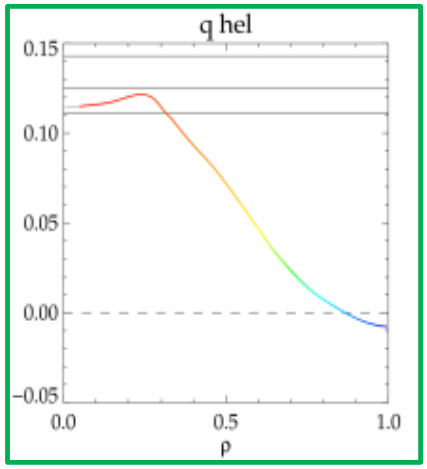

Poincare plots: secondary modes divided by 5 to match experimental amplitudes (as scaled to S= 10^7)

More efficient chaos healing by stimulating n=6 (Non Resonant)

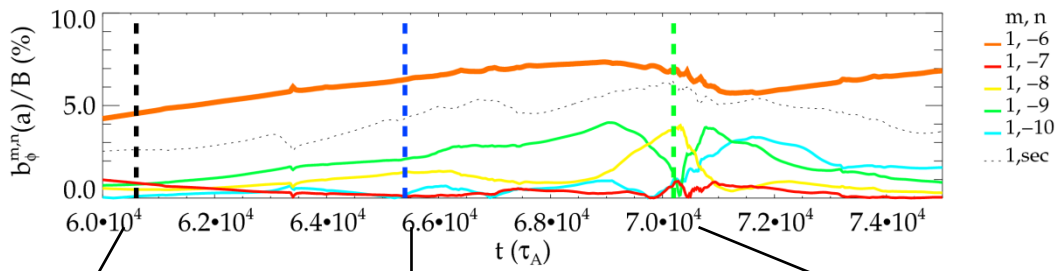

Conserved surfaces are never lost

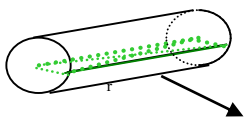

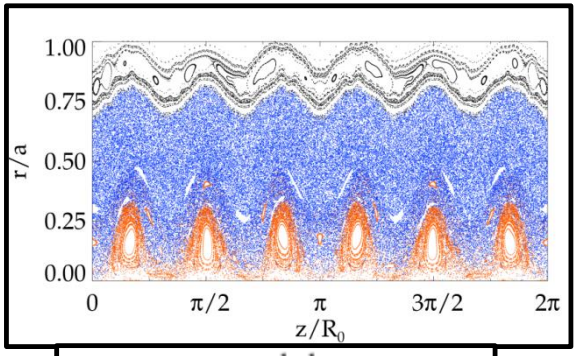

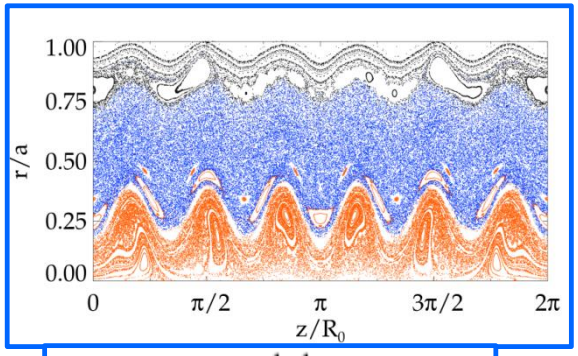

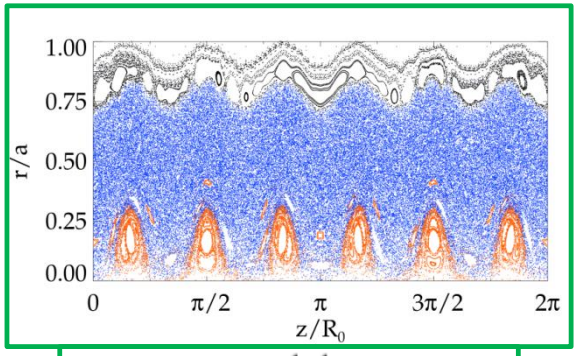

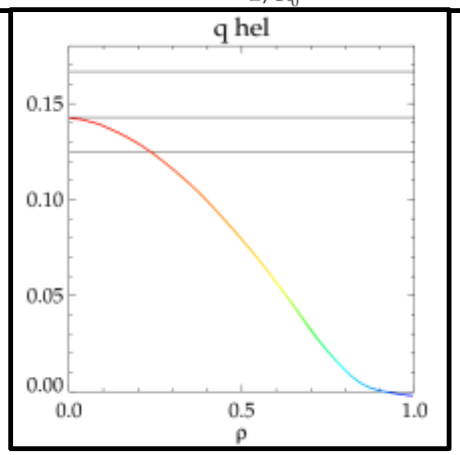

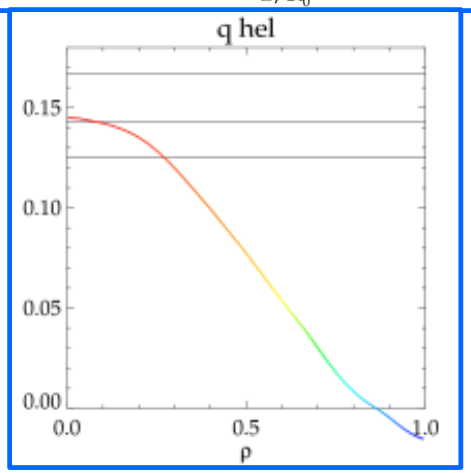

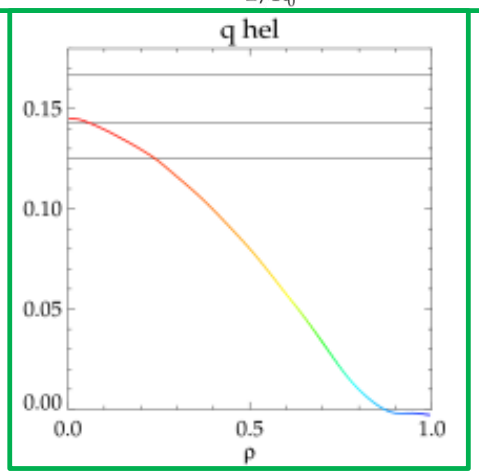

No shear reversal in such helical configurations built upon non-resonant modes …

Poincare plots: secondary modes divided by 5 to match experimental amplitudes (as scaled to S= 10^7)

A look at the reconnection events during the typical sawtoothing cycles:

Next slides:

- Magnetic energy relaxation,
- current sheets formation,
- mode phase locking,
- excitation of Alfven waves

The typical sawtoothing cycle

F(t)

Mode amplitude bz(a)% m,n

Total MAGNETIC energy

Total KINETIC energy

Magnetic Energy and Helicity dissipation rates

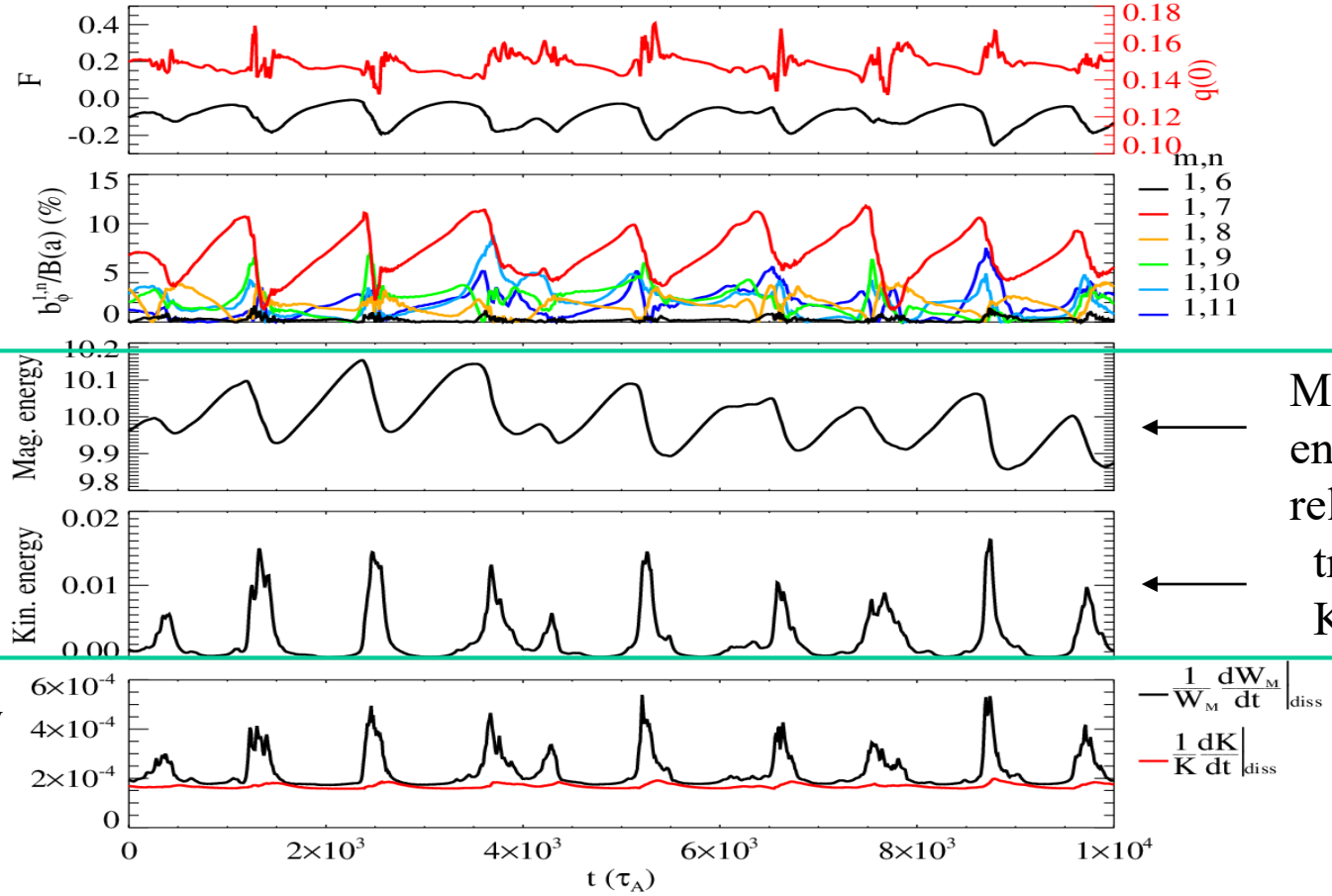

Magnetic energy relaxations transfer to Kinetic one

current sheets formation mode phase locking and excitation of Alfven waves

RFP $S=10^5$, $P=10$

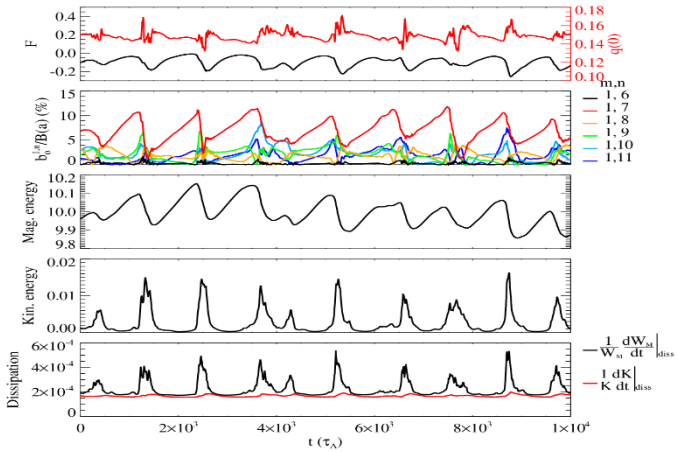

$J \cdot B$

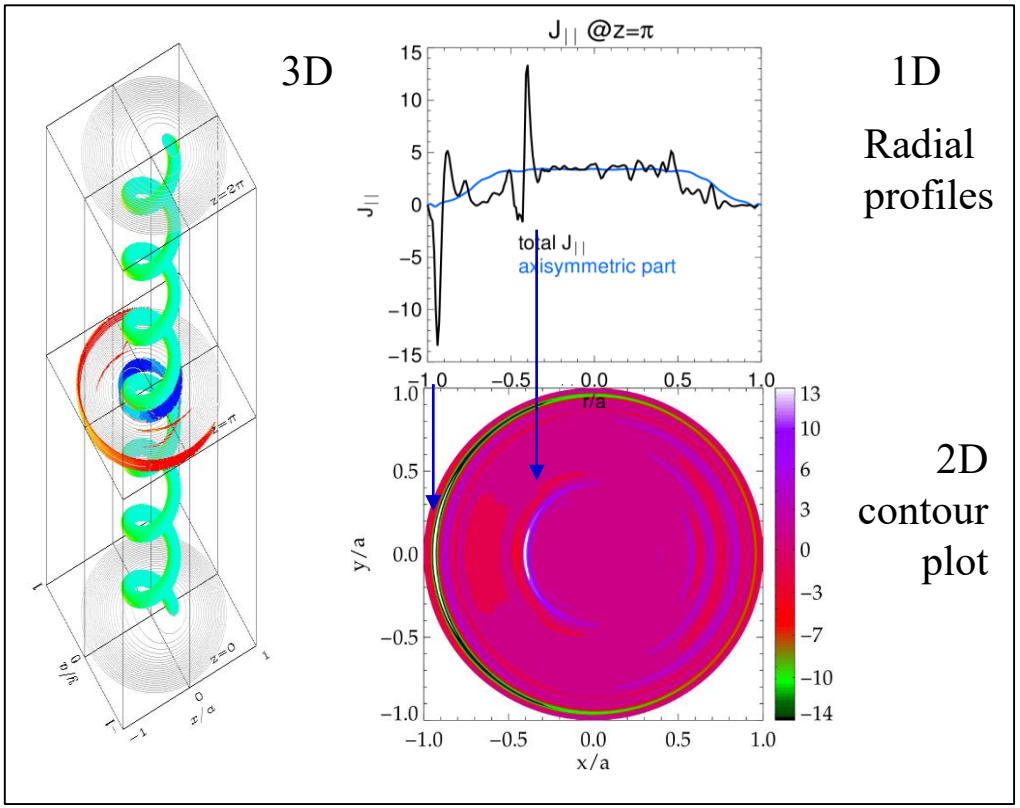

current sheets formation **mode phase locking** and excitation of Alfven waves

RFP $S=10^5$, $P=10$

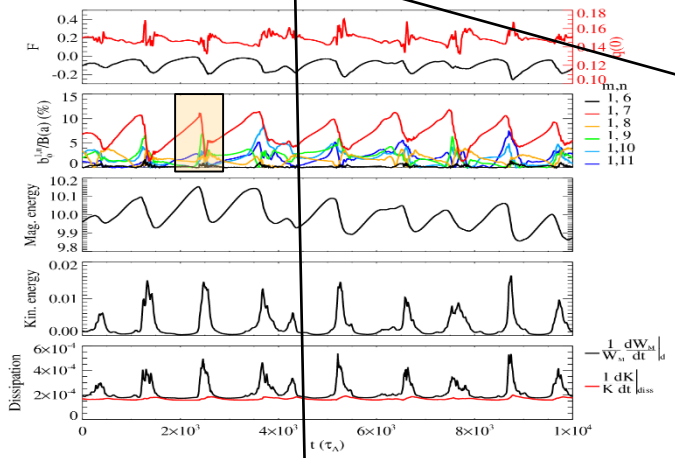

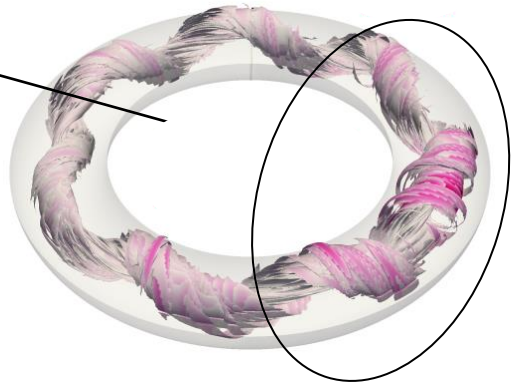

J// contours

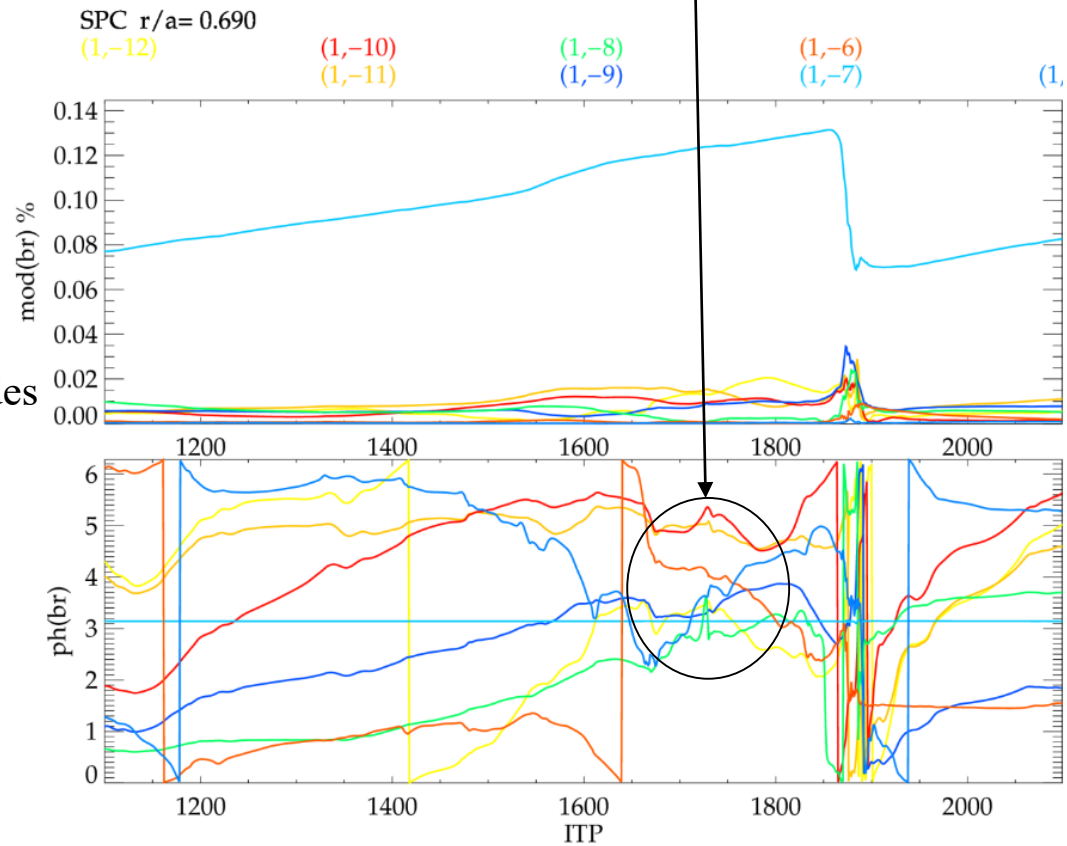

amplitudes

phases

current sheets formation mode phase locking and **excitation of Alfven waves**

RFP $S=10^5$, $P=10$

RFX-mod like density profile assigned

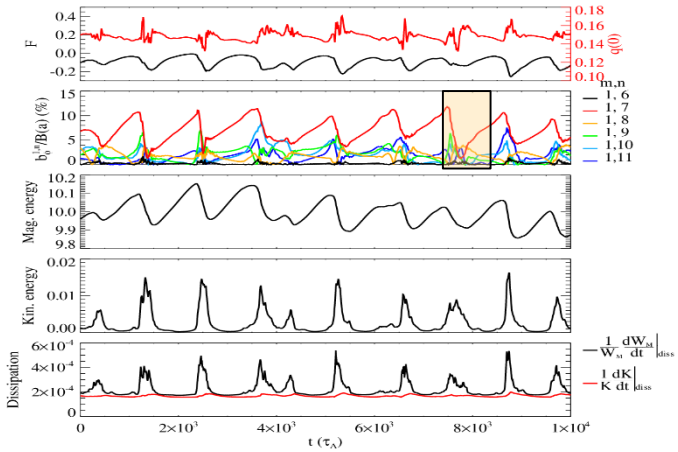

Poster session #1: 08/10/2019 15-17 pm
P1-10 Kryzhanovskyy Artur Alfvén waves in nonlinear 3D MHD modelling of RFP plasmas

Alfvén Eigenmodes (in particular the GAE and the 1st CAE) are excited by magnetic reconnection event.

Alfvén waves spectrum
(m=1, n=0) r= 0,6a

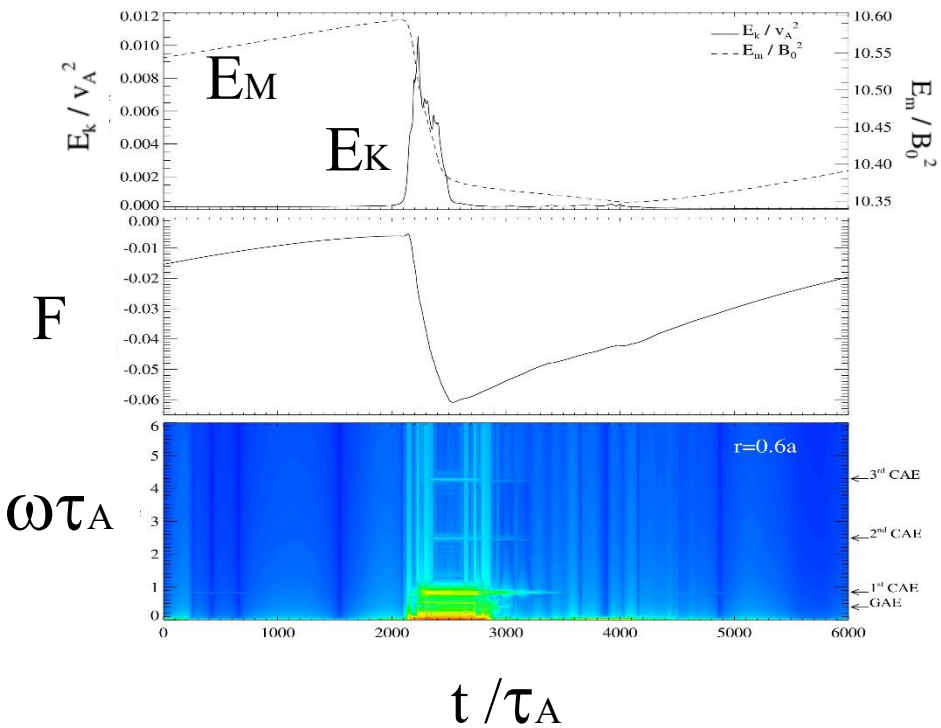

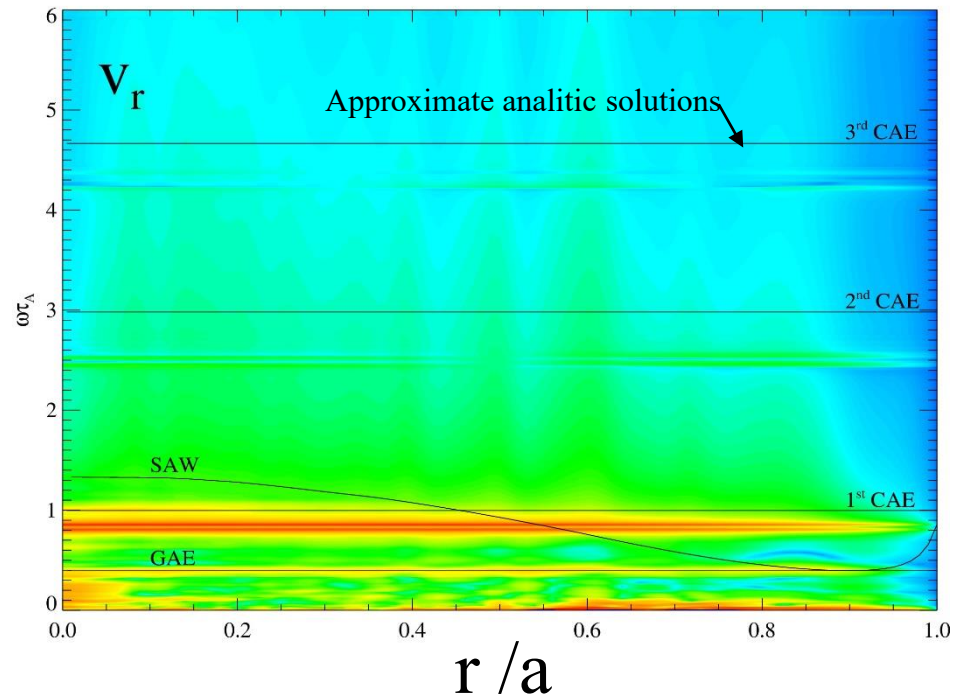

Artur Kryzhanovskyy - Master Thesis 2018 - PhD work

Experimentally observed in RFPs:
Spagnolo NF 2011 and therein refs, Koliner PRL 2012

Back to Chaos healing effect due to helical structure

… when we excite via suitable MP a Non-Resonant helical regime

We started to develop:
numerical tools to detect Lagrangian Coherent Structures able to confine magnetic filed lines

Borrowed from ordinary fluid context

(spreading of "passive" entities: pollution, contaminants, pollen, …)

Collaboration with Grasso (CNR – ISC Torino, PoliTO), Pegoraro (Pisa Univesity), Borgogno (PoliTO Torino), Rubino (ENEA-Frascati)

Lagrangian Coherent Structures detection tool

Confining magnetic structures may exist hidden in the chaotic sea surrounding the conserved magnetic surfaces (KAM), “remnant” structures: small leakage Cantor sets.

Lagrangian Coherent Structures: coherent patterns that organize the transport of field lines, provide a signature of Cantor sets.

Two techniques have been developed and compared for our cases:

- FTLE “ridges” *[Shadden et al 2005 Physica D 212]*
- “most repelling structures” *[Haller, Yuan Physica D 2000 Haller Annu. Rev. Fluid Mech. 2015]*

Rubino, Borgogno, Veranda et al PPCF 2015
Di Giannatale Falessi Grasso Pegoraro Schep, PoP2018 a,b
Di Giannatale, Falessi, Grasso et al, Varenna Lausanne Fusion Theory Conference, Journal of Physics: Conf. Series 2018
Pegoraro et al PPCF 2019
Di Giannatale PhD Thesis 2019
Veranda, Bonfiglio, Cappello, DiGiannatale, Escande to appear in NF 2019

Lagrangian coherent structures **detected** nearby conserved surfaces

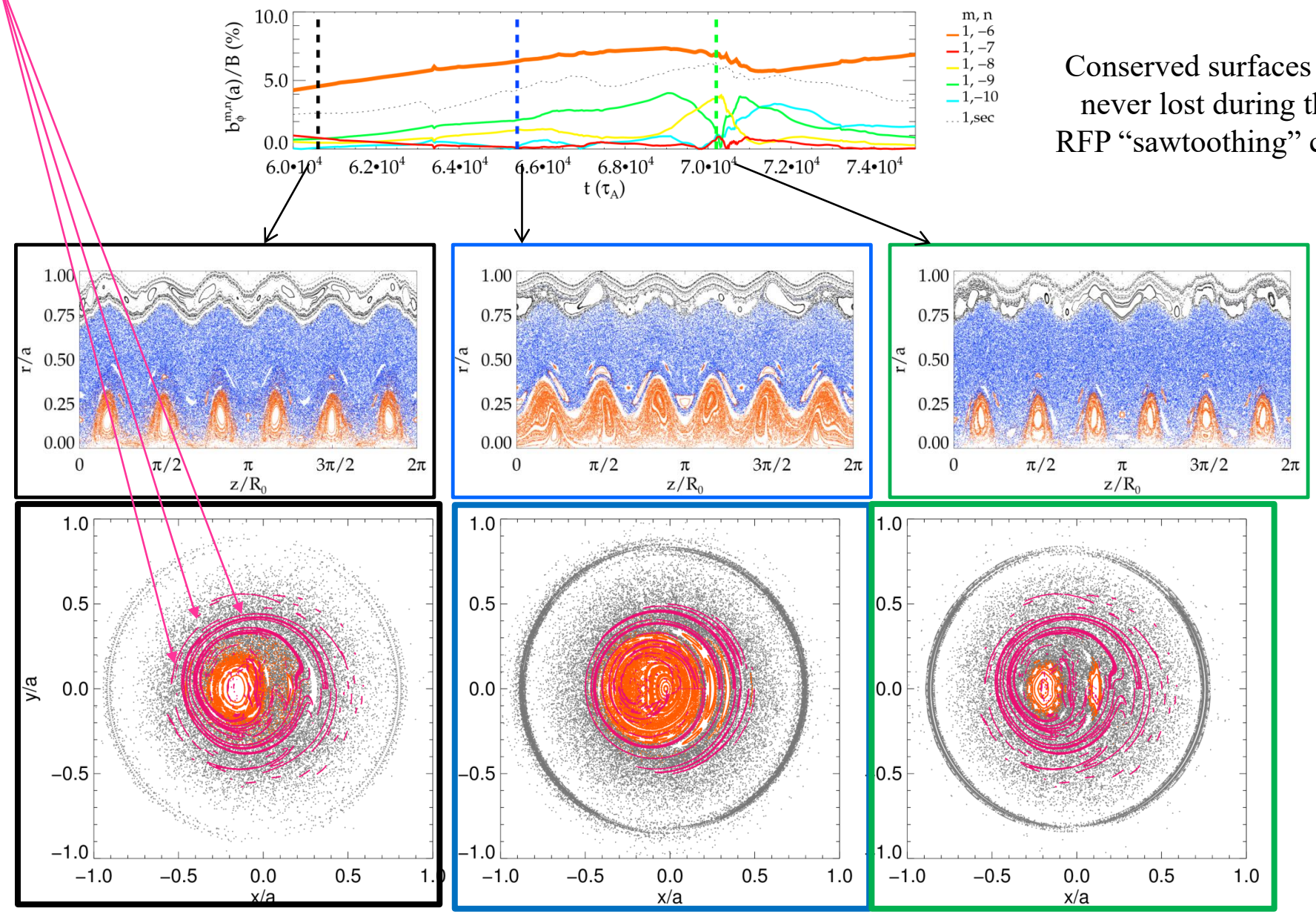

Conserved surfaces are never lost during the RFP "sawtoothing" cycle

The possibility to convey the experimental discharge toward a “new” chosen helical solution exploiting suitable MPs, in particular, low n non resonant helix, has been tested in RFX-mod ..

Dynamics successfully confirmed in RFX-mod experiment

Small edge Magnetic Perturbations (MP) **can drive new helical regimes**, with different pitch:

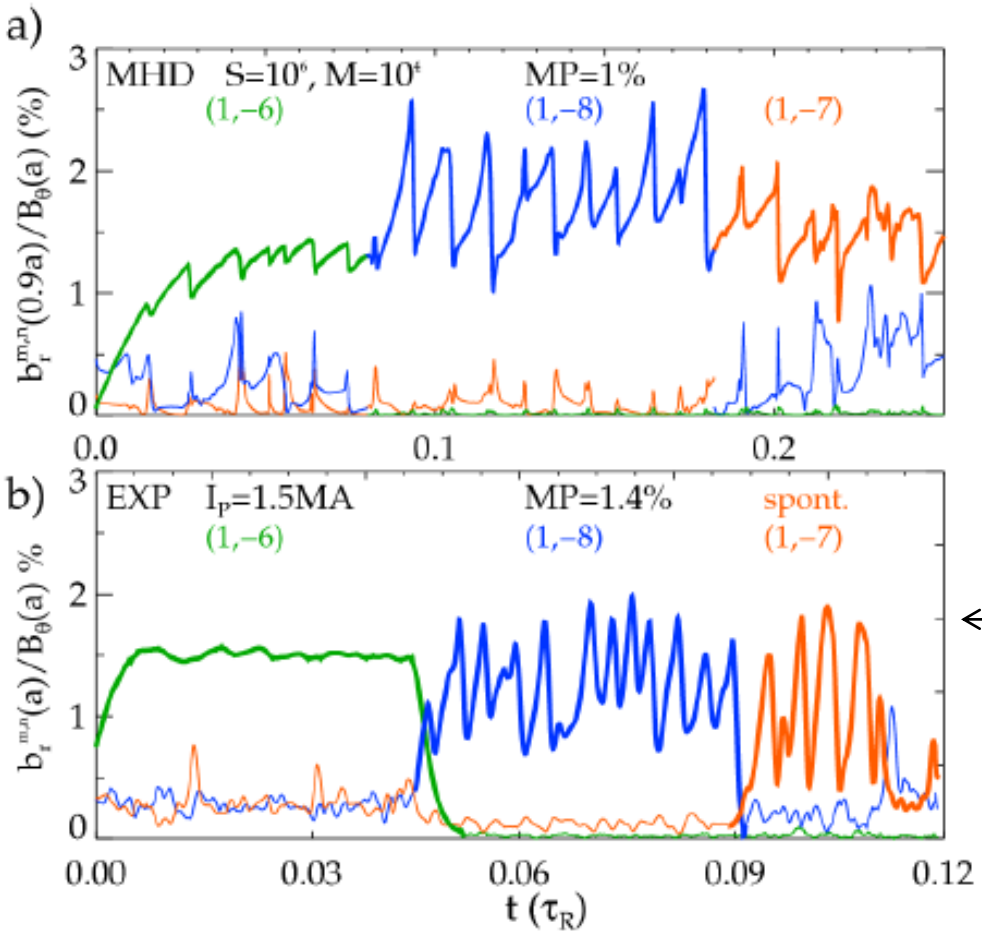

simulation

Successful RFX-mod experiments:
alternative *n*s stimulated by seed MP

Veranda, Bonfiglio, Cappello et al NF 2017

Summary

Helical self-organization characterizes the Reversed Field Pinch:

- Experiments show formation of thermal and impurity particle barriers,
- 3D MHD shows magnetic chaos healing and hidden coherent structures

(Lagrangian Coherent Structures LCS),

- New global helical regimes stimulated by seed Magnetic Pertubations,
  - ✓ Characterized by tunable amplitude and frequency of «sawtoothing»,
  - ✓ Suggested by MHD and obtained in RFX-mod,
  - ✓ 3DMHD Non resonant modes provide more efficient chaos healing

Await for further experiments in RFX-mod**2** from 2021

Where we expect lower secondary modes,
due to closer conductive shell and more effective feedback coils action.

Dissipation & MP sawtoothing
-RFP, and
-Tokamak

MPs lead to steady helical saturation in RFP

Similar to the ones obtained at high dissipation

Veranda PPCF 2013
Bonfiglio PPCF 2015

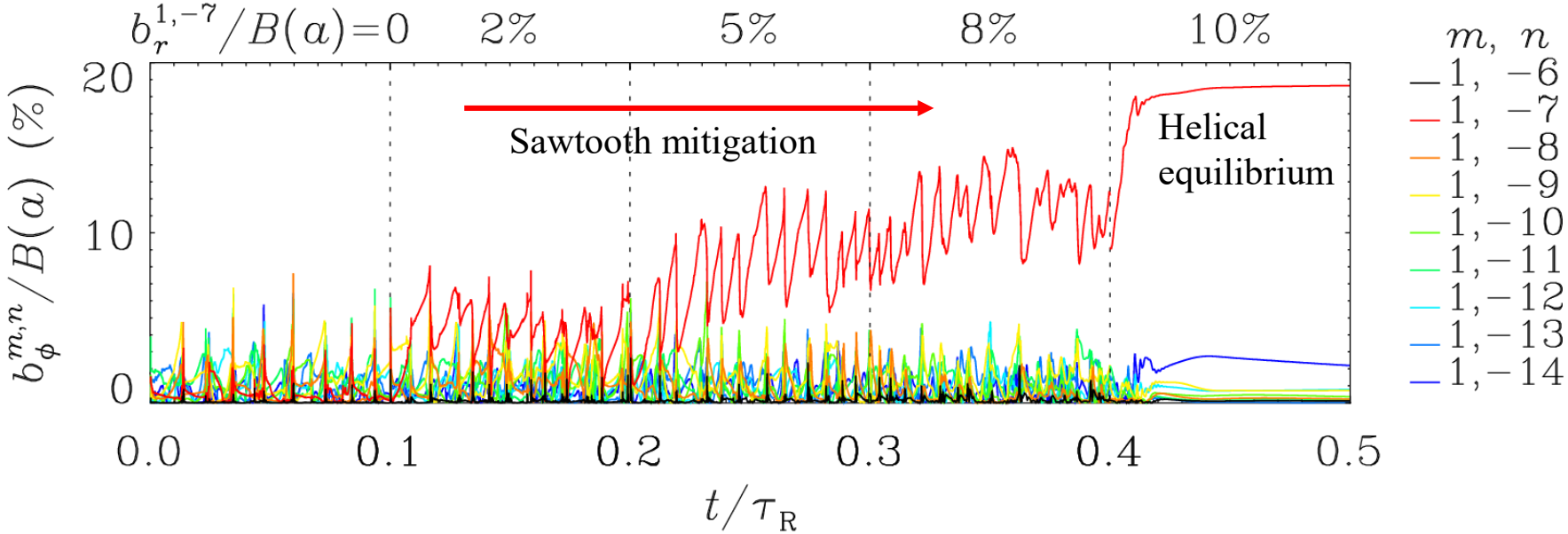

… to be explored in experiments

Circular tokamak in viscoresistive SpeCyl simulations: periodic sawtoothing (**low dissipation**)

snake (**high dissipation**)

Bonfiglio PoP 2010

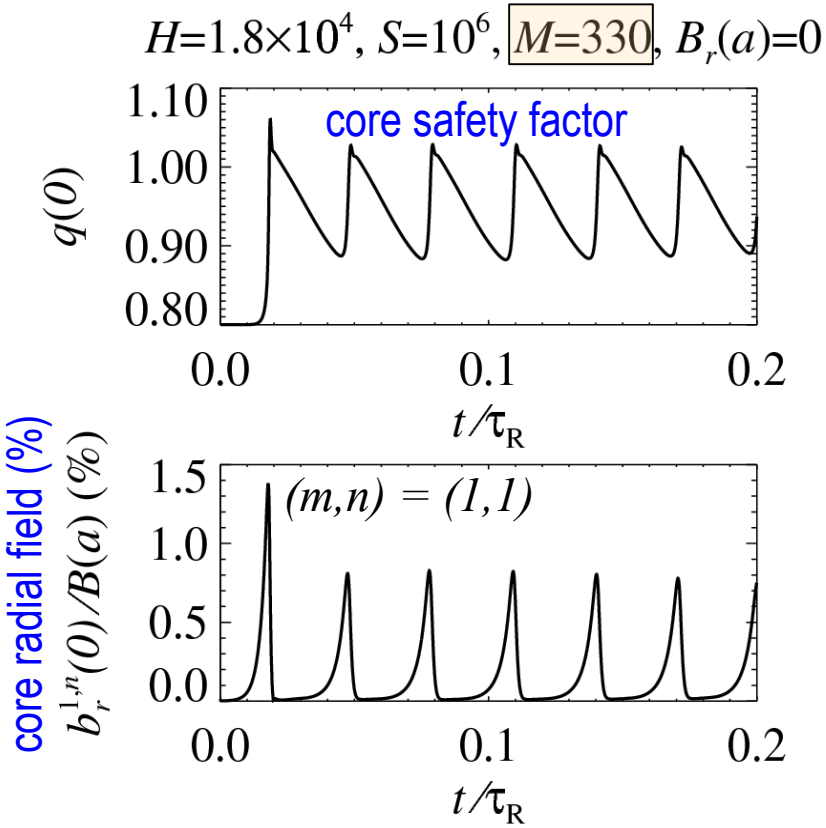

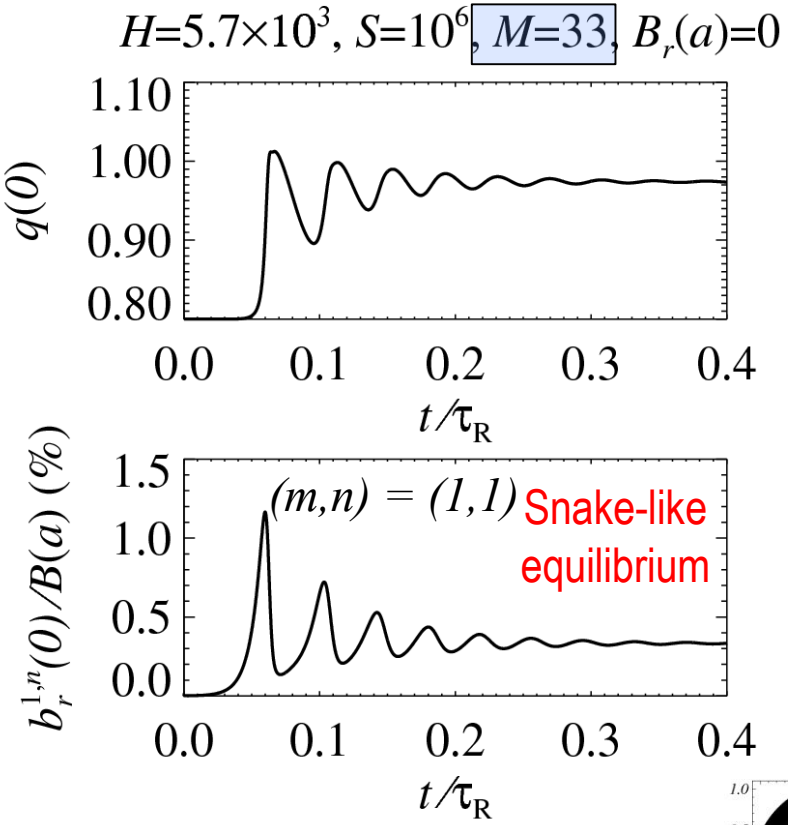

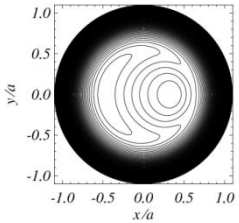

Circular tokamak in viscoresistive SpeCyl simulations: + MP (1,1) periodic sawtoothing (low dissipation) approaching snake (same dissipation but MP applied)

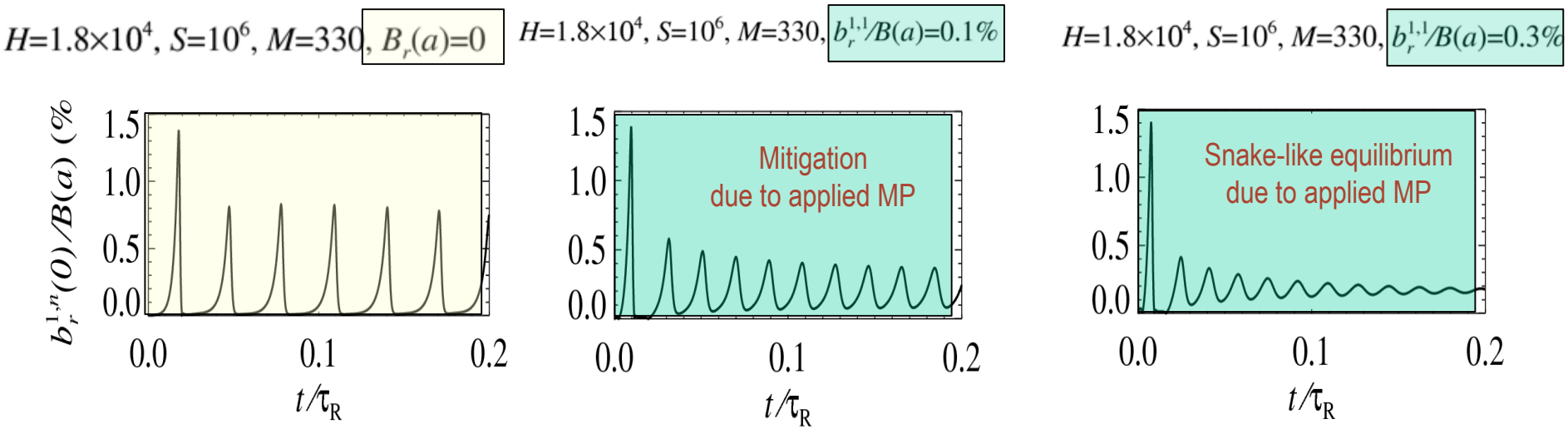

Dissipation & MP produce similar dynamical effects as in RFP

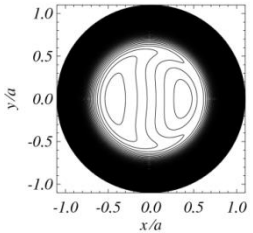

Bonfiglio, Escande , Zanca, Cappello NF 2011
Veranda, Bonfiglio Cappello et al EPS 2012
Bonfiglio, Veranda , Cappello et al PPCF 2015

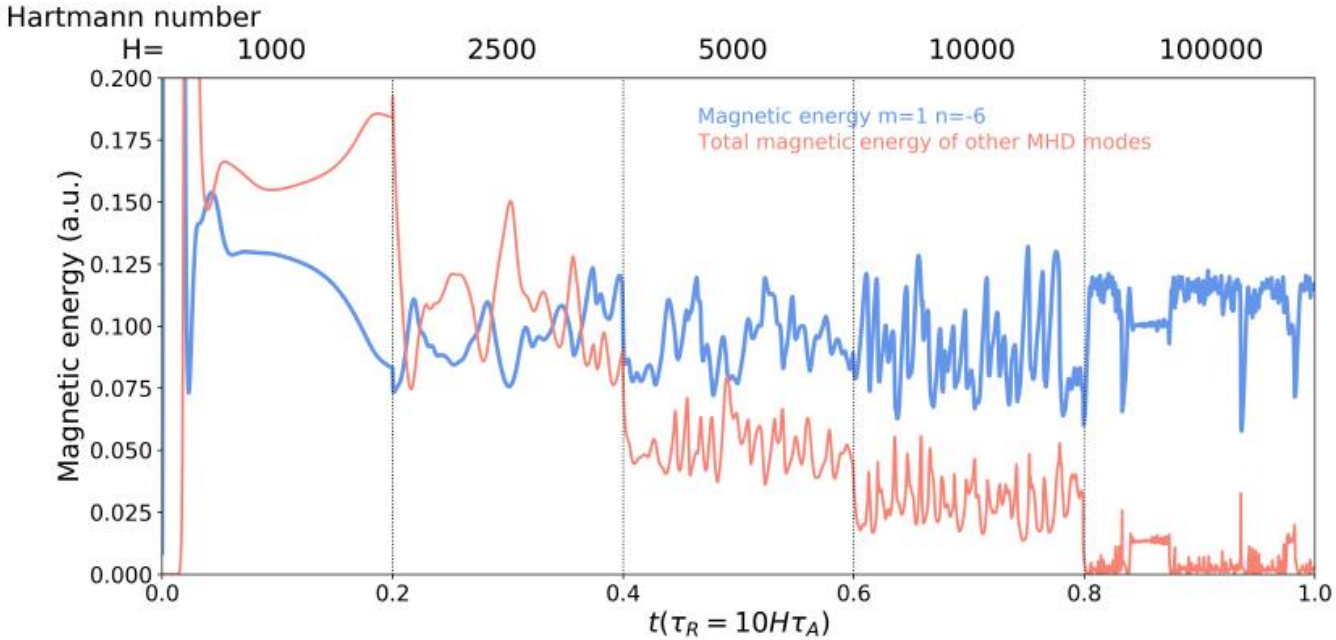

Figure 4. In 3D nonlinear MHD simulations quasi helical states with a chosen helical twist ($h = 6$ in this case) can emerge only with MP and at low dissipation. This explains the experimental observation from RFP experiments: there, QSH are observed only when plasma current is increased. In this simulation S and M vary, with constant $P = S/M = 10^2$. We also have $S = P^{1/2}H = 10H$.

$MP\_{}_{1,6} = 4\%$

Veranda et al to appear in Nuclear Fusion 2019

RFX device evolution: plasma radius and magnetic front-end

				Shell proximity
(1992 1999)	RFX	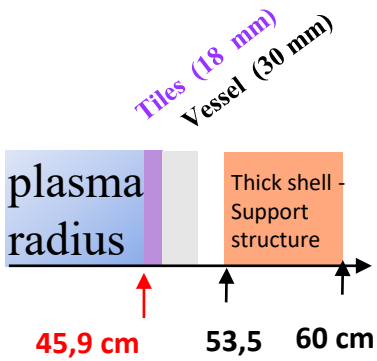	**Thick shell**	b/a = 1.17
(2004 2015)	RFX-mod	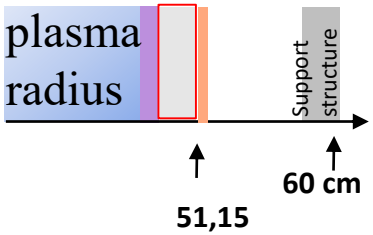	thin shell + control coils	b/a = 1.11
start 2021…	RFX-mod**2**	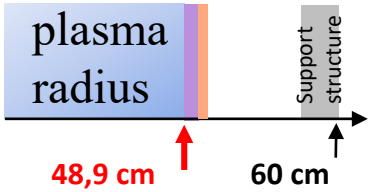	**Removed original vacuum vessel**	b/a = **1.04**

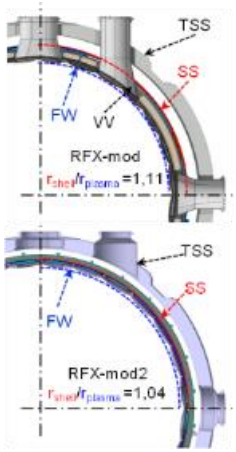

r_saddle sensors = .5065

r_sadle coils = .5815

r_pick_up coils = .510

Bondary conditions SpeCyl, several options:

"typical" boundary conditions for mean fields B o,o:

- B'z =0 (**constant magnetic flux Φ**)
- Constant Ez (or **constant total toroidal current Iz**)
  - Ideal boundary
  - With MP on B r m,n (~ 2%, 4 %...)
  - Thin shell + vacuum layer
- velocity field: no slip.

For $b_{m,n}$

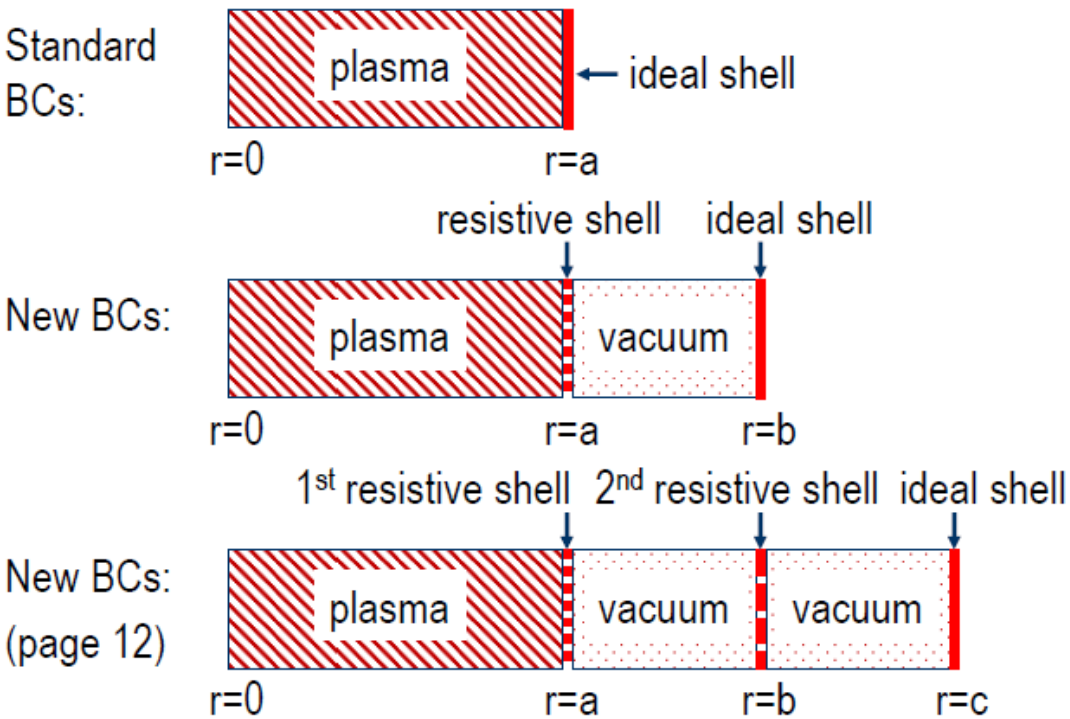

[1] S. Cappello and D.F. Escande, Phys. Rev. Lett **85**, 3838 (2000)
[2] R. Lorenzini, et al., Nature Physics **5**, 570 (2009); J.S. Sarff, et al., Nucl. Fusion **53**, 104017 (2013)
[3] D. Bonfiglio, M. Veranda, S. Cappello, et al., Phys. Rev. Lett **111**, 085002 (2013)
[4] M. Veranda, D. Bonfiglio, S. Cappello, et al., Nucl. Fusion **57**, 116029 (2017)
[5] L. Marrelli, R. Cavazzana, et al., Nucl. Fusion **59**, 076027 (2019)
[6] S. Cappello and D. Biskamp, Nucl. Fusion **36**, 571 (1996)
[7] D. Bonfiglio, L. Chacón, and S. Cappello, Phys. Plasmas **17**, 082501 (2010)
[8] T. C. Hender, C. G. Gimblett, and D. C. Robinson, Nucl. Fusion **29**, 1279 (1989)
[9] D. Schnack and S. Ortolani, Nucl. Fusion **30**, 277 (1990); R. Paccagnella et al., Nucl. Fusion **47**, 990 (2007)

First implementation of the technique to identify ridges

- simulation case (schematic one):

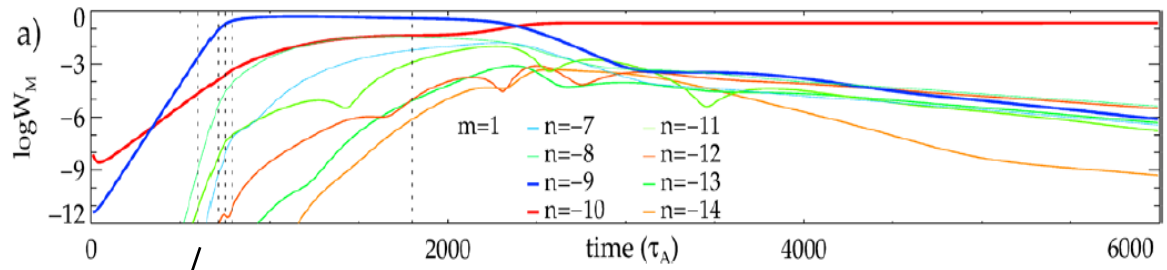

- Poincare' plot: developing chaos

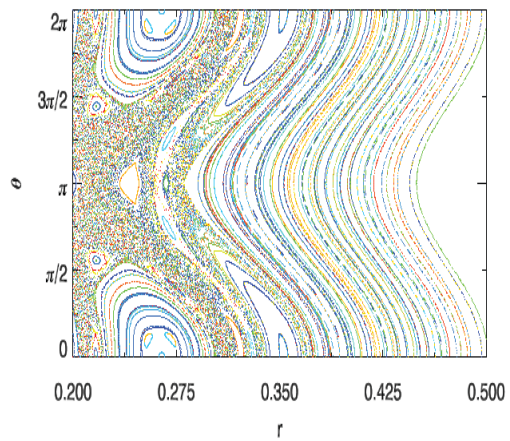

(integration length order of 1000 toroidal turns)

*[Rubino, Borgogno, Veranda, Bonfiglio, Cappello, Grasso **PPCF (2015)**]*

First implementation of the technique to identify ridges

- simulation case (schematic one):

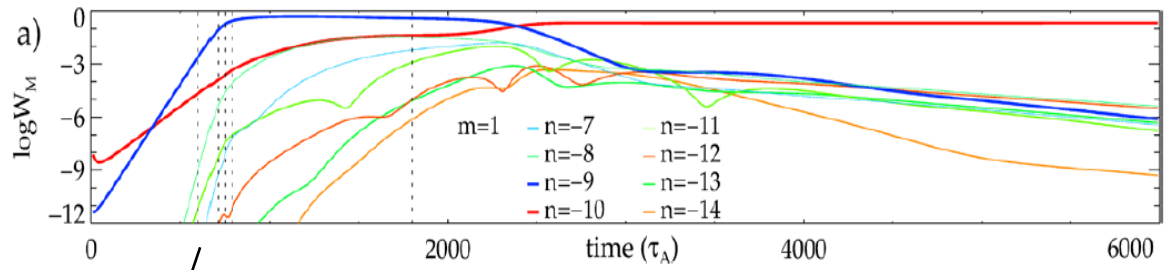

- Poincare' plot: developing chaos

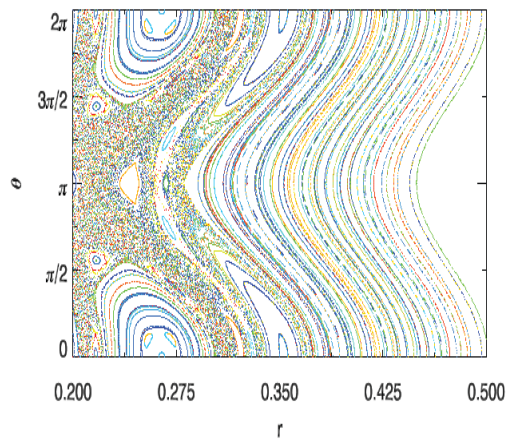

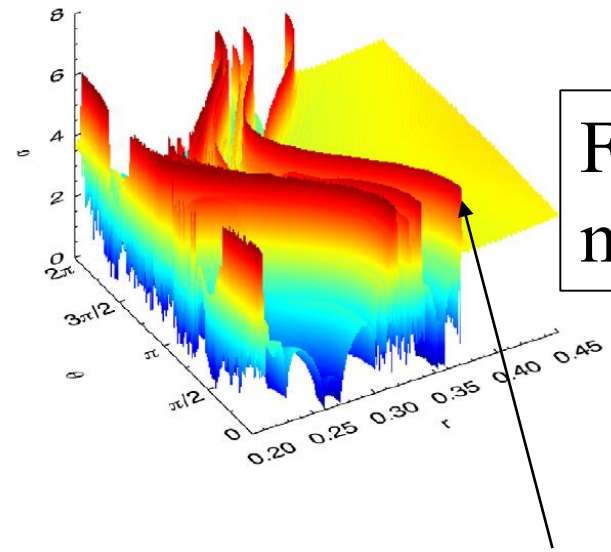

FTLE map

(integration length order of 1000 toroidal turns)

- Algorithm to extract extrema, which identify the ridges …

*[Rubino, Borgogno, Veranda, Bonfiglio, Cappello, Grasso **PPCF (2015)**]*

"Ridges": barriers to the transport of magnetic field lines

Black "curves": RIDGES

Color: magnetic field lines integrated for 100 toroidal turns

(>> FTLE computation time = 10 toroidal turns)

Ridges detect confining cantori structures

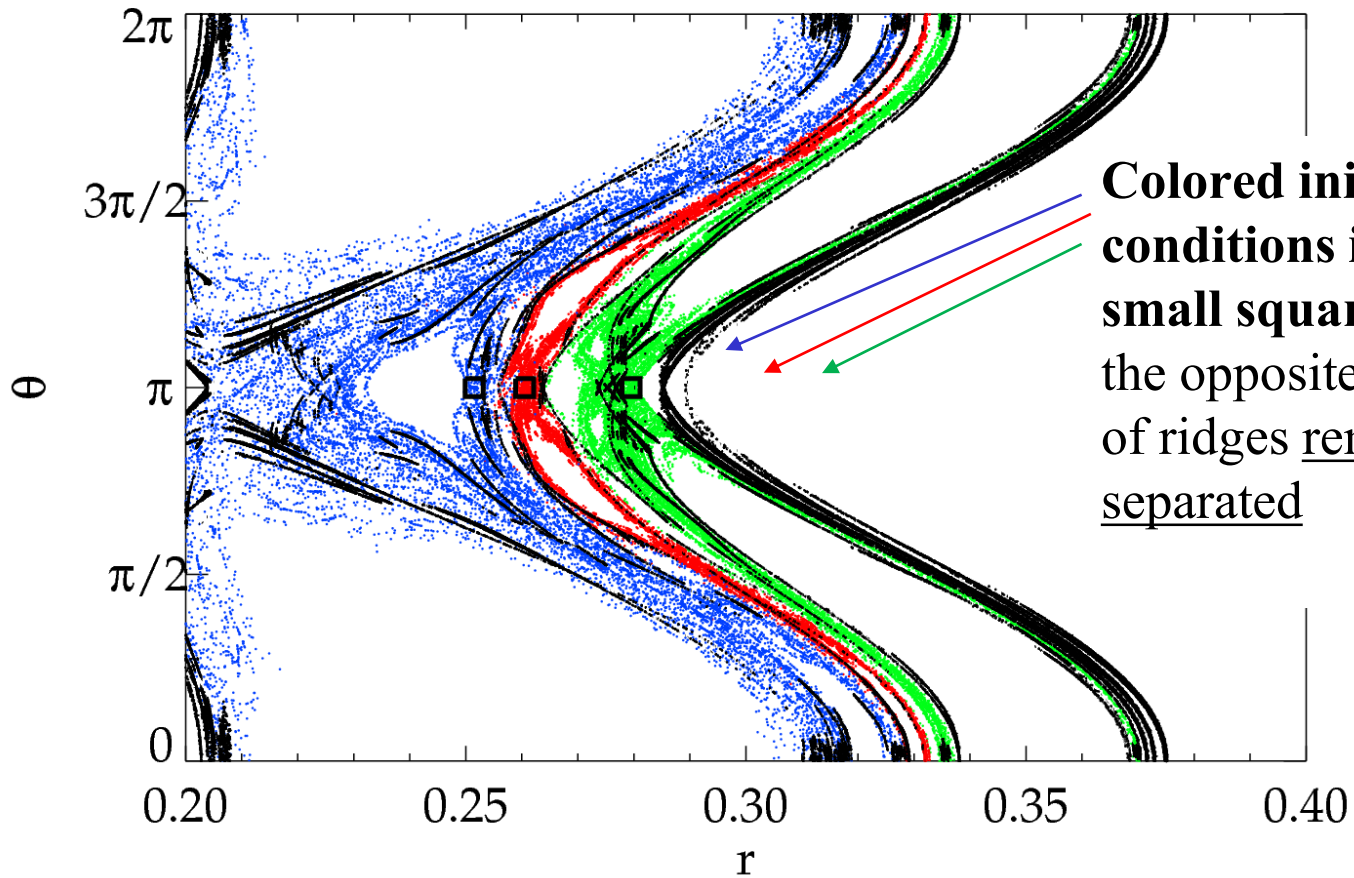

Colored initial conditions in the small squares at the opposite side of ridges remain separated

LCS (Haller) and "Ridges" (Shadden) techniques comparison:

No significant differences in our cases:

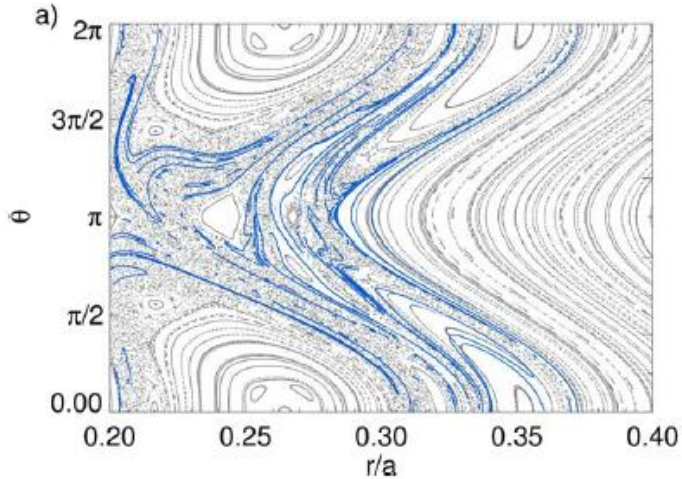

Figure 2. Poincaré map and Lagrangian coherent structures (LCS) of the magnetic configuration corresponding to the snapshot taken at $t = 600\ \tau_A$, i.e. before the formation of the quasi-helical state. LCS are overplotted in blue. In this picture we show only the relevant radial region around the $m = 1$, $n = 9$ helical core (at $r = 0.26a$, $\theta = 0$), where a weakly chaotic magnetic field is present.

Plasma Phys. Control. Fusion **61** (2019) 044003

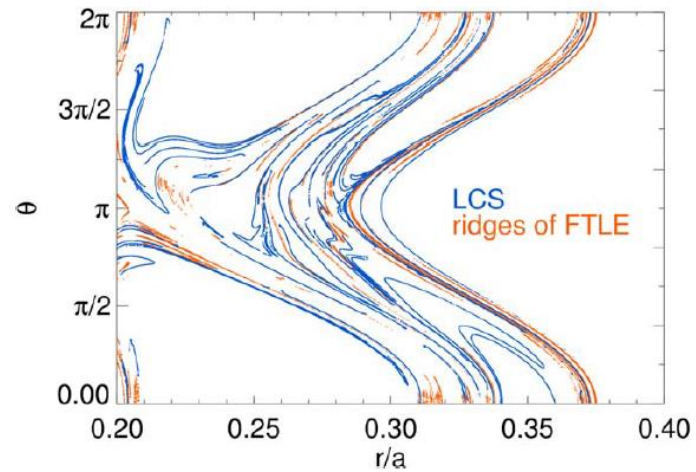

Figure 4. Comparison between the structure of repelling LCS in blue (the same as the ones in figure 3) and the ridges of the finite time Lyapunov exponents (FTLE) in orange (same as computed in figure 7 of [46]). They are qualitatively similar but LCS offer the deepest insight of the topological structure of coherent structures.

Pegoraro F., Bonfiglio, Cappello, Di Giannatale, Falessi, Grasso, Veranda, PPCF (2019)

Lagrangian Coherent Structure (LCS)

- What:
  - In a 2D configuration are material lines advected by the fluid which organize the flow transport processes by attracting or repelling the nearby elements

- use
  - LCSs divide the phase space in regions that cannot exchange particles under the finite time considered ($t-t_0$)

Two different definitions:

1) LCSs as ridges of FTLE field. Ref Shadden et all 2005. Physica D 212 (3-4), 271{304
2) LCSs as " the most attracting or repelling material lines " Ref G. Haller, A variational theory of hyperbolic Lagrangian coherent structures, Phys. D 240 (7) (2011) 574-598

Implication of Haller's definition: in addition to other requirements, repelling LCS are found integrating the eigenvector field related to minimum eigenvalue of Cauchy-Green (CG) matrix. Such matrix gives indications about how strong and in which direction a blob of initial conditions, namely particles, evolve under the flow map F.

Cauchy-Green matrix $$C(x_0) = \left[\nabla F_{t_0}^{t}(x_0)\right]^T \nabla F_{t_0}^{t}(x_0)$$

A qualitative description

Qualitatively the difference between the two methods stays in the fact that only the second one (Haller's method) assures that the LCS are material lines, that is an invariant curve under the flow, and thus they cannot be crossed by other particles.

Moreover, the Haller's method is "*Lagrangian*": the barriers are found integrating the eigenvectors of the CG strain tensor.

A graphical definition

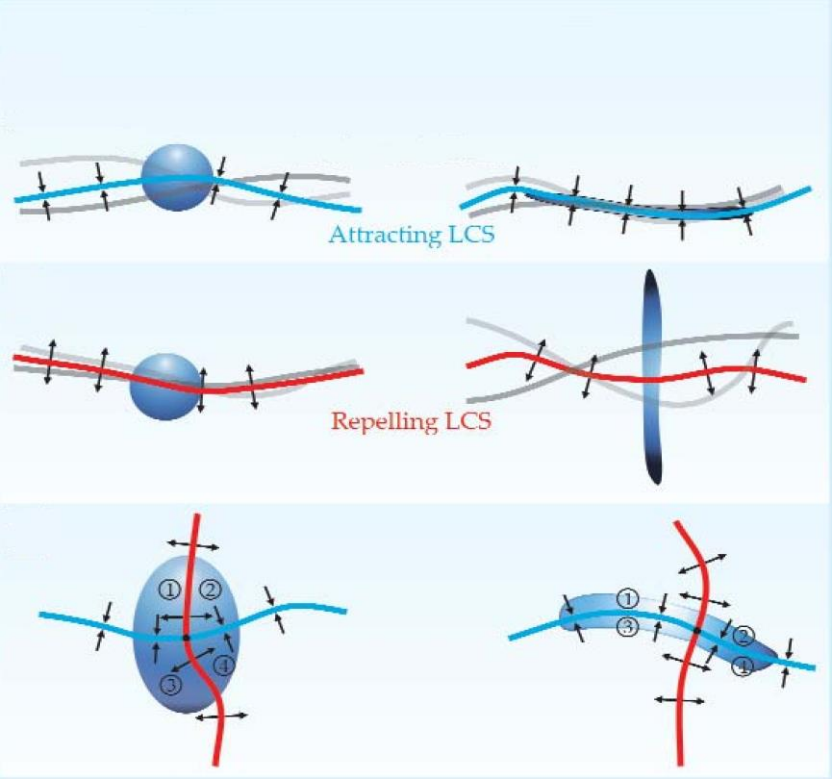

On the opposite, the ridge method only focuses on an analysis point by point (*Eulerian*).

Mathematically speaking:

1) the Haller's method focuses on FTLE and eigenvector of CG matrix.

2) The ridge method only focuses on FTLE and to eigenvectors associated to FTLE Hessian matrix.

RFP Toy model: useful to describe the "slinky -phase locking- effect "

After kinking …

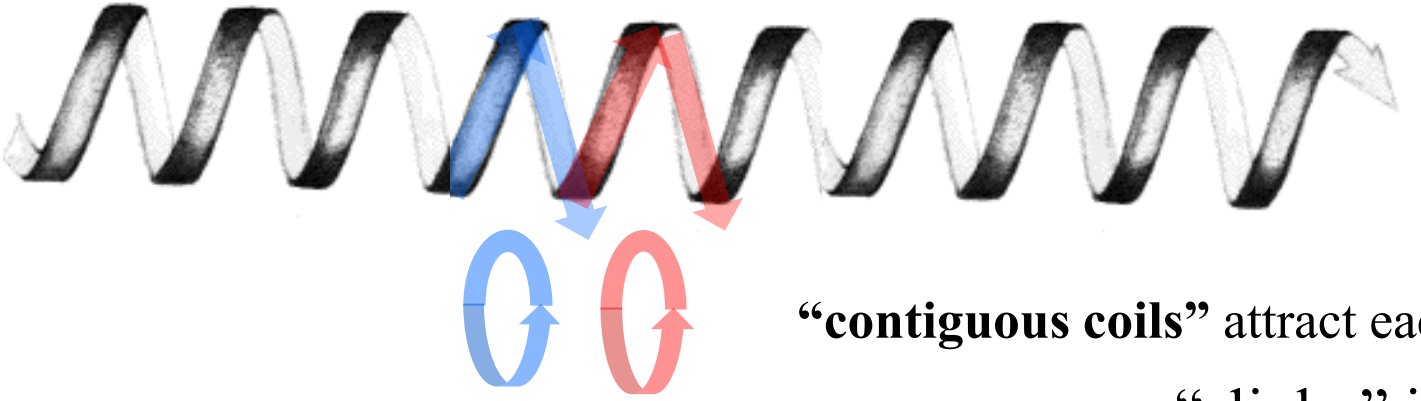

"contiguous coils" attract each other …

…"slinky" instability

… localized collapse

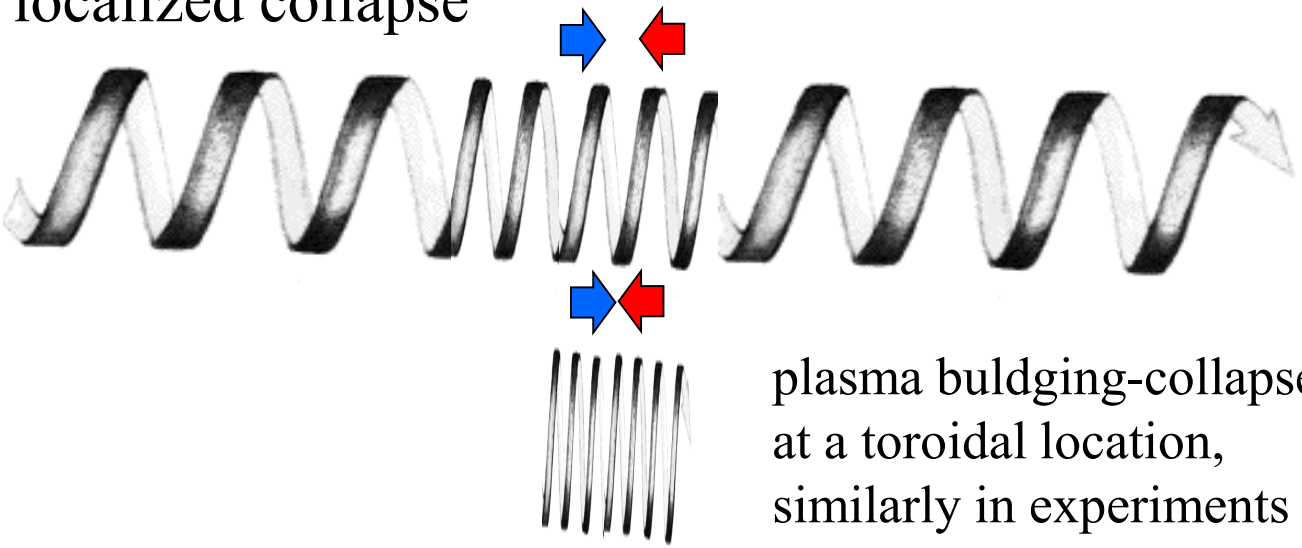

plasma buldging-collapse
at a toroidal location,
similarly in experiments
and nonlinear modeling…

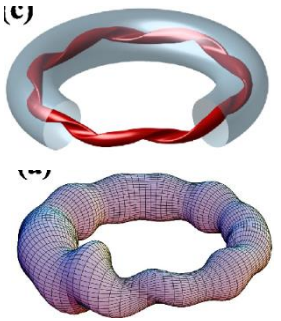

Cappello et al., Theory of Fusion Plasmas - Varenna 2008

When QSH dominant mode GROWS: separatrix expulsion occurs, and

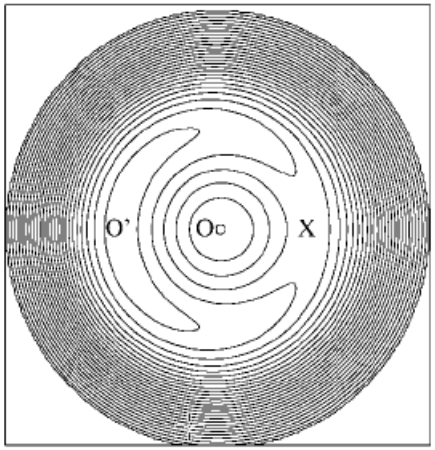

(a)

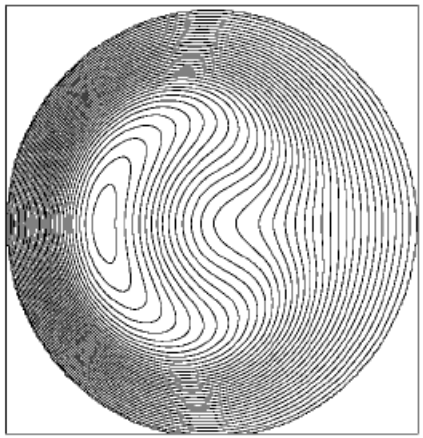

(b)

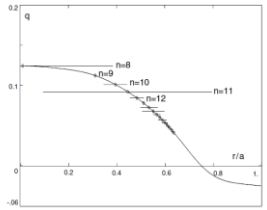

FIG. 2. q profile and magnetic islands width (shown by horizontal bars) of different $m = 1$ modes.

…clean helical topology emerges

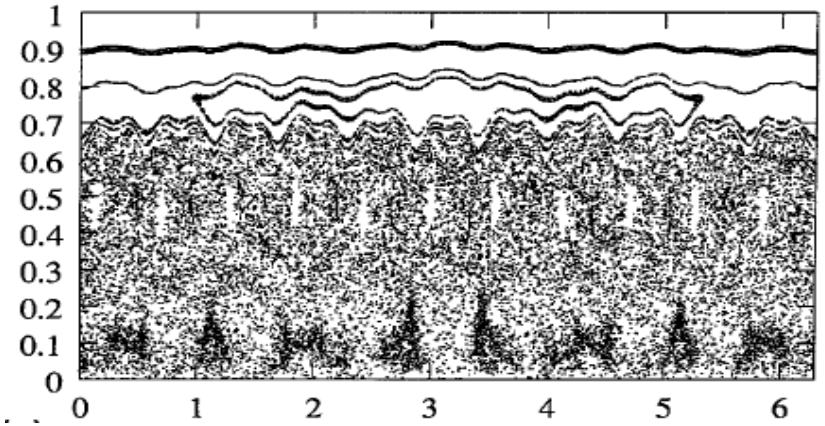

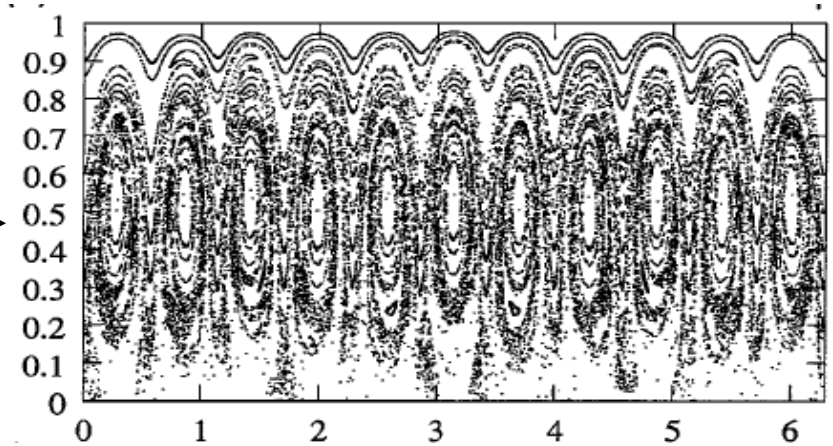

Escande, Paccagnella, Cappello et al PRL 2000

LCS (blue) and Connection length maps

LCS mark radii where large Lc gradients are seen

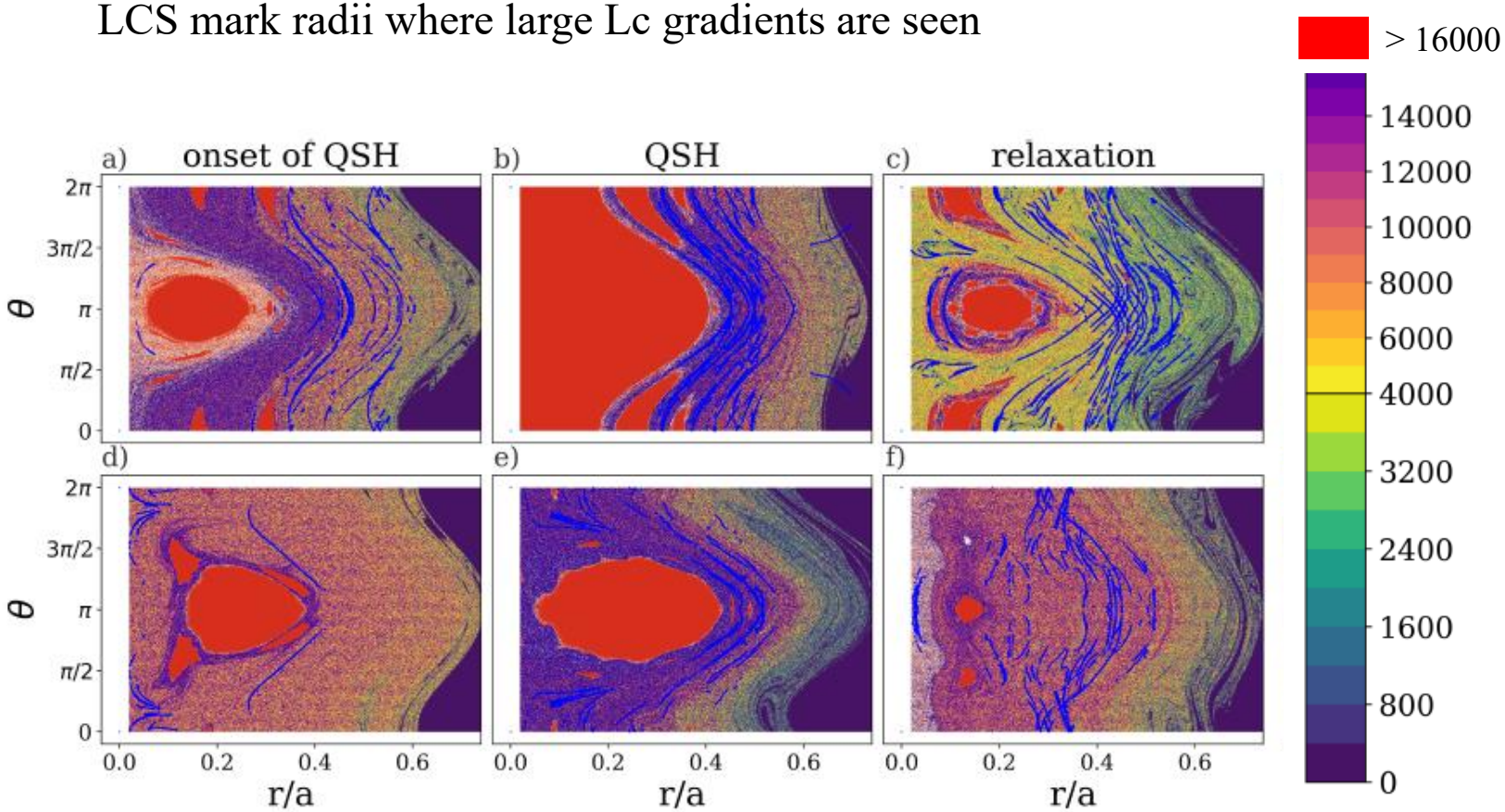

Figure 9. Bundles of Lagrangian Coherent Structures (LCS, blue lines) are a common feature of quasi-helical regimes. We plot the connection length to the edge confining structures of magnetic field lines. In red we color the regions where $L_c = L_{c,max} = 10^5$. The blue LCS divides regions with different connection length.

T_e, n_e get a helical shape - T_e steep gradients …

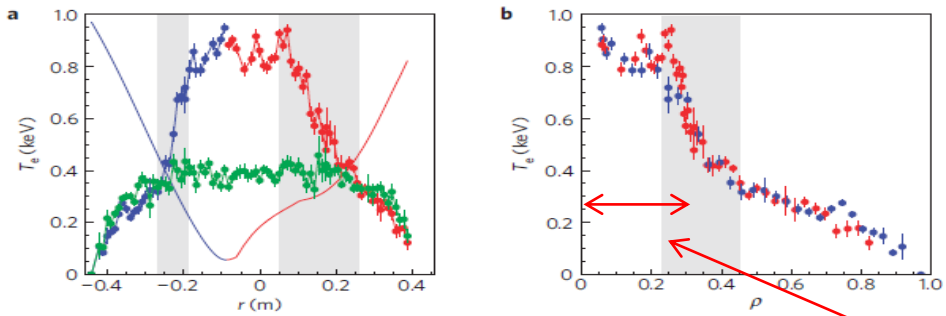

Lorenzini et al NatPhys 2009

… not stationary …
Temporal evolution of thermal structure under investigation

Grad (Te) vs time

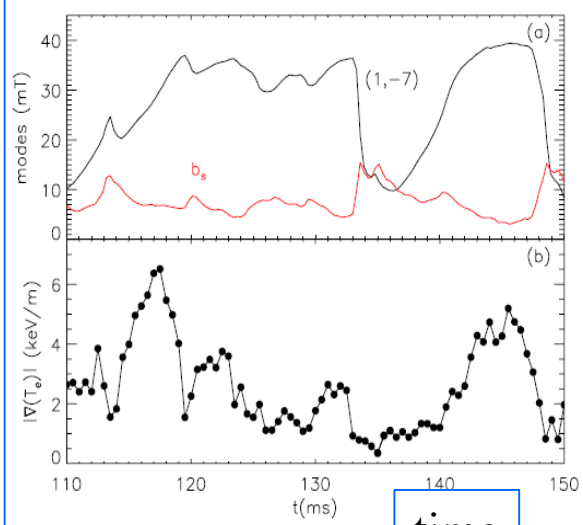

time

Franz et al NF 2013
Gobbin et al PPCF 2013

Thermal structure width: increases with helical amplitude

Secondary modes

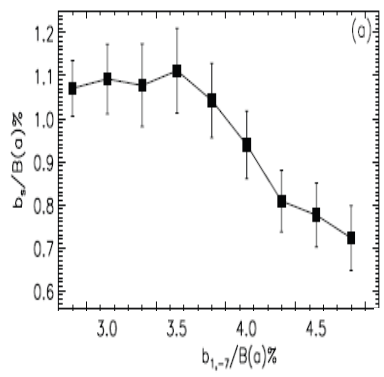

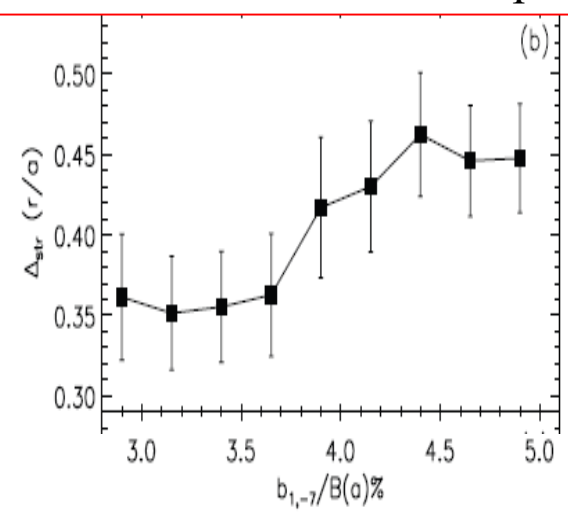

helical mode amplitude

helical mode amplitude

Gobbin et al PPCF 2015

the barrier foot is close to the vanishing magnetic shear location

Helical q: q(ρ) gives the number of toroidal turns field lines perform for one poloidal turn around the helical axis

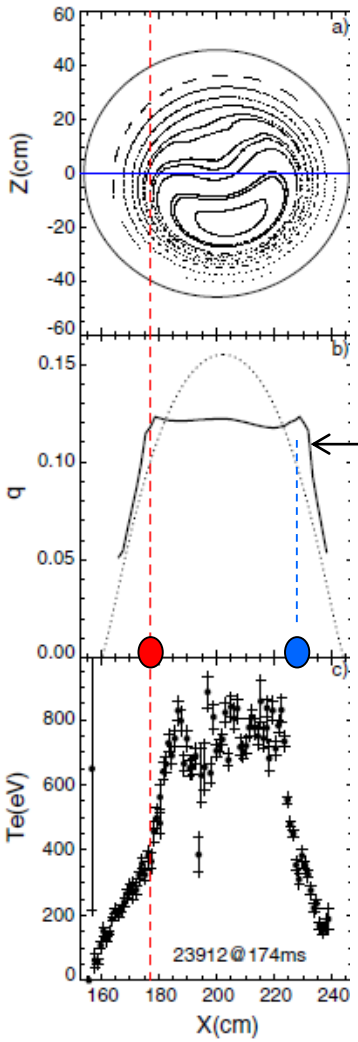

Helical flux surfaces

Helical q

Te

Position of the eITB vs the maximum_q location for RFX-mod experimental SHAx states.

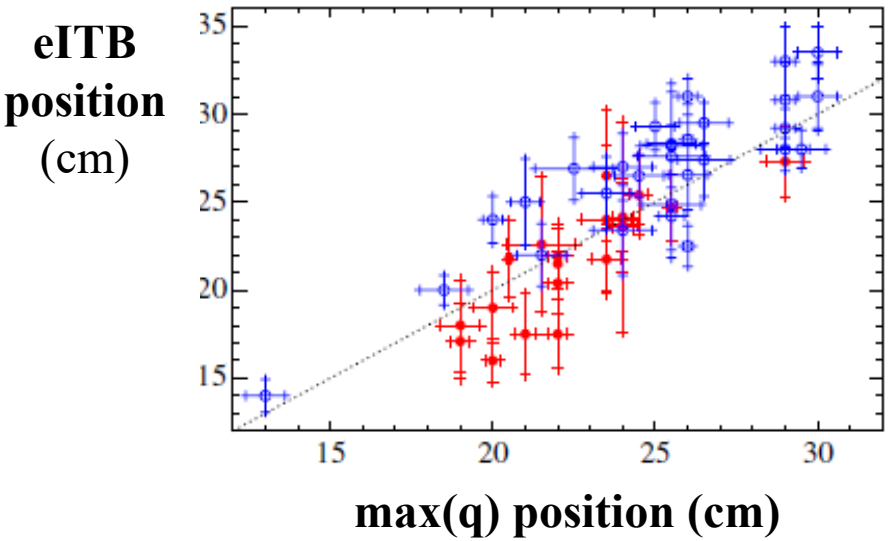

Error bars in the abscissas are due to uncertainties in equilibrium reconstruction.

Gobbin, Bonfiglio, Escande et al PRL 2011

RFP helical self-organization

Isotopic effect: Deuterium discharges

QSH improvement: Persistence & Te

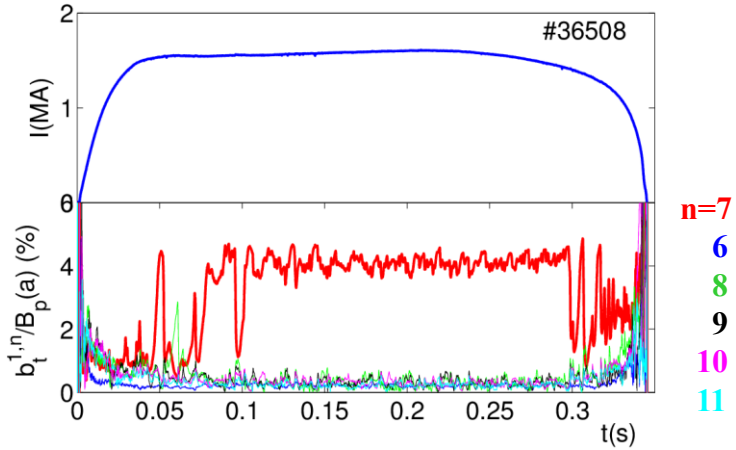

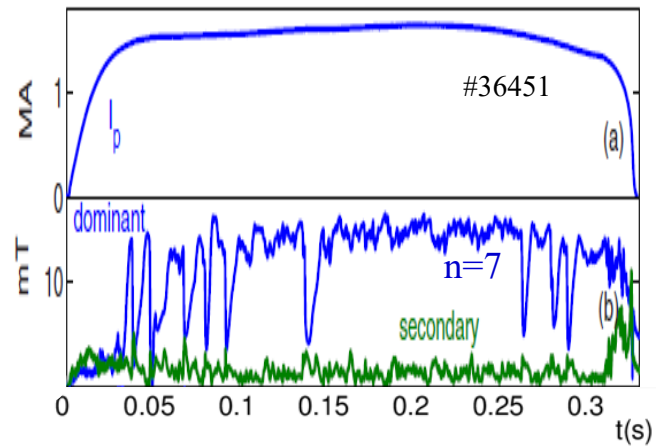

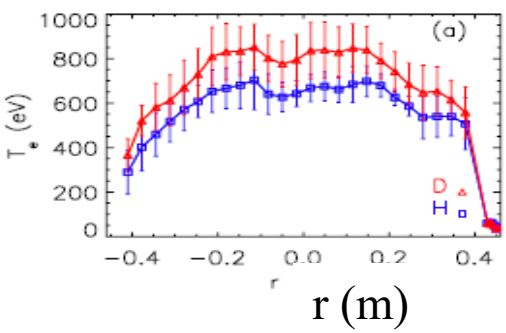

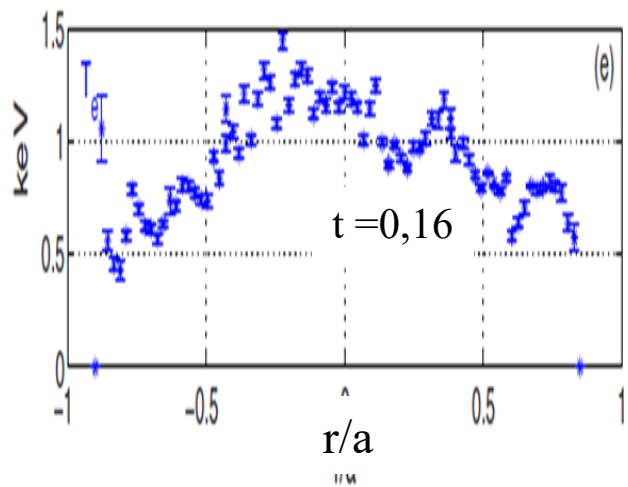

Lorenzini, Agostini, Auriemma et al NF 2015

Puiatti, Dal Bello, Marrelli, et al. NF 2015

Taylor's relaxation theory for the RFP.

Gained quickly an enormous success due to its ability to explain field reversal.

In fact, at the beginning, the solenoidal effect of the toy model appeared too small to provide a convincing explanation…

J. B. Taylor PRL 1974
J. B. Taylor Rev. Mod Phys. 1986

Taylor's relaxation theory for the RFP.

Taylor's conjecture involves
the **Magnetic Helicity** associated with a flux tube

$$K_V = \int_V \mathbf{A} \cdot \mathbf{B} \, d^3x$$

(**A:** vector potential)

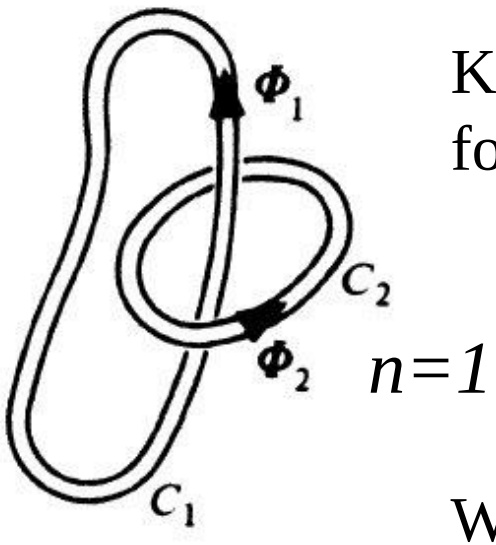

$n=1$

K is related to the topological complexity of B field, for example, for the two flux tubes knotted *n* times:

$$K_V = (+/-) \; n \, \Phi_1 \Phi_2$$

Woltjer theorem (1958) showed that for an ideal plasma (must conserve Kv for any flux tube αi) the minimum energy solution requirement leads to the force free equation

$$\nabla \wedge \mathbf{B} = \alpha_i \, \mathbf{B}$$

Taylor's relaxation theory for the RFP.

Conjecture:
small resistivity allows for total magnetic helicity conservation in a flux conserving volume

search for minimum energy states with constraint on $\mathbf{K_0}$ and $\mathbf{\Phi}$

$$K_0 = \int_{Volume} \mathbf{A} \cdot \mathbf{B}\, d^3x$$

INVARIANT

$$\Phi = \int_S \mathbf{B} \cdot d\mathbf{s}$$

CONSERVED

$$W = \int_{Volume} \frac{\mathbf{B}^2}{2\mu_0} \cdot d^3x$$

(internal energy neglected)

Variational principle (related Euler-Lagrange equation), which ends up to coincide with force free condition:

$$\nabla \wedge \mathbf{B} = \mu \mathbf{B}$$

μ is the Lagrange multiplier determined by the invariants of the problem $\mathbf{K_o}$ and $\mathbf{\Phi}$, in particular :

$$\mu \leftrightarrow \frac{K_0}{\Phi^2}$$

being $\nabla \wedge \mathbf{B} = \mu_o \mathbf{J}$

the useful relation holds:

$$\mu = 2\Theta / a$$

Taylor 1986
Martin Taylor (Culham Rep) 1974

Axisymmetric solutions

Bessel Function Model (BFM)

For $\mu a \geq 2.4$ reversed field B_ϕ

$\Theta \geq 1.2$

compared with experimental measurements

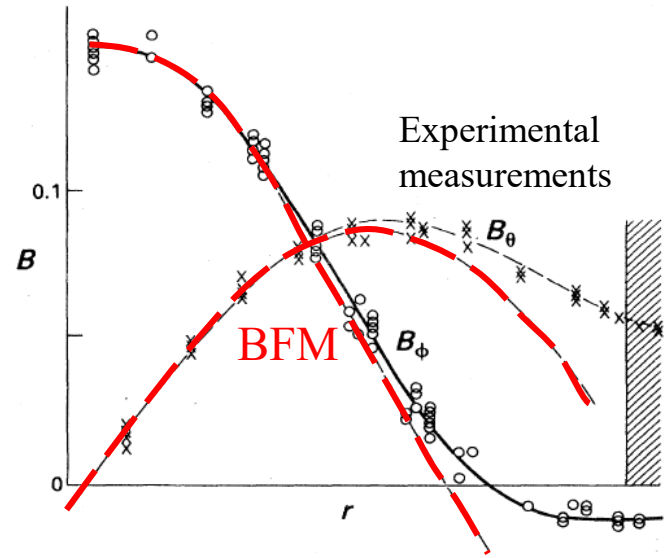

FIG. 2. Experimental and theoretical magnetic field profiles. HBTX-1A (from Bodin, 1984).

Rev. Mod. Phys., Vol. 58, No. 3, July 1986

Helical solutions for $\mu a \geq 3.12$

<u>K_o / Φ^2 determine periodicity and amplitude</u>

while $\mu a \geq 3.12$ remain fixed,

i.e. saturation of the pinch parameter at $\Theta = 1.56$

m=1, n=+5 (R/a=4)
(external helicity)

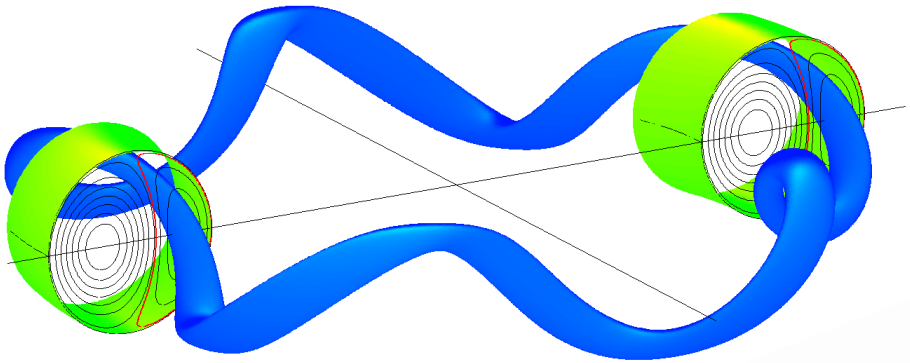

SH solutions are different from Taylor's helical solutions

Helical RFP from 3D MHD

m=1, **n = – 10**

(R/a=4)

(internal helicity)

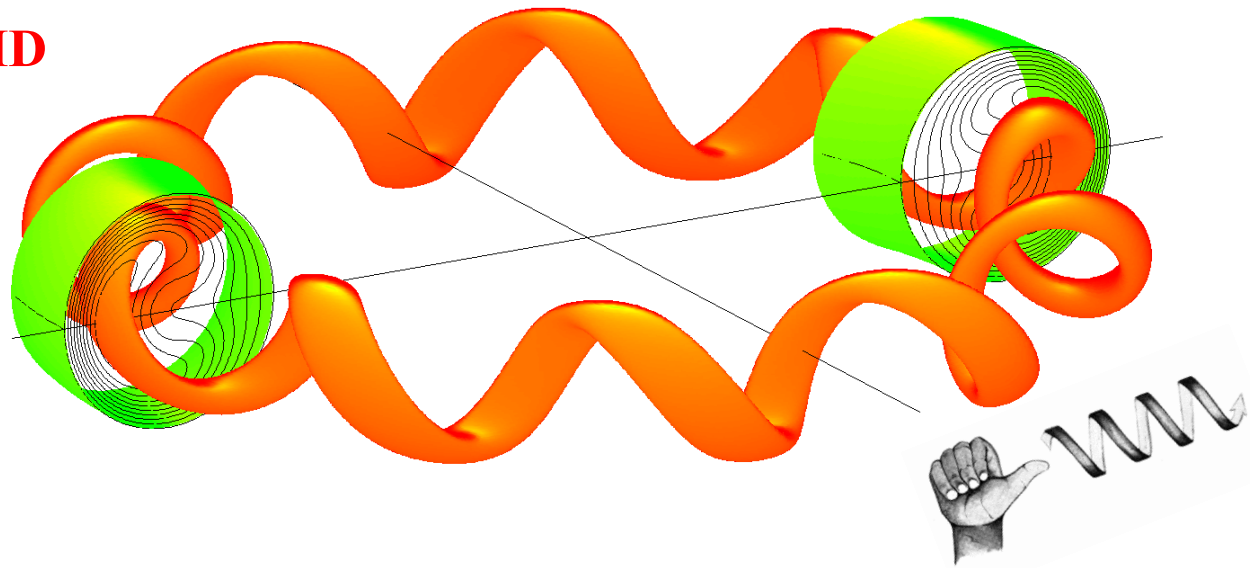

Taylor's helical state

m=1, **n = + 5**

(R/a=4)

(external helicity)

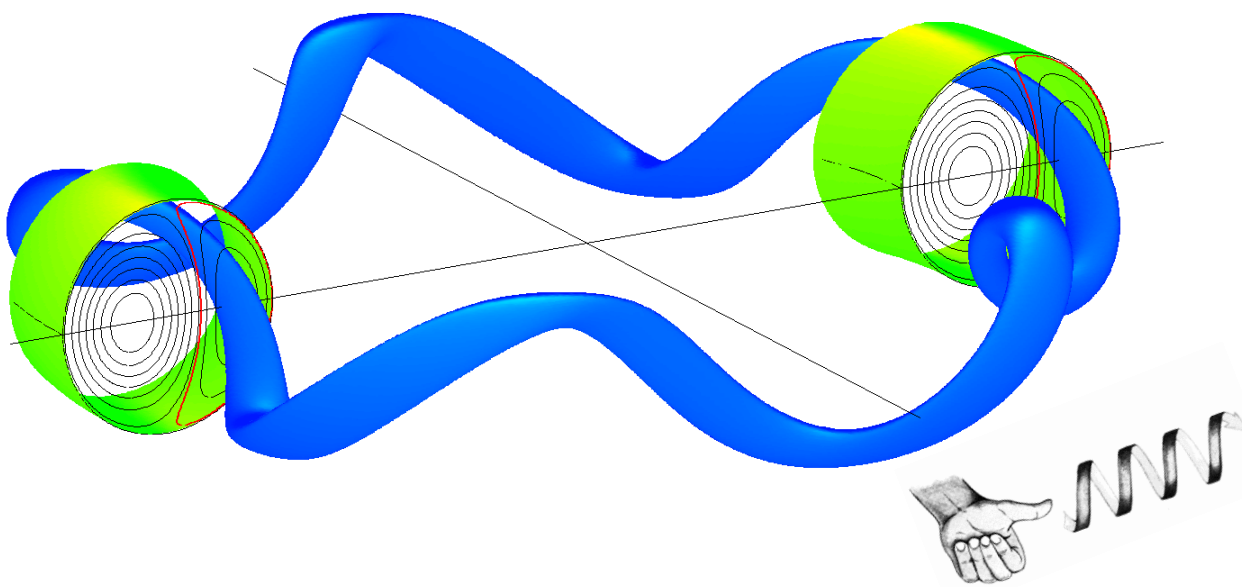

Next slides some features about the two regimes:

Saturated kink
Single Helicity - SH

Nearly periodic relaxations
Multiple Helicity - MH

SH regime: “ the simplest **RFP** ”

Magnetic flux surfaces - field lines

... and corresponding mean profile of B_T

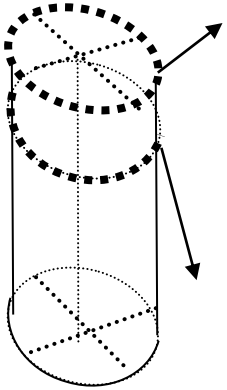

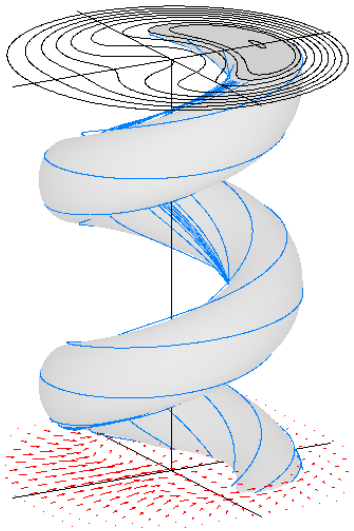

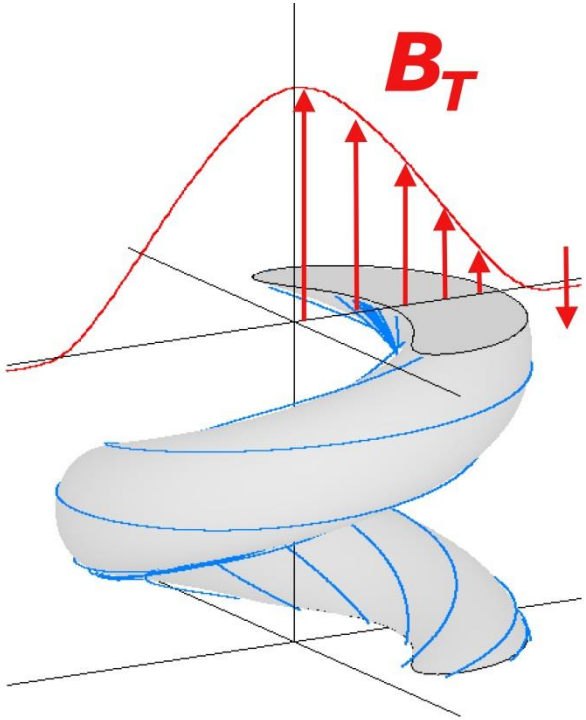

Helical Pinch Velocity

➔ drift velocity induced by the electrostatic potential …

Bonfiglio, et al PRL 2005

SH solutions resemble the toy model

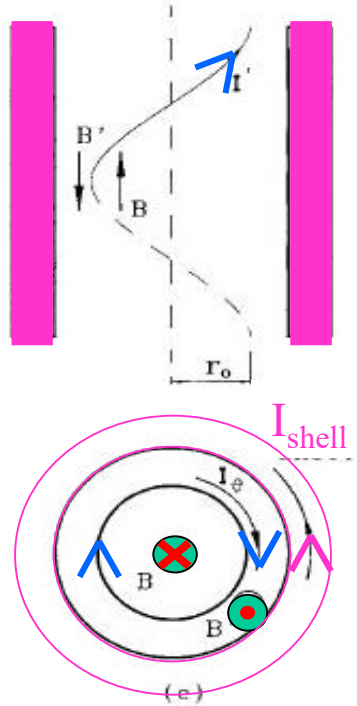

kinked wire

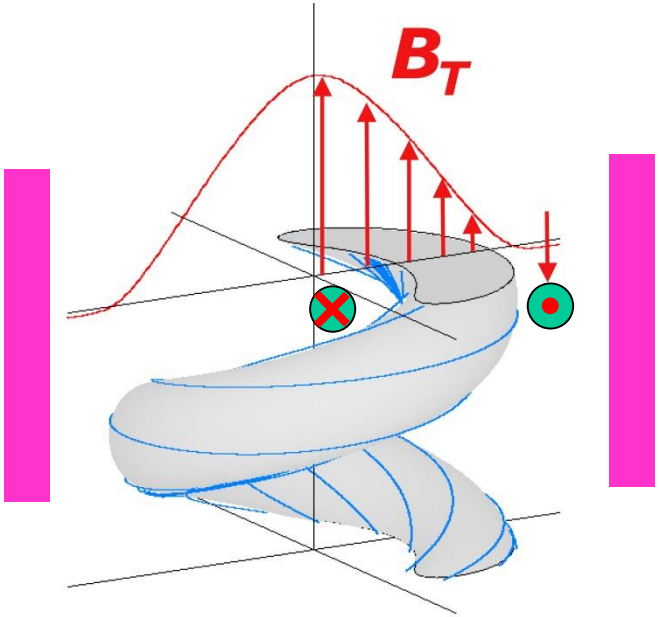

SH in viscoresistive modelling

MH regime: Nearly-periodic relaxation events

(similarly to low current experimental observations)

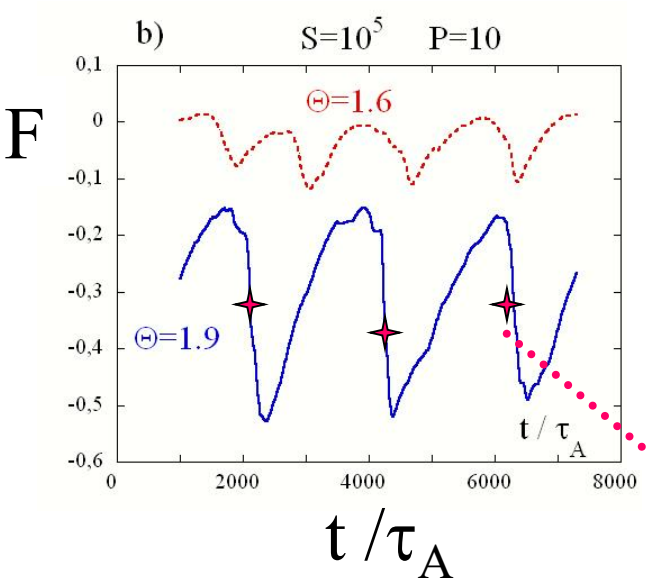

with formation of current sheets

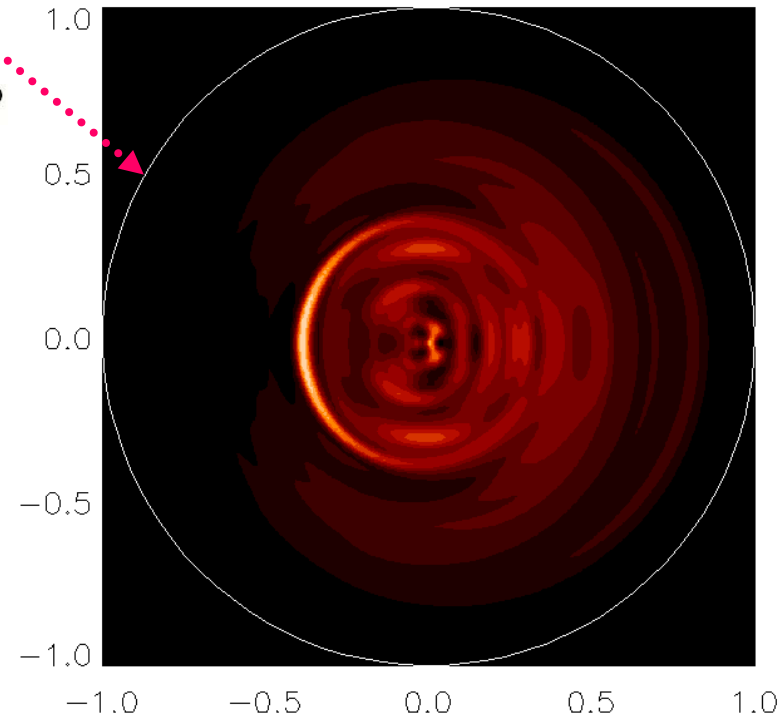

$J \cdot B$

Current density contour plots (poloidal sections)

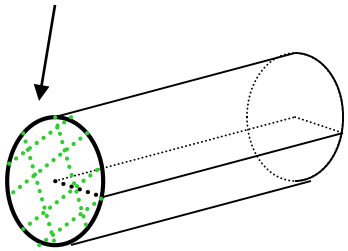

(3D: all of the modes contribute)

Bright colour => high current

Cappello & Biskamp Nucl Fus 1996

$J \cdot B$ contour plot and flow pattern

during RFP relaxation event

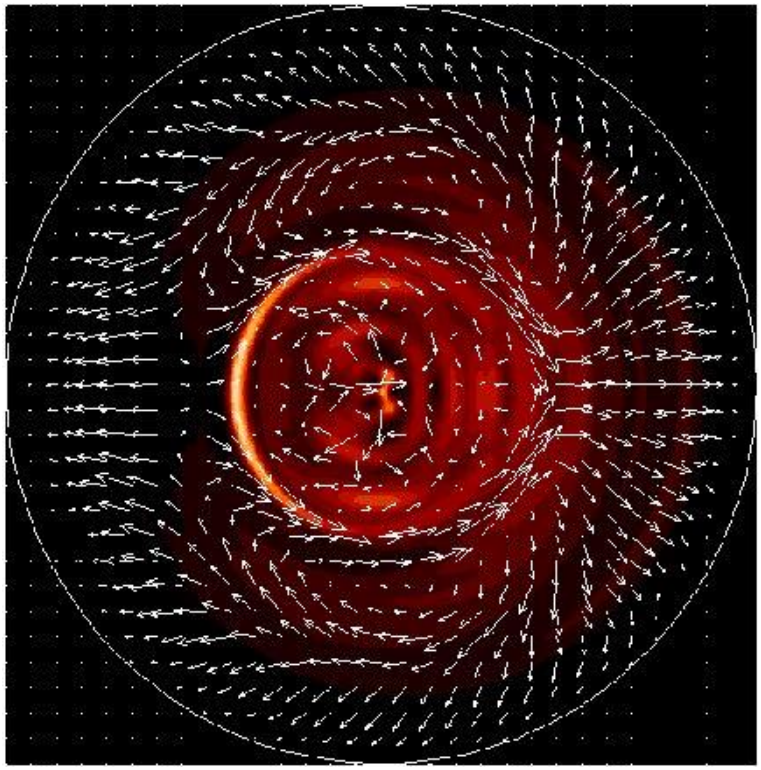

… in between relaxation events

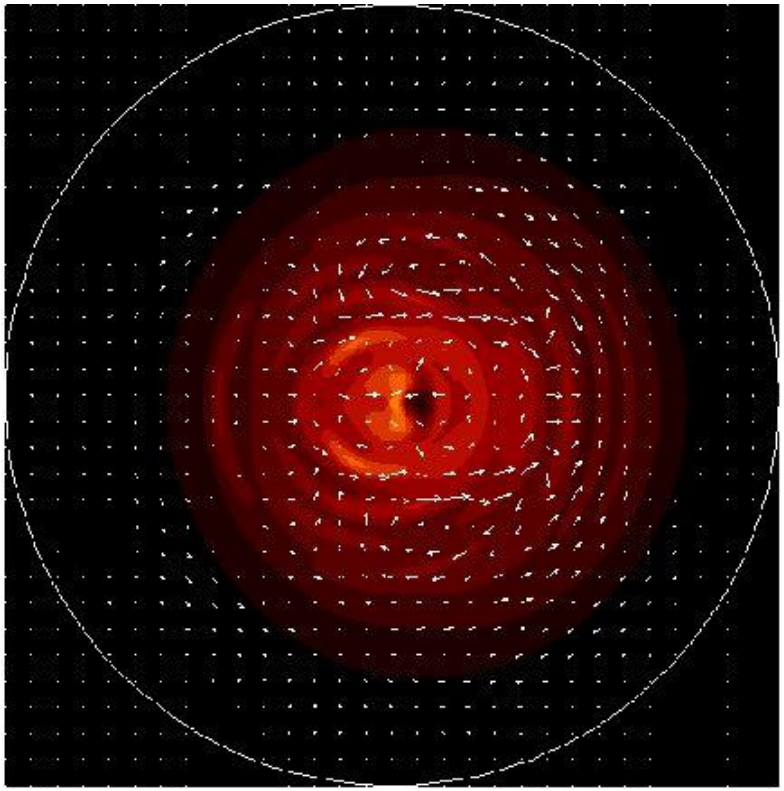

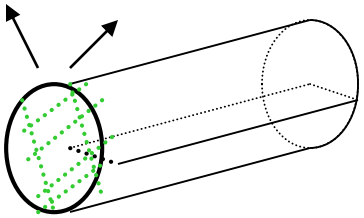

Bright colour => high current

Possible to excite different *n*s

Dominant (1,-7) and sum of secondary modes

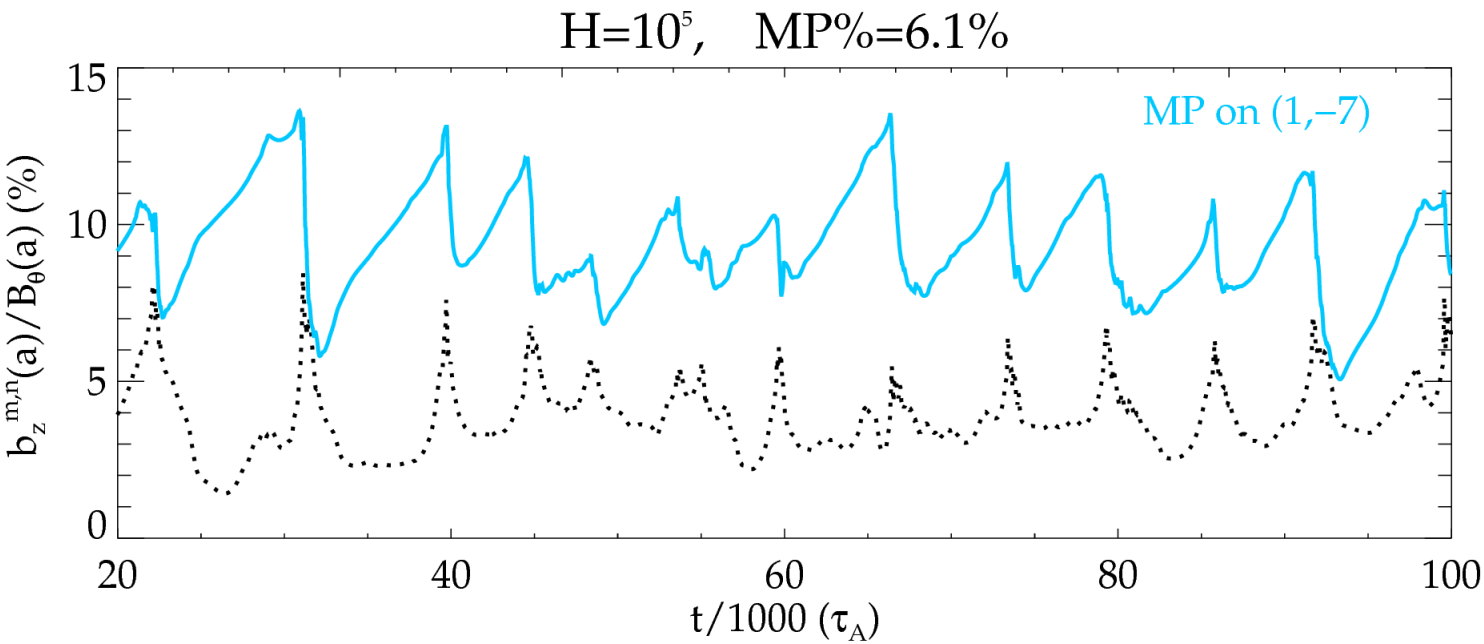

Response to different MPs : comparison

Dominant (1,-6) less reactive than -7

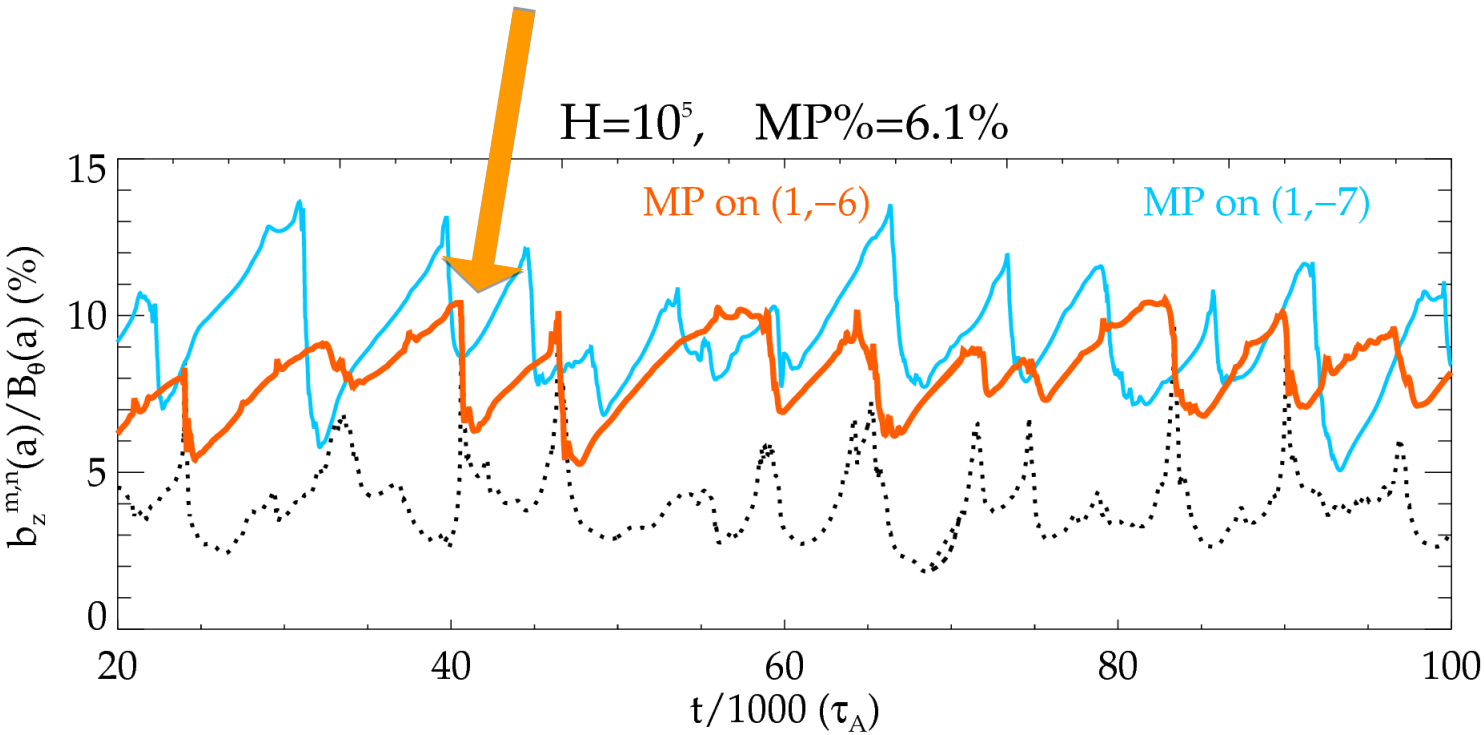

Response to different MPs : comparison

Dominant (1,-5) even less reactive

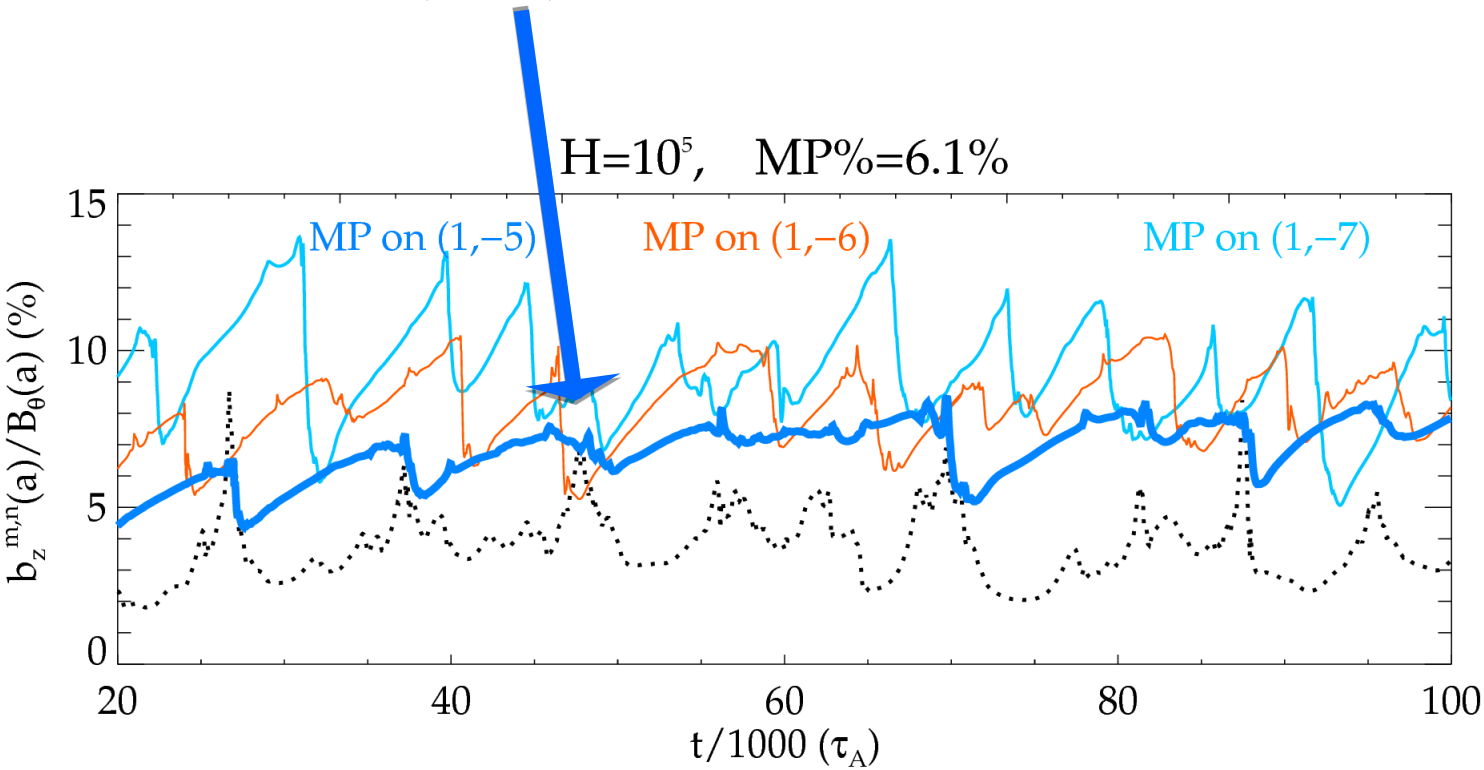

NOTE: the lower the n_{MP} -> the smaller the **Frequency&Amplitude** of cyclic oscillations

Moving around:

- Ultra-low-q and Low-q
- Circular Tokamak-like

2D (3D) visco-resistive MHD nonlinear simulations

circular cylindrical **(Ultra) low-q**

(SpeCyl – PIXIE3D)

(Ultra) low-q: Numerical modelling and Taylor's solutions

Bonfiglio NF 2008

Starting from RFP: Bz(a) is driven **upward** and **downward** again:

q(t)

Mode energies

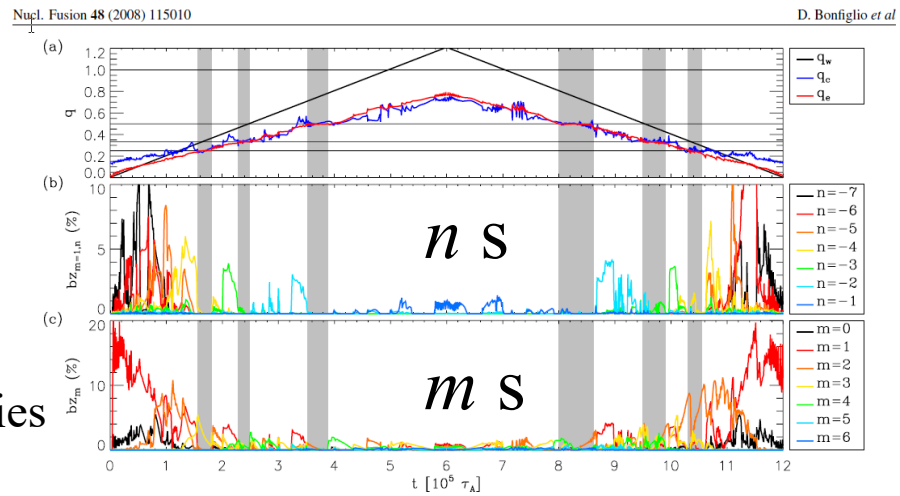

F(t)

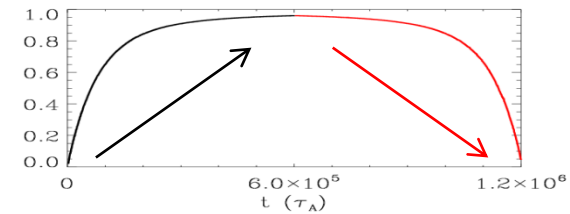

The initial phase (low-q) is closer to BFM than <u>Ultra-low-q</u> and <u>RFP</u>

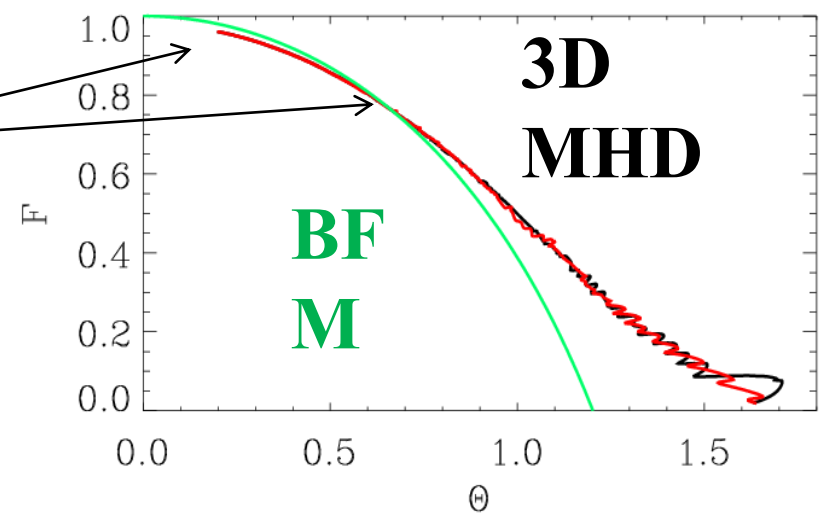

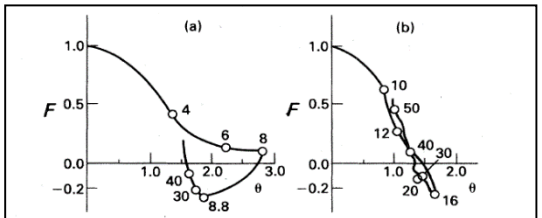

FIG. 5. Time-dependent F-θ curve for HBTX1. Times in μsec: (a) Fast mode; (b) slow mode (from Bodin and Newton, 1980).

2D (3D) visco-resistive MHD nonlinear simulations

circular cylindrical TOKAMAK

(SpeCyl – PIXIE3D)

Nonlinear verification benchmark **SpeCyl** – **PIXIE3D**

PIXIE3D is a massively parallel code in arbitrary curvilinear geometry
conservative, solenoidal finite-volume discretization in space,
fully implicit temporal advance.

Bonfiglio, Chacòn, Cappello POP 2010

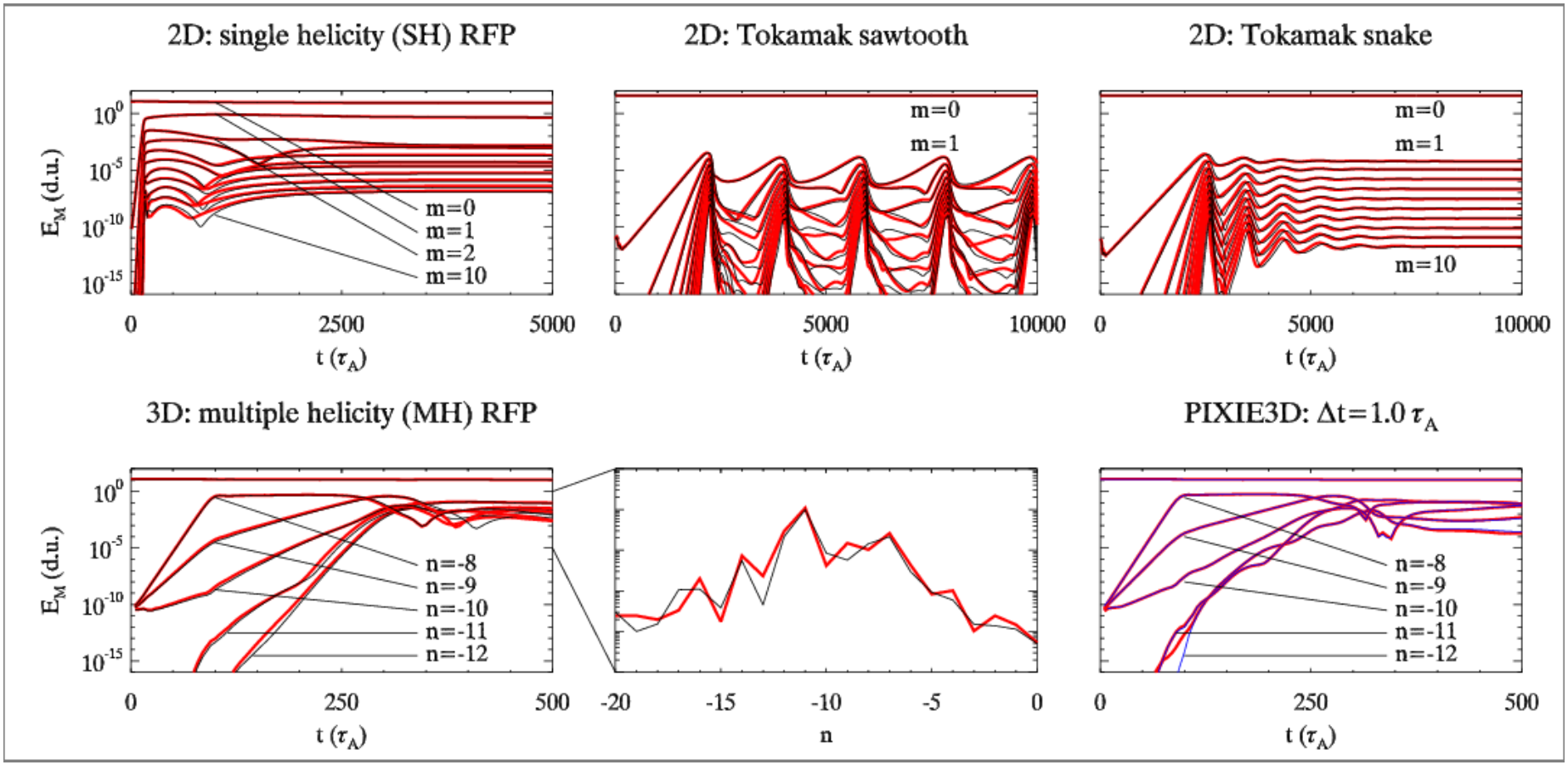

*Magnetic energy evolution from **SpeCyl** and PIXIE3D (black and red curves respectively).*
Top panels 2D) *RFP and Tokamak.*
Bottom 3D *left) RFP case. Bottom right) PIXIE3D with different time steps (red $\Delta t=5x10^{-3}$ blue $\Delta t=1\ \tau A$)*

Circular tokamak:
periodic sawtoothing (**low dissipation**)

Magnetic energy relaxation and current sheet formation

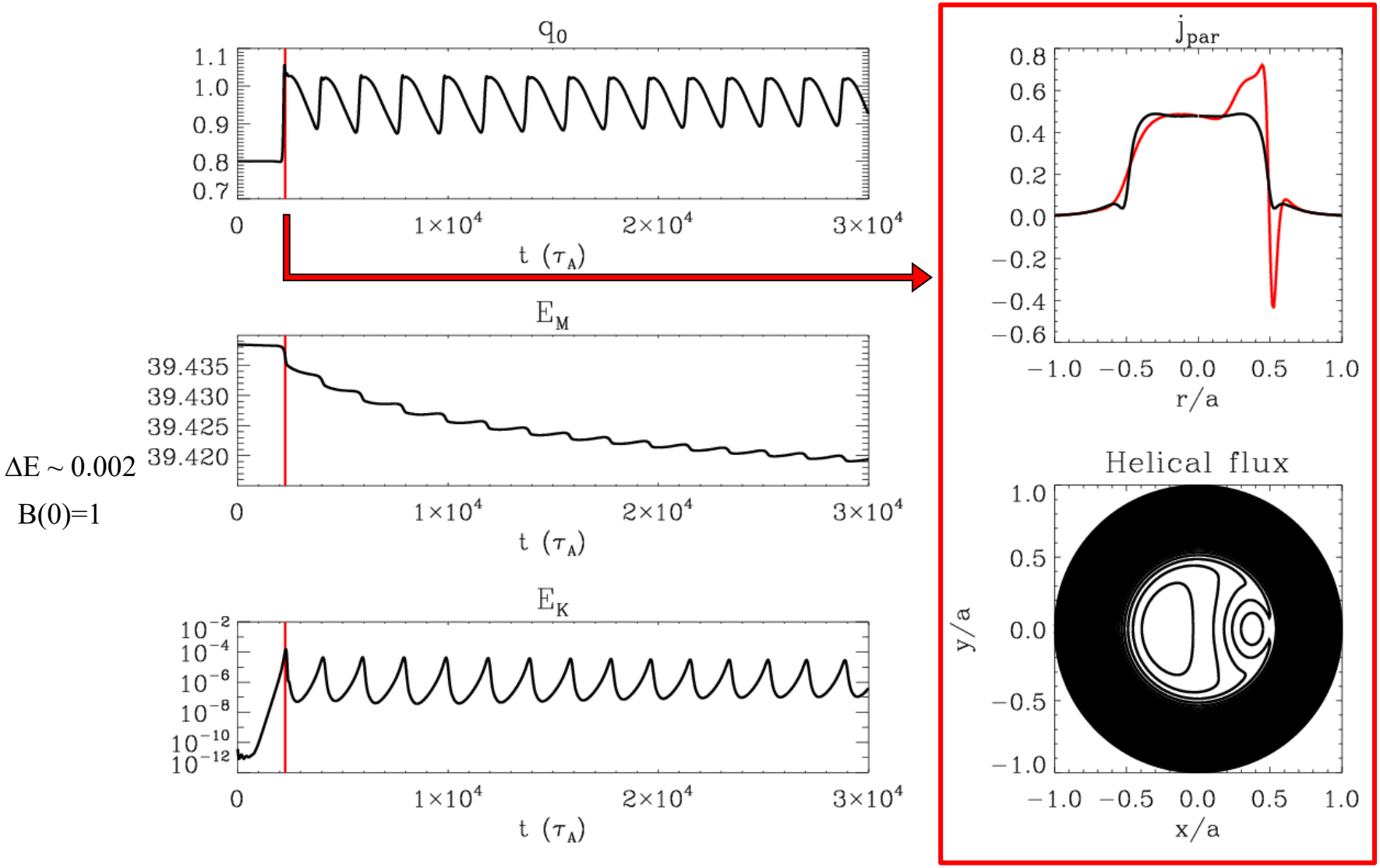

$\Delta E \sim 0.002$

B(0)=1

SpeCyl & PIXIE3D model equations

PIXIE3D (supplementary terms in red)

Continuity equation:

$$\partial_t \rho + \nabla\cdot(\rho\, \mathbf{v} - D\, \nabla\rho) = 0 \text{ (SpeCyl: } \rho \equiv 1)$$

Momentum equation:

$$\partial_t (\rho\, \mathbf{v}) + \rho\, (\mathbf{v}\cdot\nabla)\, \mathbf{v} + \rho\, \mathbf{v}\, (\nabla\cdot\mathbf{v}) = \mathbf{J}\times\mathbf{B} - \nabla p + \nu\nabla^2\mathbf{v}$$

Energy equation:

$$\partial_t T + \mathbf{v}\cdot\nabla T + (\gamma-1)\, [\, T\, \nabla\cdot\mathbf{v} - (\chi\nabla^2 T + Q)/(2\, n)] = 0$$

Faraday-Ohm equation:

$$\partial_t B = \nabla \times (\mathbf{v}\times\mathbf{B} - \eta\mathbf{J} - d_i/\rho\, (\, \mathbf{J}\times\mathbf{B} - \nabla p_e) + \nu_e\nabla^2\mathbf{J})$$

Gauss's law for magnetism: $\nabla\cdot B = 0$

RFX device evolution: plasma radius and magnetic front-end

Taylor's relaxation theory for the RFP

Taylor' conjecture (weak formulation of Woltjer's theory) is based on a minimum energy principle, (strictly meaningful for closed system),

The theory, with few ingredients, predicts minimum energy solutions with reversed Bz for high enough values of the pinch parameter Θ,
thus solutions toward which **the system should tend to**,
… **the RFP dynamo flows -essential for the RFP life- are neglected**.

There are several discrepancies :

- B(r) are smoother then Bessel … - μ *is not a constant*,
- a helical solution should be achieved … - *different from the ones observed* (*neither in exp nor in 3D nonlinear modelling*)
- after saturation of the pinch parameter - *not observed* (*neither in exp nor in 3Dmod*)

Such deficiencies should not surprise us,
the **RFP is not a closed system, it is a driven one** and we should not expect to obtain more then what promised by the Taylor's minimum energy solution itself !

RFP self-organization

ruled by Hartmann number

MHD Numerical simulations

Turbulent ⟷ **MH** : 3D non linear coupling resistive-kink tearing modes

↑

RFP

Numerical simulations

(cylindrical approx.)

$\mathbf{H \sim (\nu\eta)^{-1/2}}$

↓

Laminar ↔ **SH** : 2D Stationary **helical symmetric** configurations

Model equations

3D MHD nonlinear code SpeCyl

Cappello & Biskamp
Nucl. Fus. 1996

$$\frac{\partial \boldsymbol{B}}{\partial t} = \nabla \wedge (\boldsymbol{v} \wedge \boldsymbol{B}) - \nabla \wedge (\boxed{\eta}\, \boldsymbol{J})$$

$$\frac{\mathrm{d}\boldsymbol{v}}{\mathrm{d}t} = \boldsymbol{J} \wedge \boldsymbol{B} + \boxed{\nu}\, \nabla^2 \boldsymbol{v}$$

$$\rho \equiv 1, p \equiv 0$$

$\eta = \tau_A / \tau_R$

$\nu = \tau_A / \tau_v$

(Lundquist: $S = 1 / \eta$)

simple visco - resistive approximation

(ideal boundary)

re-scaling : $t \rightarrow \bar{t} = \sqrt{\frac{\eta}{\nu}}\, t$ $\quad \mathrm{v} \rightarrow \bar{\mathrm{v}} = \sqrt{\frac{\nu}{\eta}}\, \mathrm{v}$

Model equations … transformed

… re-scaling : $t \to \bar{t} = \sqrt{\frac{\eta}{\nu}}\, t$ $\quad \mathrm{v} \to \bar{\mathrm{v}} = \sqrt{\frac{\nu}{\eta}}\, \mathrm{v}$

$(\eta, \nu) \Rightarrow (H, P)$

Hartmann: **$H = (\nu\eta)^{-1/2}$**

highlighted also in
D. Montgomery et al. PPCF 92-93
Tebaldi,Ottaviani JPP 99
(linear stab.)

magnetic Prandtl: **$P = \nu / \eta$**

$$\frac{\partial \bar{B}}{\partial \bar{t}} = \nabla \wedge (\bar{\mathrm{v}} \wedge \bar{B}) - \nabla \wedge (H^{-1} \bar{J})$$

$$\frac{1}{P} \frac{d\bar{\mathrm{v}}}{d\bar{t}} = \bar{J} \wedge \bar{B} + \nabla^2 (H^{-1} \bar{\mathrm{v}})$$

$$\rho \equiv 1, p \equiv 0$$

"H" is the important parameter when inertia is negligible

Cappello & Escande PRL 2000

Introduce m=0 mode energy as dynamical indicator

$\delta B_{m=1}, n$

m=1 modes
nonlinearly drive
m=0 modes

MH

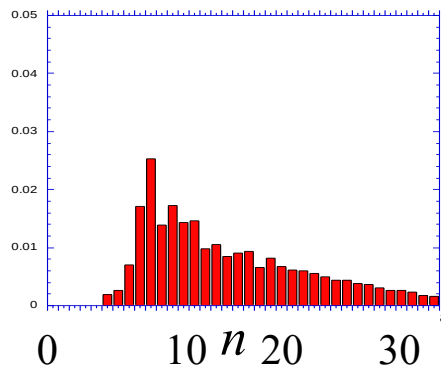

QSH

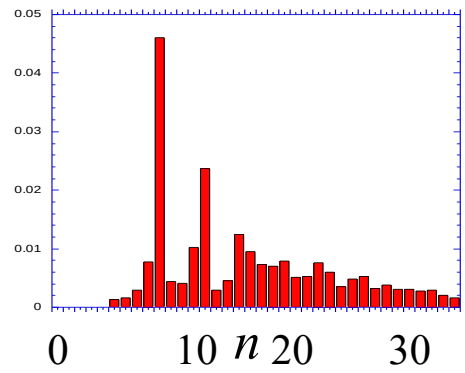

$\log \delta E_{m=0}$

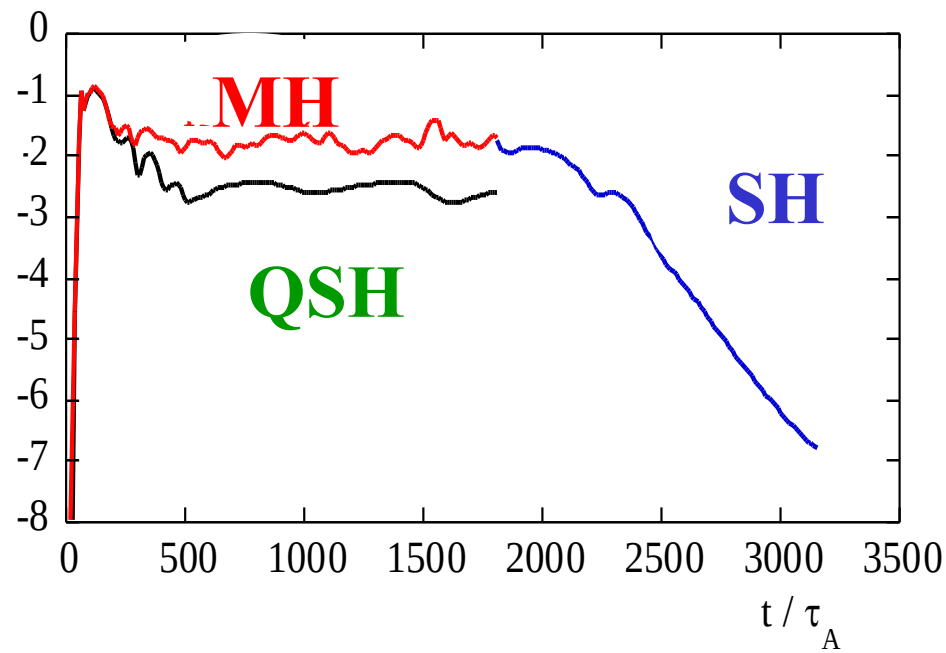

m = 0 modes are a <u>good indicator</u> of the dynamical regime

next slide : **RFP transition diagram**

m=0 mode energy

(Time averaged)

vs.

Hartmann number

Dynamical regimes in the numerical RFP : Transition diagram SH - QSH - MH

Numerical results

$\Theta = 1.9$

$E^{M}_{m=0}$

S=3.3x10^3 (P: 2/3-10)
S=3.0x10^4 (P: 1-5000)
S=10^5 (P = 10)

Two **S**ingle **H**elicity basins:

m/n 1/-12, 1/-11

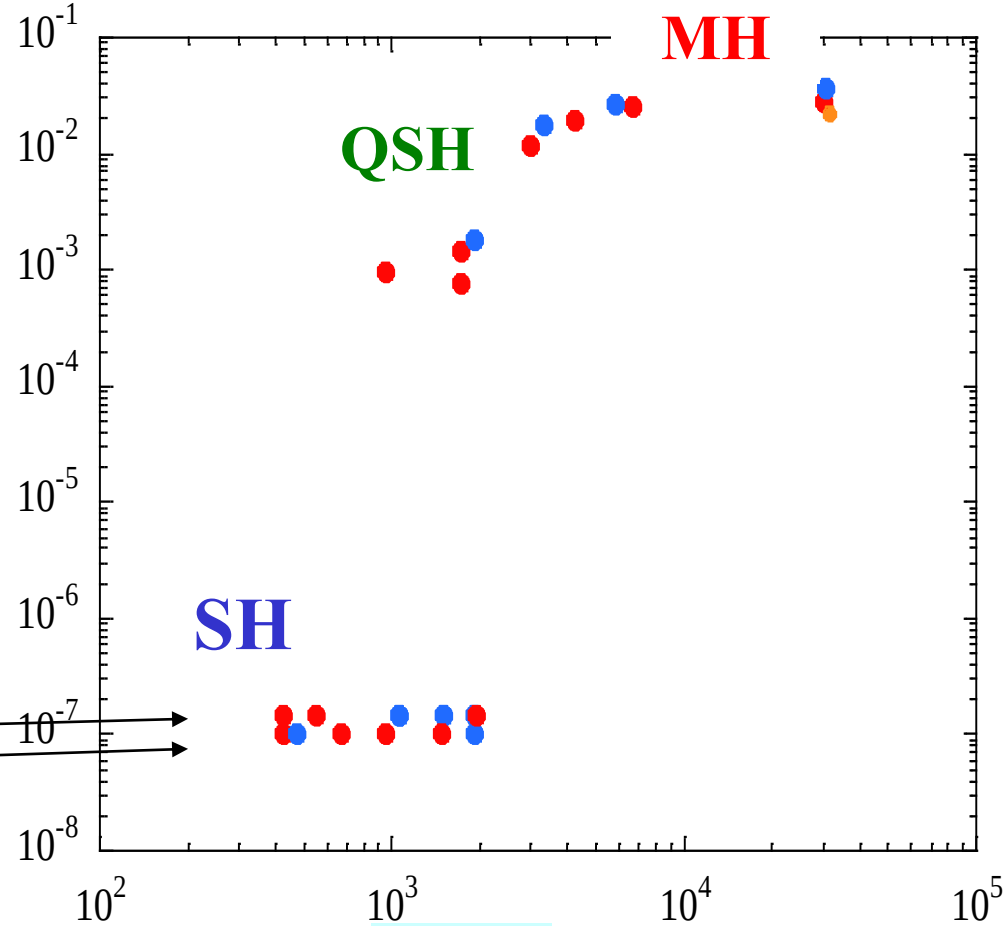

R/a =4

$H = 1/(\nu\eta)^{1/2}$

Cappello & Escande PRL 2000
Cappello PPCF 2004

- **transition to QSH – SH in viscoresistive MHD**

Most updated numerical transition diagrams (PPCF 2004)
minor dependence also on magnetic Prandtl and Θ

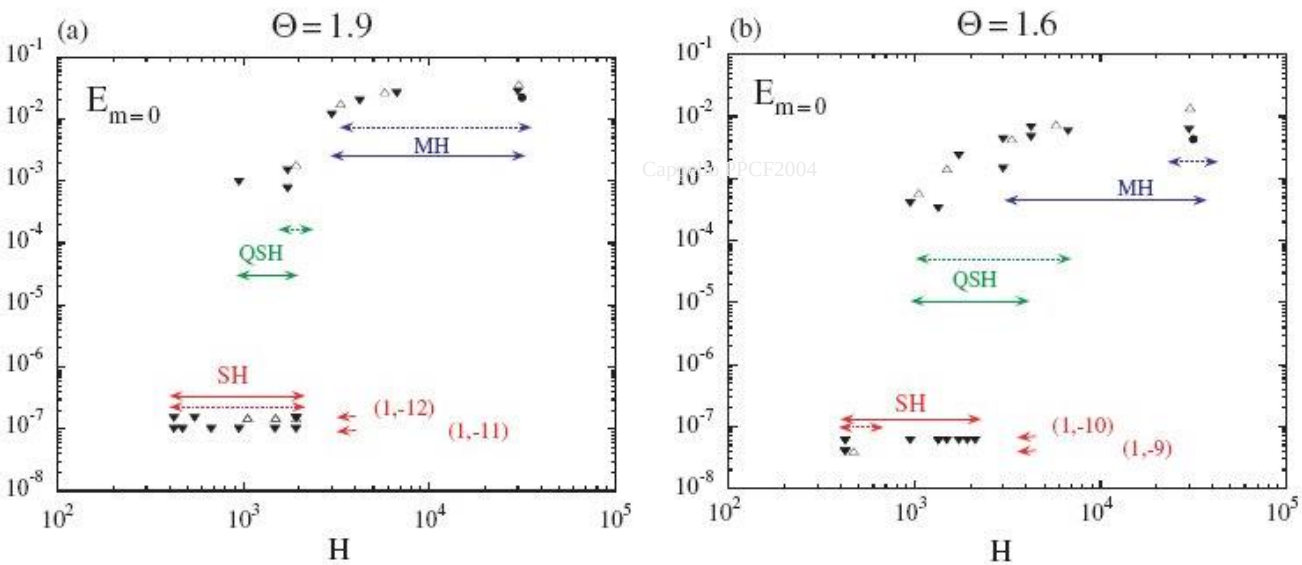

Figure 1. Transition diagrams at two values of the pinch parameter: (*a*) $\Theta = 1.9$, (*b*) $\Theta = 1.6$. The plots show the time-averaged magnetic energy of the $m = 0$ modes against the Hartmann number. Open triangles are used for $S = 3.3 \times 10^3$ with $P = [0.012, 50]$, black triangles for $S = 3.0 \times 10^4$ with $P = [1, 5000]$, the black circle is used for the case $S = 1.0 \times 10^5$ with $P = 10$. Note that for a convenient representation in the log-scale plot the vanishing SH $m = 0$ mode energy is represented as a finite conventional value with different offsets associated with the different preferred helicities developed by the system. The intervals associated with the different dynamical regimes, MH/QSH/SH, are highlighted by the horizontal bars (plain line $S = 3.0 \times 10^4$, dashed line $S = 3.3 \times 10^3$); at $S = 1.0 \times 10^5$ with $P = 10$ a MH regime is found.

Continuous transition ruled by ην (no MP)

High, intermediate, **low** dissipation

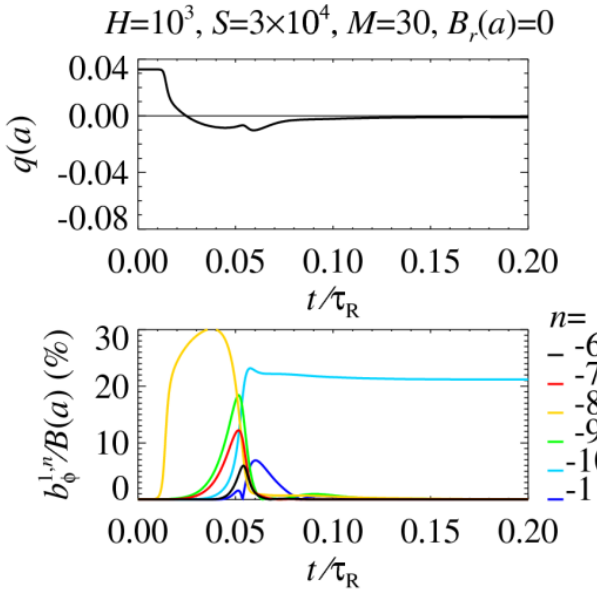

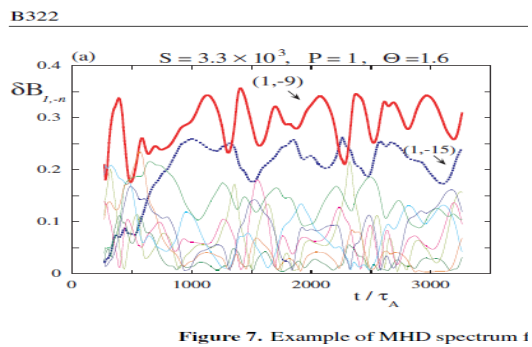

Figure 7. Example of MHD spectrum f

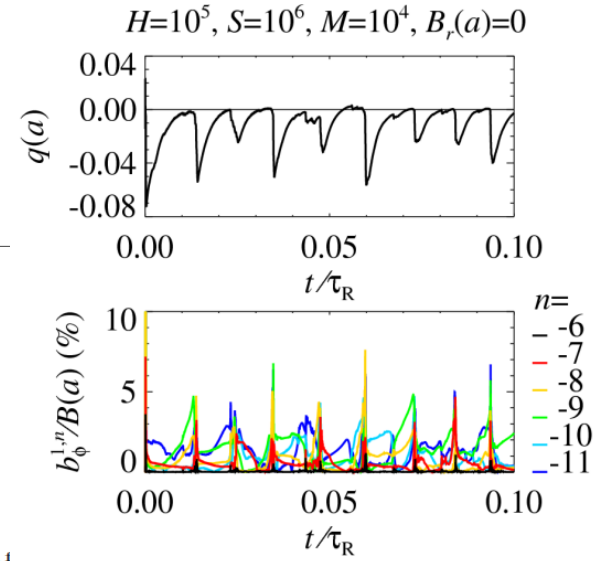

SH

MH

Cappello PPCF 2004

QSH regime:

Poincaré plot in **numerical** QSH regime

Topology reconstructions from **experimental** measures

conserved helical structure

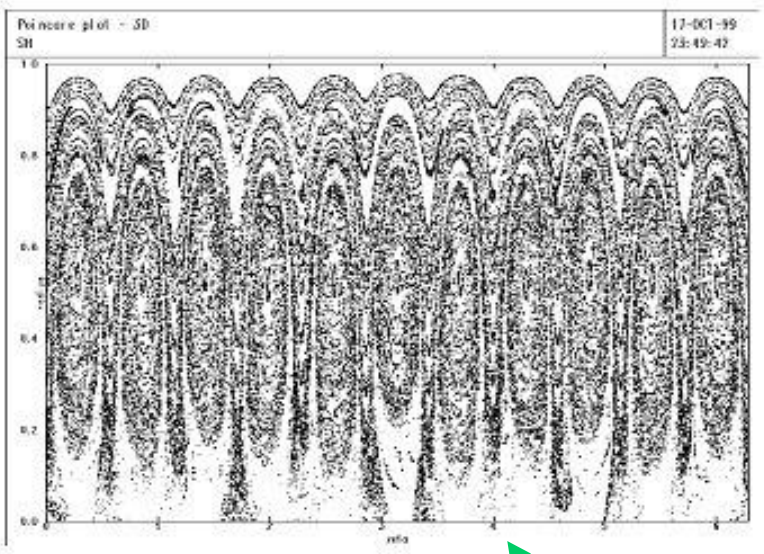

no separatrix

Escande et al. PRL 2000

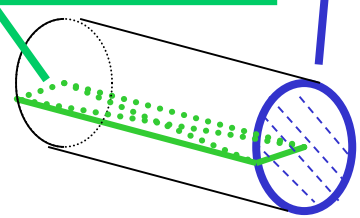

SXR emissivity

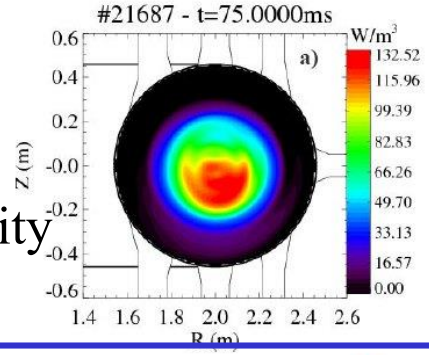

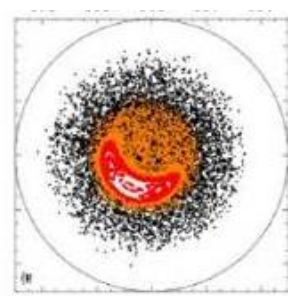

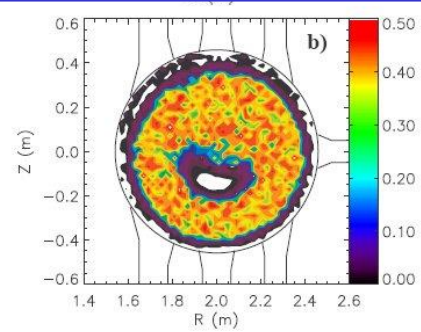

Gobbin et al. – Bonomo et al. - Innocente et al. EPS 2007

Lorenzini et al. PRL 2008

RFP plasma discharge set up

Historical observations (‘*50ties* several toroidal pinches – ZETA –):

Quiescent regimes observed after B_T field reversal

RFP plasma discharge set up

Historical observations (‘*50ties* several toroidal pinches – ZETA –):

Quiescent regimes observed after B_T field reversal

Let us introduce two useful dimensionless parameters

Reversal parameter

$$F \equiv \frac{B_T(a)}{\langle B_T(r) \rangle}$$

Pinch parameter

$$\Theta \equiv \frac{B_P(a)}{\langle B_T(r) \rangle} \longrightarrow \propto \frac{I}{\Phi}$$

Quiescent regimes observed after B_T field reversal

… Faithfully replicated in modern experiments: RFX examples

F = **- 0.01**

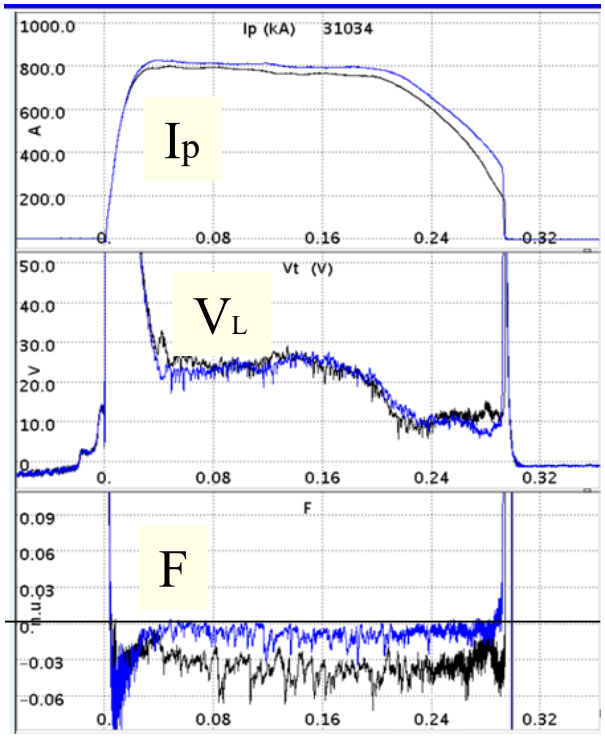

F > 0 disruptive instability

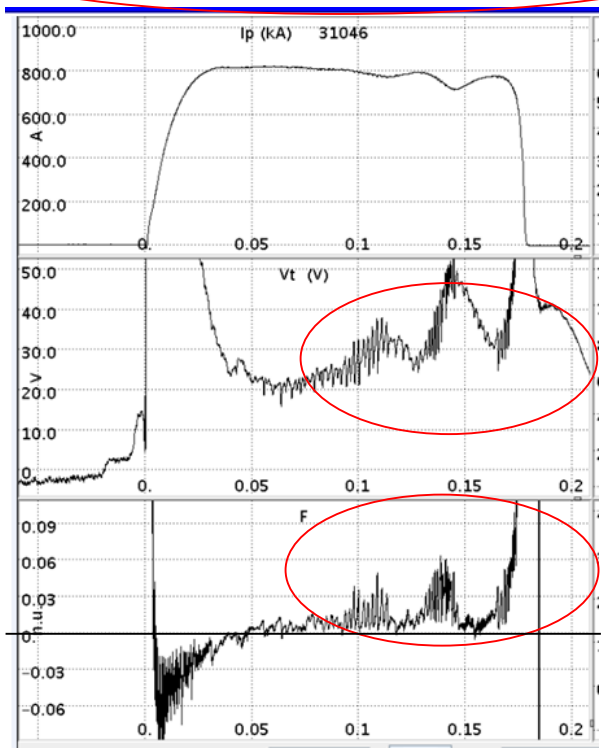

temporal trajectory in the F – Θ plane

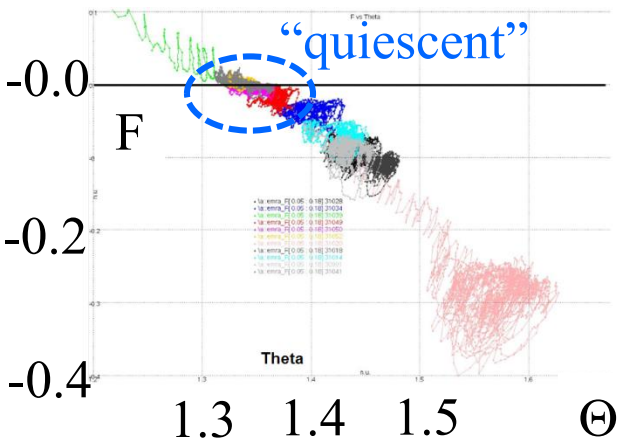

M. Zuin & RFX team
RFX internal presentation
2011.12.02

Example of QSH regime similar to experimental ones

$H=10^5$, $S=10^6$, $M=10^4$, $b_r^{1,-7}/B(a)=2\%$ ← with MP (1,7)

Typical RFP sawtoothing

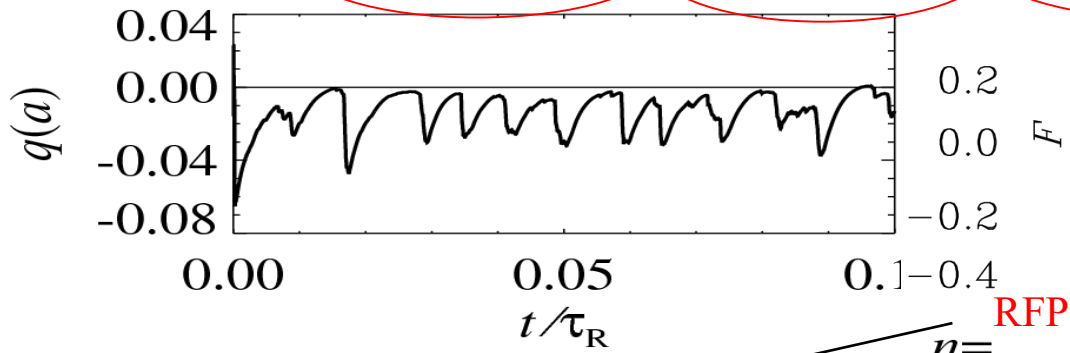

RFP "sawtoothing" cycle

Mode amplitude

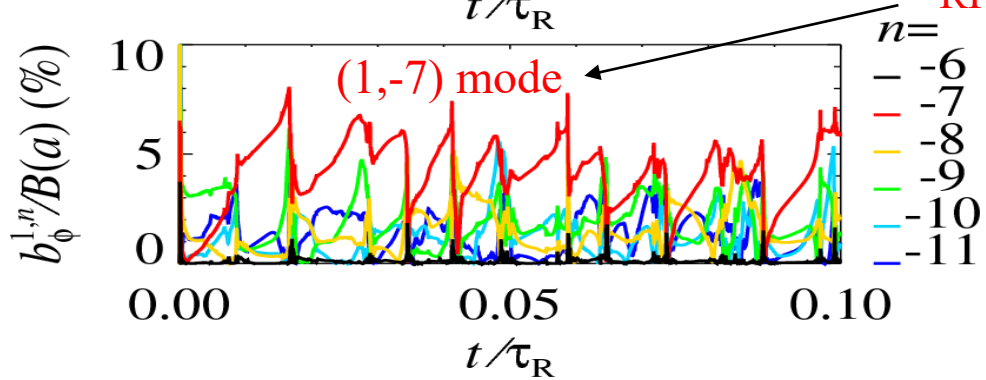

Bonfiglio NF 2011
Veranda PPCF 2013
Bonfiglio PRL 2013

The amplitude of secondary modes decreases with S,
The threshold MP% to excite a dominant mode decreases with S too.

RFX-mod:
I ≥ 1MA
S ≥ 5 10^6

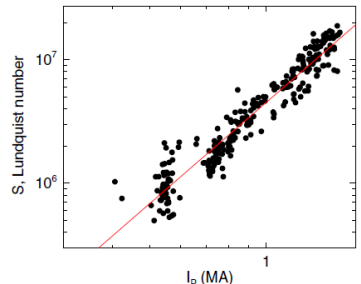

Piovesan, Zuin et al NF 2009

RFX-mod discharges

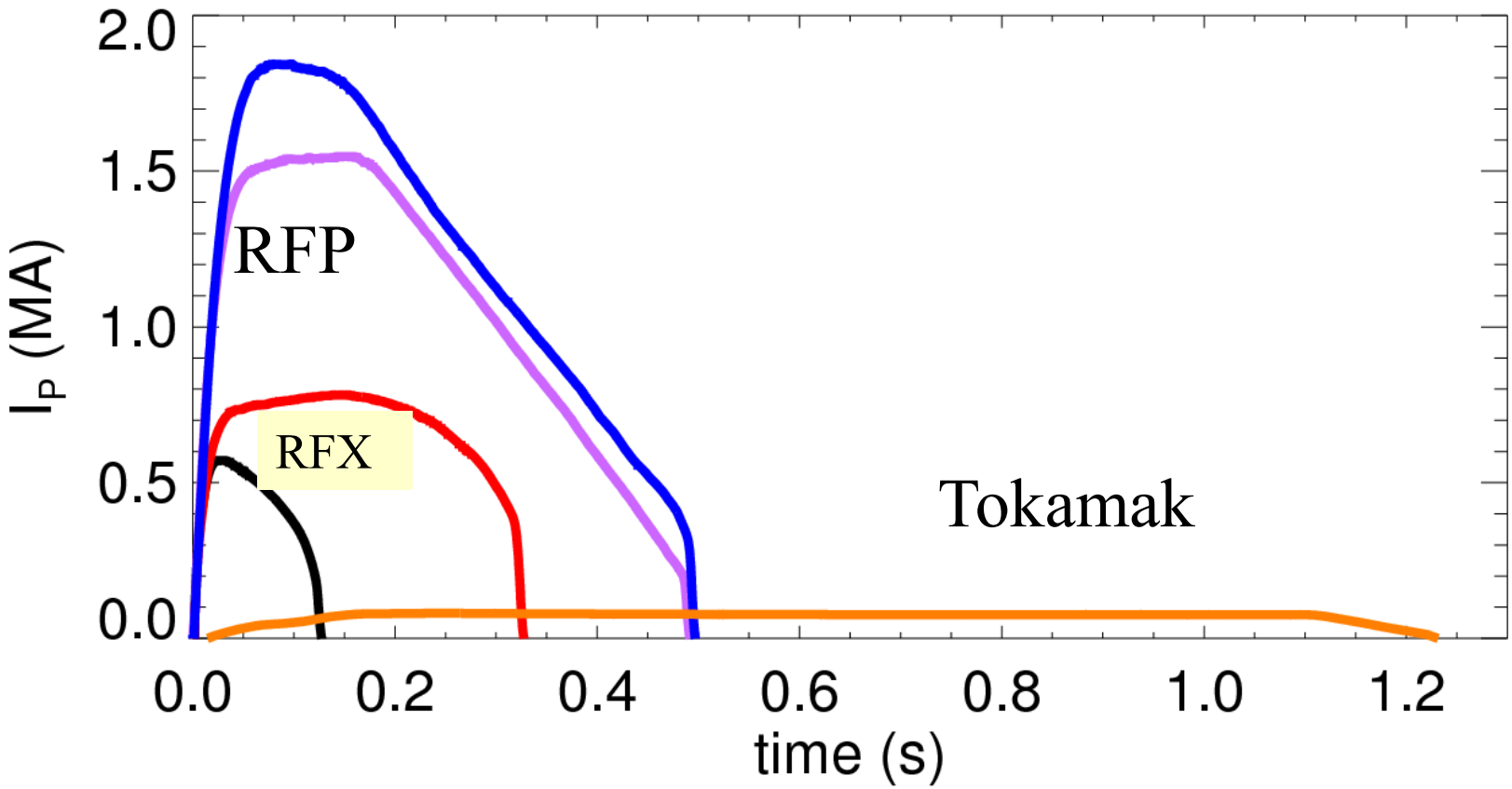

Shear Alfvén Wave and Compressional Alfvén Wave

SAW

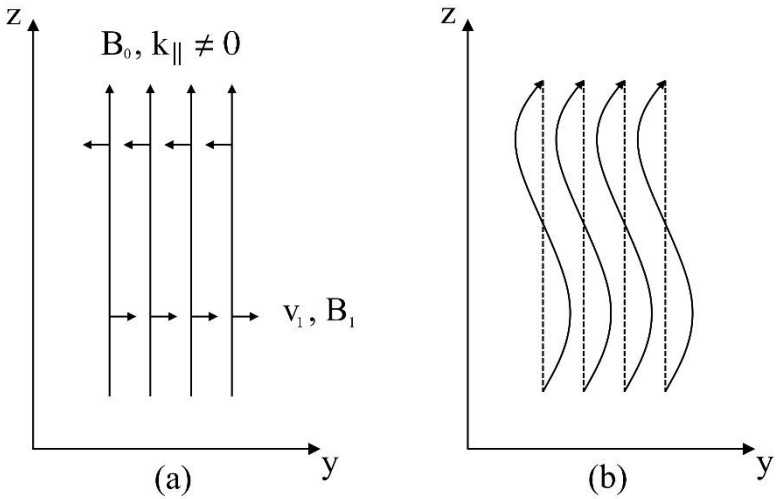

- The field lines are bent, giving the rise to a magnetic tension.
- There is no density or particle pressure perturbation for this mode.

CAW

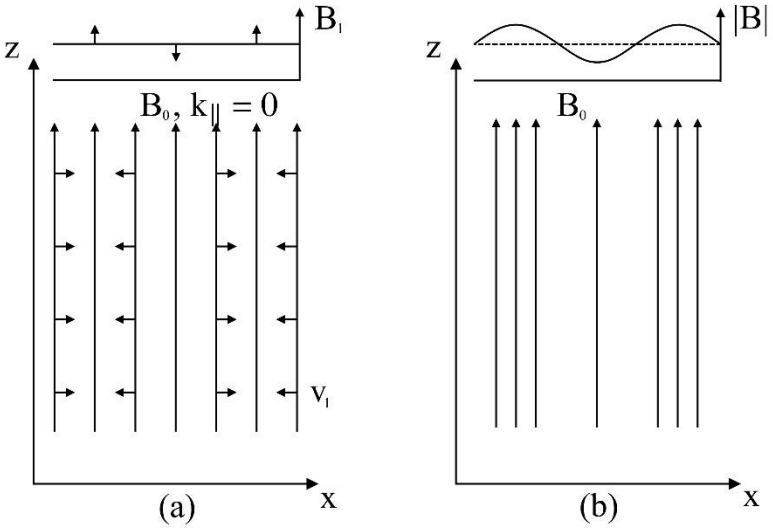

- These modes are compressive in nature, even if the sound speed is zero (cold plasma approximation).
- There are density perturbation in the wave, and perturbations of the magnetic field parallel to $\mathbf{B}_0$.

Experimental observations of AE in RFX-mod plasmas

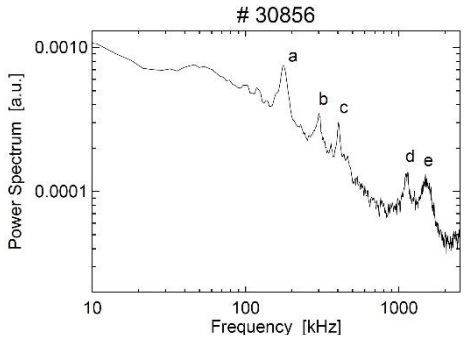

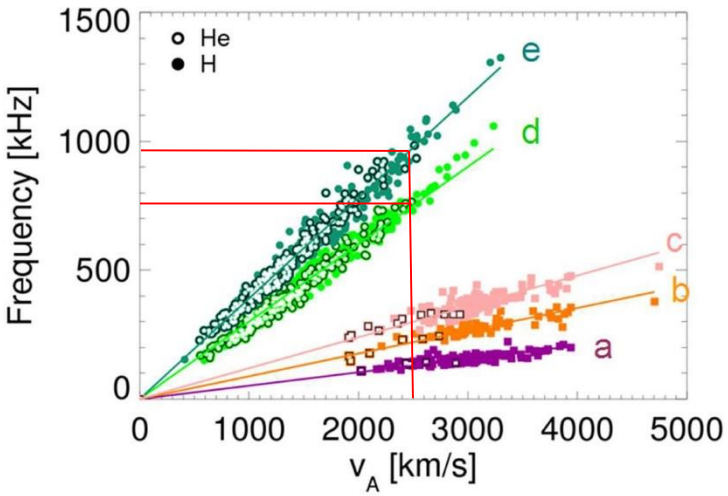

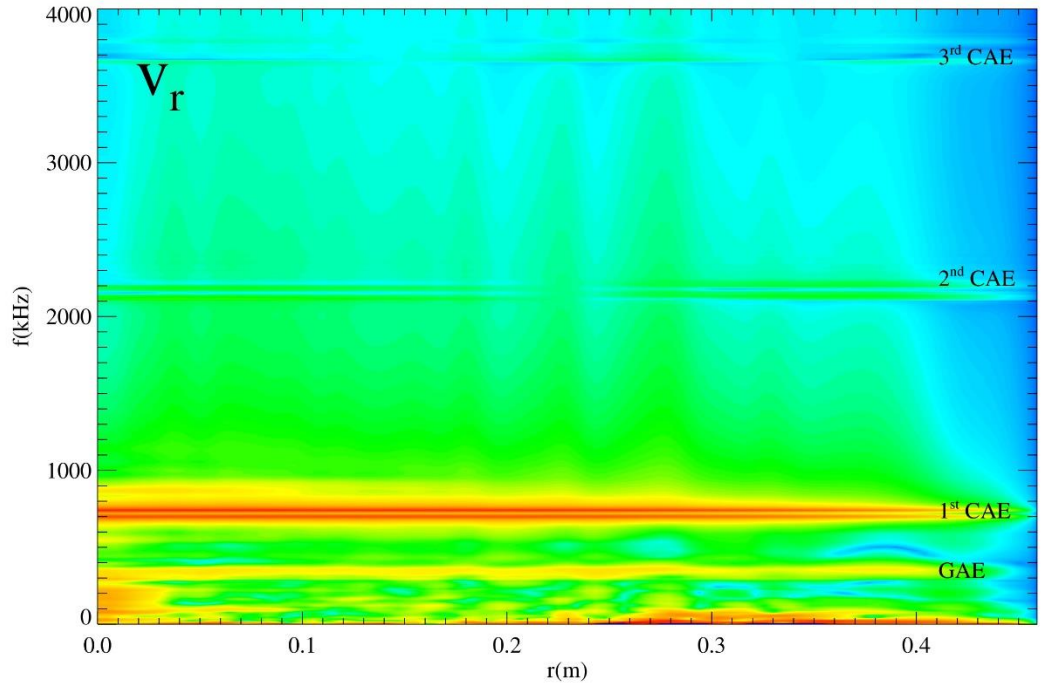

- Power spectrum of a $\dot{b}_p$ (r/a=1) signal evaluated during a SHAx state.
- d and e peaks are present during almost the full discharge duration.
- Physical units by taking $v_A = 2500$ km/s.

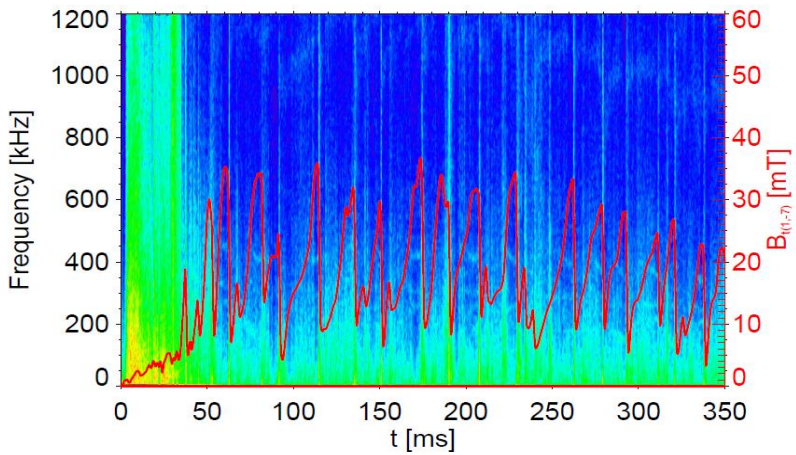

Figure 5.11: Spectrogram of U-probe $\dot{B}_\theta$ signal. The red line is the (m,n)=(1,-7) toroidal magnetic field component.

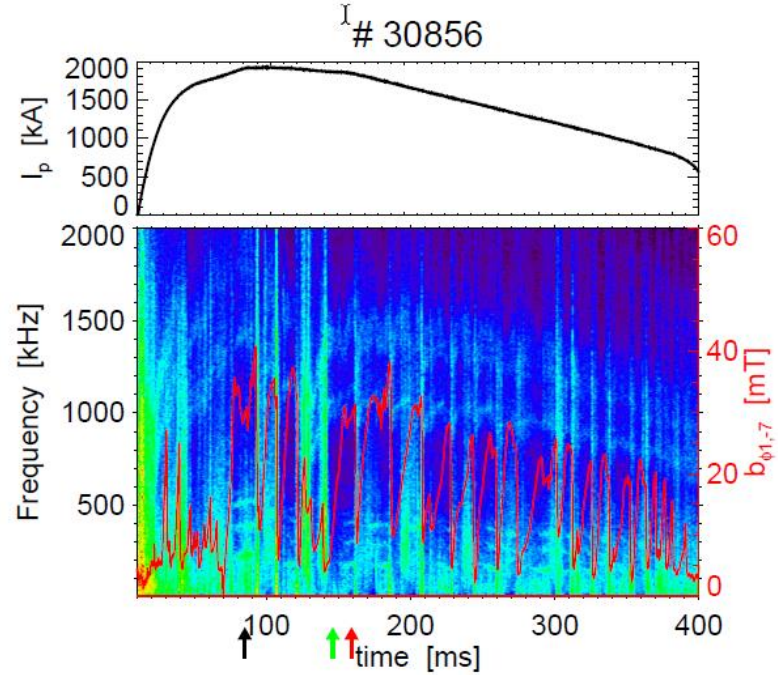

FIG. 1: Top: plasma current I_p time trace; bottom: spectrogram of a $\dot{b}_p$ signal and (red line) amplitude of the dominant $m/n = 1/-7$ mode (y-axis on the righthand side). The three arrows refer to the three time instants for the analysis in figure 3

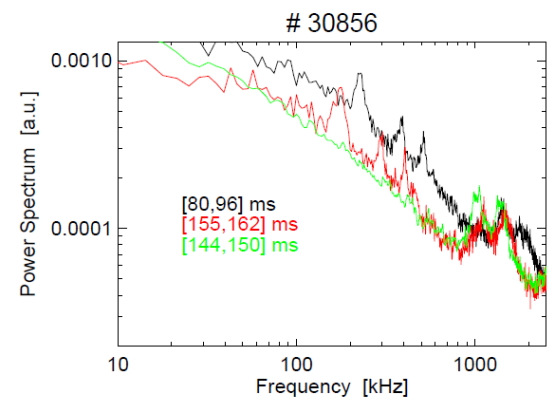

FIG. 3: Power spectrum of a $\dot{b}_p$ signal evaluated during the three time instants indicated by the arrows of figure 1: black and red lines refer to SHAx states, the green one to an axisymmetric state.

Spagnolo PhD Thesis 2012

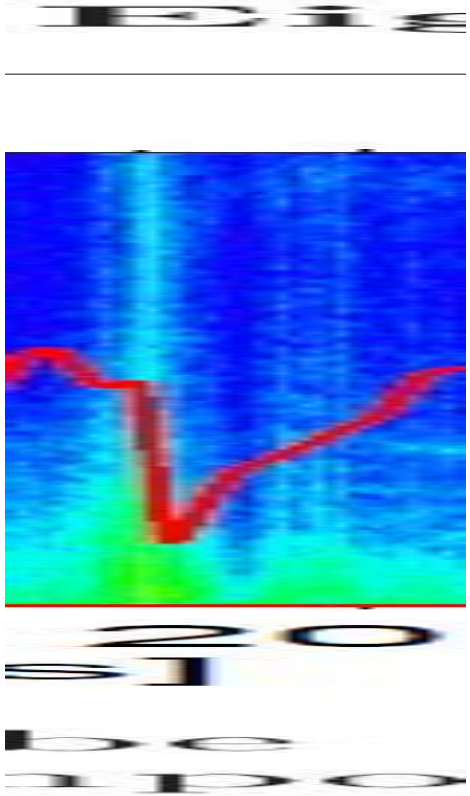

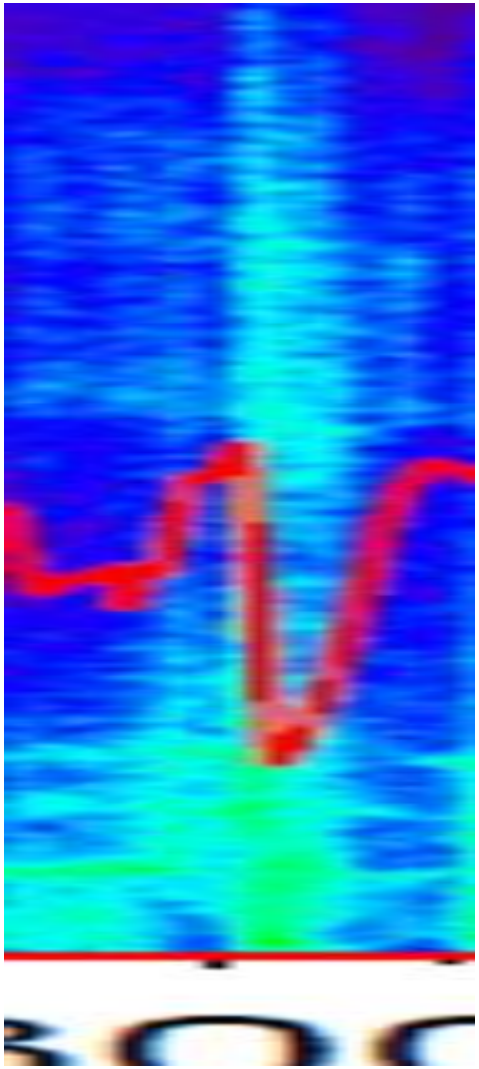

(1992 – 1999)

RFX

(2004 – 2015)

RFX-mod

(2021 ...)

RFX-mod2

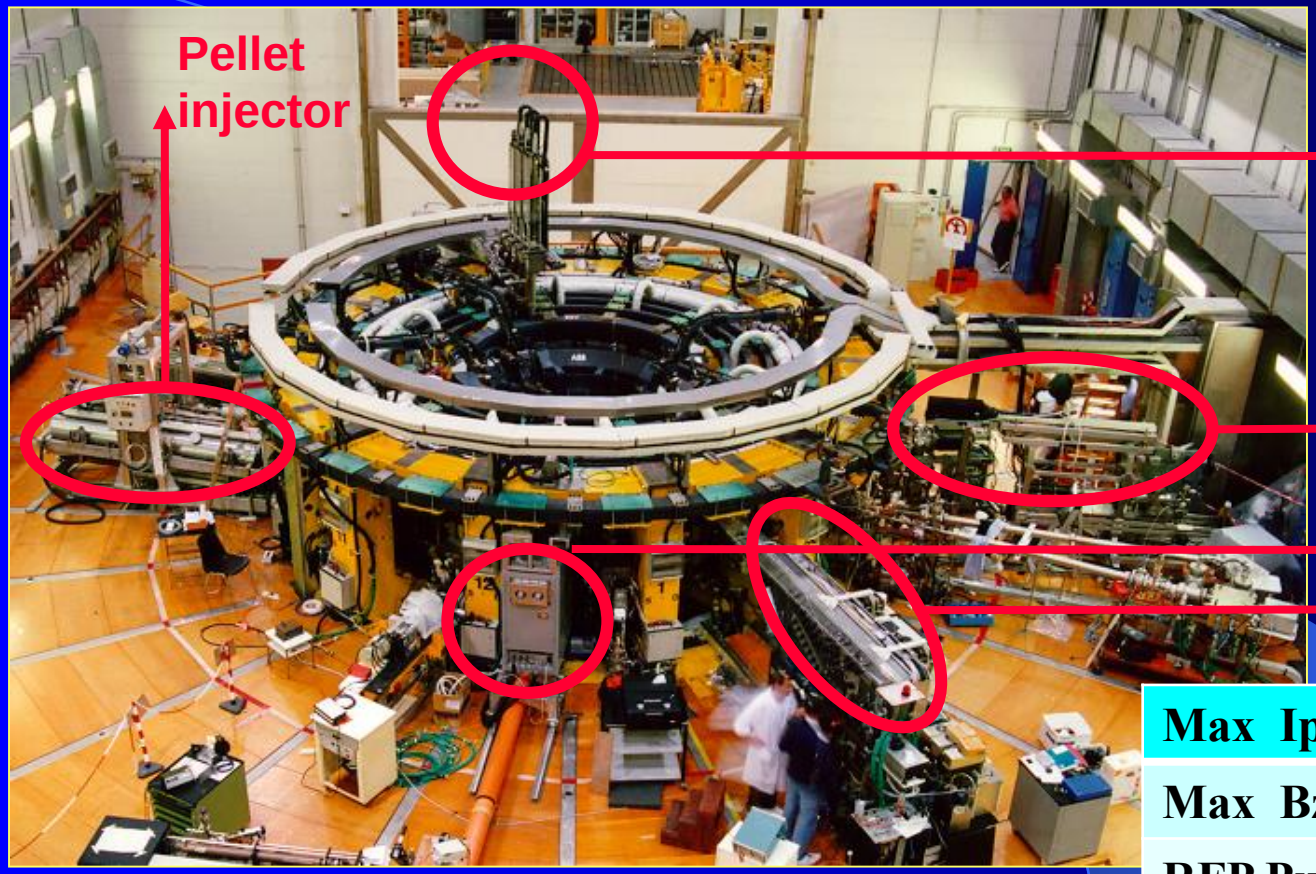

Max Ip	2 MA
Max Bz	0.7 T
RFP Pulse duration	0.6 s
Tokamak Pulse	1 s

screw-pinch

Un altra quantità utile per descrivere queste configurazioni è il fattore di sicurezza q(r), è legato al passo di avvolgimento elicoidale del campo magnetico sulle sue superfici:

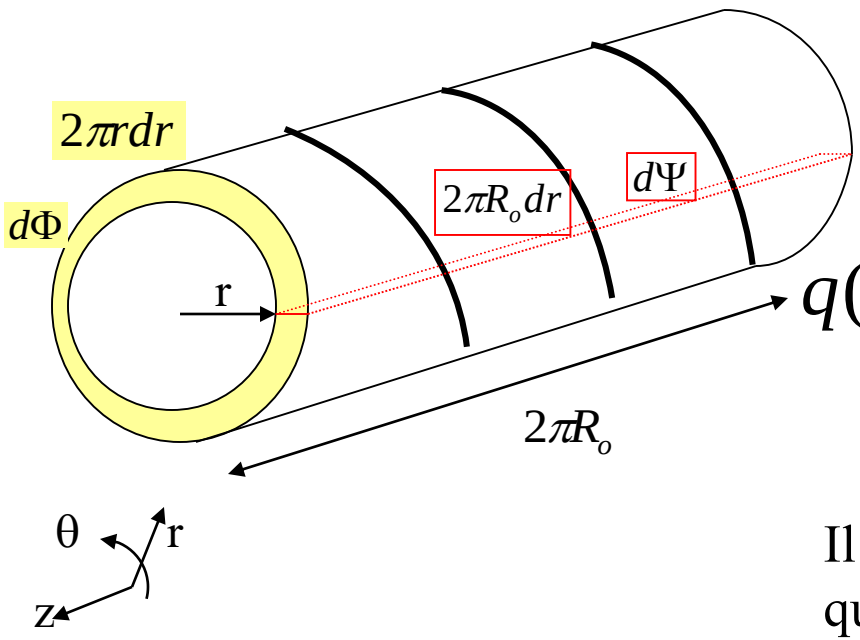

$$q(r) = \frac{d\Phi}{d\Psi} = \frac{2\pi r dr\ B_z}{2\pi R_o dr\ B_\vartheta} = \frac{r B_z(r)}{R_o B_\vartheta(r)}$$

Il fattore di sicurezza è un altra quantità importante per la stabilità...

Abstract

Recent Developments in the Studies of Plasma Self-Organization in the Reversed-Field Pinch and Impact on Transport Properties

We will review key results from the 3D nonlinear MHD numerical modeling of Reversed-Field Pinch helical self-organization processes. **Magnetic transport-barrier formation** and **nearly periodic reconnection events** are found to be at play [1-4], akin to the experimental observation of thermal transport barriers and residual "back-transition" cycles when approaching helical regimes in high current discharges [4-7].

Similarities with Tokamak visco-resistive MHD snake/sawtooth–like phenomena will be discussed, as well as aspects at odds with the **original Taylor's relaxation theory** for the Reversed Field Pinch [8].

We will describe the recent successful technique to "channel" the system towards chosen **"stimulated" macroscopic helical** shapes by applying suitable (either Resonant or Non-Resonant) Magnetic Perturbations at the edge of the plasma, as predicted by nonlinear MHD modeling and observed in recent RFX-mod experiments [2].

In so doing, we are able to modify the transport properties of the configuration, with the two-fold objective of:

- developing "handles" for the understanding of transport barrier formation processes and
- exploring new routes for optimization of pinch configurations.

We have found that the magnetic chaos healing effect by helical structure development [9] appears to be more robust in the case of Non-Resonant helical regimes [2].

This line of research will be further explored in the upgraded RFX-mod2 device in Padova-Italy, expected to start operation in 2021.

References:

[1] S. Cappello et al., *Nuclear Fusion* **51**, 103012 (2011); S. Cappello *PPCF* **46**, B313 (2004)
[2] M. Veranda, D. Bonfiglio, S. Cappello, et al., *Nuclear Fusion* **57**, 116029 (2017)
[3] F. Pegoraro, D. Bonfiglio, S. Cappello, G. Di Giannatale, M V Falessi, D. Grasso and M. Veranda, *PPCF* **61**, 044003 (2019)
[4] D. Bonfiglio, M. Veranda, S. Cappello, et al., *Phys. Rev. Lett* **111**, 085002 (2013)
[5] R. Lorenzini, et al., *Nature Physics* **5**, 570 (2009);
[6] P. Piovesan, M. Zuin, et al., *Nuclear Fusion* **49**, 085036 (2009)
[7] J.S. Sarff, et al., *Nuclear Fusion* **53**, 104017 (2013)
[8] S. Cappello et al., *Theory of fusion plasmas Book Series*: AIP Conf. Proc. **1069** 27 (2008)
[9] D.F. Escande, R. Paccagnella, S. Cappello, et al *Phys. Rev. Lett* **85**, 3169 (2000)

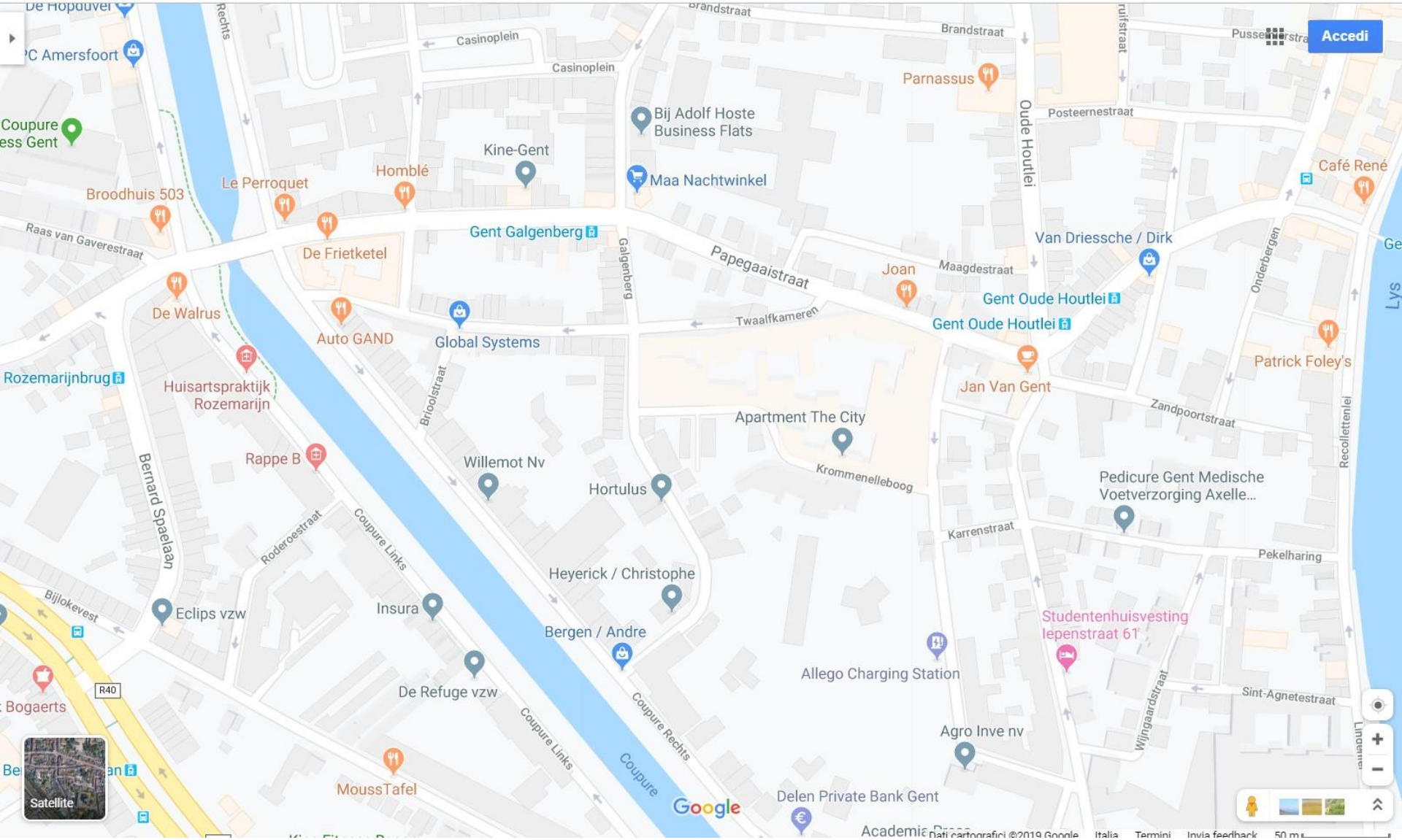
Accedi
Casinoplein
Brandstraat
Parnassus
Posteernestraat
Oude Houtlei
Bij Adolf Hoste
Business Flats
Kine-Gent
Maa Nachtwinkel
Homblé
Le Perroquet
Broodhuis 503
Café René
Raas van Gaverestraat
Gent Galgenberg
De Frietketel
Galgenberg
Papegaaistraat
Van Driessche / Dirk
Joan
Maagdestraat
Gent Oude Houtlei
Twaalfkameren
Onderbergen
De Walrus
Auto GAND
Global Systems
Patrick Foley's
Rozemarijnbrug
Huisartspraktijk
Rozemarijn
Jan Van Gent
Zandpoortstraat
Brioolstraat
Apartment The City
Rappe B
Willemot Nv
Hortulus
Krommenelleboog
Recollettenlei
Pedicure Gent Medische
Voetverzorging Axelle...
Bernard Spaelaan
Roderoestraat
Coupure Links
Karrenstraat
Pekelharing
Heyerick / Christophe
Bijlokevest
Eclips vzw
Insura
Bergen / Andre
Studentenhuisvesting
Iepenstraat 61
Allego Charging Station
R40
De Refuge vzw
Sint-Agnetestraat
Coupure Rechts
Wijngaardstraat
Agro Inve nv
Coupure
MoussTafel
Delen Private Bank Gent
Satellite
Google
Dati cartografici ©2019 Google
Italia
Termini
Invia feedback
50 m